

University of Windsor

Scholarship at UWindor

Electronic Theses and Dissertations

Theses, Dissertations, and Major Papers

5-10-2022

Enhancing Thermoelectric Generator Performance

Xi William Wang
University of Windsor

Follow this and additional works at: <https://scholar.uwindsor.ca/etd>



Part of the [Energy Systems Commons](#)

Recommended Citation

Wang, Xi William, "Enhancing Thermoelectric Generator Performance" (2022). *Electronic Theses and Dissertations*. 8902.

<https://scholar.uwindsor.ca/etd/8902>

This online database contains the full-text of PhD dissertations and Masters' theses of University of Windsor students from 1954 forward. These documents are made available for personal study and research purposes only, in accordance with the Canadian Copyright Act and the Creative Commons license—CC BY-NC-ND (Attribution, Non-Commercial, No Derivative Works). Under this license, works must always be attributed to the copyright holder (original author), cannot be used for any commercial purposes, and may not be altered. Any other use would require the permission of the copyright holder. Students may inquire about withdrawing their dissertation and/or thesis from this database. For additional inquiries, please contact the repository administrator via email (scholarship@uwindsor.ca) or by telephone at 519-253-3000ext. 3208.

Enhancing Thermoelectric Generator Performance

By

Xi (William) Wang

A Dissertation
Submitted to the Faculty of Graduate Studies
through the Department of Mechanical, Automotive & Materials Engineering
in Partial Fulfillment of the Requirements for
the Degree of Doctor of Philosophy
at the University of Windsor

Windsor, Ontario, Canada

2022

© 2022 Xi (William) Wang

Enhancing Thermoelectric Generator Performance

by

Xi (William) Wang

APPROVED BY:

N. Zioui, External Examiner
Université du Québec à Trois-Rivières

A. Emadi
Department of Electrical and Computer Engineering

N. Eaves
Department of Mechanical, Automotive, & Materials Engineering

A. Fartaj
Department of Mechanical, Automotive, & Materials Engineering

P. Henshaw, Co-Advisor
Department of Civil and Environmental Engineering

D. S-K. Ting, Co-Advisor
Department of Mechanical, Automotive, & Materials Engineering

April 08, 2022

DECLARATION OF CO-AUTHORSHIP/PREVIOUS PUBLICATION

I. Co-Authorship

I hereby declare that this thesis incorporates material that is result of joint research, as follows:

Chapter 2~5 of the thesis was co-authored with P. Henshaw and D. S-K. Ting. In all cases, the key ideas, primary contributions, experimental designs, data analysis, interpretation, and writing were performed by the author. P. Henshaw and D. S-K. Ting provided feedback on refinement of editing of the manuscript.

I am aware of the University of Windsor Senate Policy on Authorship and I certify that I have properly acknowledged the contribution of other researchers to my thesis, and have obtained written permission from each of the co-author(s) to include the above material(s) in my thesis.

I certify that, with the above qualification, this thesis, and the research to which it refers, is the product of my own work.

II. Previous Publication

This thesis includes four original papers that have been previously published/submitted for publication in peer reviewed journals/conferences/book chapters, as follows:

| Thesis Chapter | Publication title/full citation | Publication status |
|----------------|--|---------------------|
| Chapter 2 | <i>X. Wang, D. S-K. Ting, P. Henshaw, "Mutation particle swarm optimization (M-PSO) of a thermoelectric generator in a multi-variable space," Energy Conversion and Management 224 (2020) 113387</i> | <i>Published</i> |
| Chapter 3 | <i>X. Wang, P. Henshaw, D. S-K. Ting, "Exergoeconomic analysis for a thermoelectric generator using mutation particle swarm optimization (M-PSO)," Applied Energy 294 (2021) 116952</i> | <i>Published</i> |
| Chapter 4 | <i>X. Wang, P. Henshaw, D. S-K. Ting, "Using Dual-MPSO method to optimize TEG with variable cross-sections based on a comprehensive thermodynamic model," Cleaner Engineering and Technology</i> | <i>Under review</i> |

| | | |
|------------------|---|---------------------|
| <i>Chapter 5</i> | <i>X. Wang, P. Henshaw, D. S-K. Ting, "Using a hyperbolic structure for furthering the dynamic performance of a thermoelectric generator," Thermal Science and Engineering Progress</i> | <i>Under review</i> |
|------------------|---|---------------------|

I certify that I have obtained a written permission from the copyright owner(s) to include the above published material(s) in my thesis. I certify that the above material describes work completed during my registration as a graduate student at the University of Windsor.

III. General

I declare that, to the best of my knowledge, my thesis does not infringe upon anyone's copyright nor violate any proprietary rights and that any ideas, techniques, quotations, or any other material from the work of other people included in my thesis, published or otherwise, are fully acknowledged in accordance with the standard referencing practices. Furthermore, to the extent that I have included copyrighted material that surpasses the bounds of fair dealing within the meaning of the Canada Copyright Act, I certify that I have obtained a written permission from the copyright owner(s) to include such material(s) in my thesis.

I declare that this is a true copy of my thesis, including any final revisions, as approved by my thesis committee and the Graduate Studies office, and that this thesis has not been submitted for a higher degree to any other University or Institution.

ABSTRACT

Waste heat recovery plays an important role for alleviating the energy crisis and mitigating climate change. The thermoelectrical generator (TEG), a solid energy convertor, is a promising technology. However, the performance of a TEG is sensitive to its geometric structure and working conditions. An improved geometric structure and matching to the working conditions can make a TEG fully utilize its thermoelectrical conversion potential.

The TEG optimization is a kind of combinatorial problem. An effective algorithm is needed to optimize a TEG's performance. The particle swarm optimization (PSO) algorithm is introduced in this study to optimize a TEG's output power, efficiency, and even some economic indices (exergy efficiency and levelized cost of energy (LOCE)). In order to address the premature convergence (which is one of the main challenges for algorithms), a mutation program is used to improve the traditional PSO method. Meanwhile, many parameter combinations related to the algorithm (such as mutation factor (μ), cognitive parameter (C_1), and social parameter (C_2)) were tried. The mutation particle swarm optimization (M-PSO) is an effective algorithm to optimize the performance for the TEG. The results indicate that it is difficult to reach the optimal state in different performance indices simultaneously, necessitating a multi-objective optimization. Although the multi-objective optimization can be solved by the M-PSO using a weighted approach, there are biases introduced when selecting a weighting factor. In order to improve the multi-objective optimization further, the ε -constraint method is introduced into the M-PSO algorithm. Through optimizing of the TEG by this method, a series of acceptable solutions are acquired, which are named Pareto solutions. After that, the technique for order preference by similarity ideal solution (TOPSIS) method was used to analyze these Pareto solutions to search for a TOPSIS ideal solution.

Additionally, a hyperbolic-shaped variable cross-section TEG was simulated. Based on a comprehensive thermodynamic model, it appears that the hyperbolic TEG is equipped with higher output power and efficiency compared to the constant cross-section one. The study also indicates that the four non-dimensional parameters (shape parameter (β), area ratio (μ), temperature ratio (θ), and resistance ratio (r_x)) have considerable influences on the hyperbolic TEG performance. In this way, it is necessary to optimize the TEG power generation and efficiency in the variable searching space of these parameters. However, differing from the traditional optimization, it is necessary to solve the control equations in every iteration when

searching for an optimal configuration based on the comprehensive model. In order to do this, the Dual-MPSO algorithm was used in the optimizing research.

Finally, a transient TEG model is established using the SIMULINK. Under a periodic source temperature varied with a sinusoidal function, it is verified that the hyperbolic TEG has a higher mean power output and overall efficiency compared to that of the traditional one. Moreover, the results indicate that the shape parameter (β) and the period of the source temperature have considerable influences on the mean power output and overall efficiency of the hyperbolic TEG.

DEDICATION

To my family

ACKNOWLEDGEMENTS

Firstly, I am grateful to my advisors Dr. P. Henshaw and Dr. D. S-K. Ting sincerely. During this period, they provide me with useful advice helping me improve my academic ability. They always encourage me to keep forward and complete this dissertation finally. Particularly, I would like to thank Dr. P. Henshaw and Dr. D. S-K. Ting for scrutinizing through every manuscript.

A special thanks is to my committee members, Dr. A. Emadi, Dr. N. Eaves, and Dr. A. Fartaj for their time and invaluable suggestions. Meanwhile, I really appreciate Dr. N. Zioui of Université du Québec à Trois-Rivières, for her willingness to serve as the external examiner which demands much of her precious time.

This work was made possible by the Natural Sciences and Engineering Research Council of Canada and Ontario Centres of Excellence.

TABLE OF CONTENTS

| | |
|--|------|
| DECLARATION OF CO-AUTHORSHIP/PREVIOUS PUBLICATION | iii |
| ABSTRACT..... | v |
| DEDICATION | vii |
| ACKNOWLEDGEMENTS | viii |
| LIST OF TABLES | xii |
| LIST OF FIGURES | xiii |
| LIST OF ABBREVIATIONS/SYMBOLS..... | xvi |
| CHAPTER 1 INTRODUCTION | 1 |
| <i>1.1 Background and Motivation</i> | 1 |
| <i>1.2 Objective and Scope</i> | 3 |
| <i>1.3 Thesis Organization</i> | 3 |
| <i>References</i> | 5 |
| CHAPTER 2 MUTATION PARTICLE SWARM OPTIMIZATION (M-PSO) OF A THERMOELECTRIC GENERATOR IN A MULTI-VARIABLE SPACE..... | 7 |
| <i>2.1 Introduction</i> | 7 |
| <i>2.2 Energy analysis for a TEG</i> | 10 |
| <i>2.3 Modelling validation</i> | 13 |
| <i>2.4 Single-objective optimization for the TEG via M-PSO method</i> | 16 |
| <i>2.4.1 Variables and dimension in the searching space</i> | 19 |
| <i>2.4.2 Comparison of PSO and M-PSO algorithm in optimizing problem</i> | 21 |
| <i>2.4.3 The influence of parameters in the M-PSO method on the optimization of results</i> .. | 25 |
| <i>2.4.4 The optimized results for the output power and efficiency of the TEG module</i> | 31 |
| <i>2.5 Multi-objective Optimization for the TEG Via M-PSO Method</i> | 32 |
| <i>2.6 Conclusions</i> | 34 |
| <i>Acknowledgments</i> | 35 |
| <i>References</i> | 35 |

CHAPTER 3 EXERGOECONOMIC ANALYSIS FOR A THERMOELECTRIC GENERATOR USING MUTATION PARTICLE SWARM OPTIMIZATION (M-PSO)39

| | |
|---|----|
| 3.1 Introduction | 39 |
| 3.2 Thermodynamic Analysis for a TEG | 43 |
| 3.2.1 Analysis based on the 1st law of thermodynamics for a TEG module | 43 |
| 3.2.2 Analysis based on the 2nd law of thermodynamics for a TEG module | 46 |
| 3.2.3 Cost-effectiveness analysis for a TEG module | 47 |
| 3.2.4 Model establishment for a TEG module | 49 |
| 3.3 Single-objective Optimization for a TEG Using M-PSO Algorithm | 50 |
| 3.3.1 The influence of related parameters in the M-PSO method on the optimized results | 52 |
| 3.3.2 The optimized results for the exergy efficiency and LCOE of the TEG module | 59 |
| 3.4 Multi-objective Optimization for a TEG using ξ-constraint combined with M-PSO algorithm | 60 |
| 3.5 Conclusions | 66 |
| Acknowledgments | 67 |
| References | 67 |

CHAPTER 4 USING DUAL MUTATION PARTICLE SWARM METHOD TO OPTIMIZE THE VARIABLE CROSS-SECTION OF A THERMOELECTRIC GENERATOR BASED ON A COMPREHENSIVE THERMODYNAMIC MODEL....72

| | |
|---|-----|
| 4.1 Introduction | 72 |
| 4.2 Thermodynamic Analysis for a TEG | 76 |
| 4.2.1 Thermoelectric theory for a variable cross-sectional TEG module | 76 |
| 4.2.2 Material properties of the TEG module | 79 |
| 4.2.3 Control equations of the TEG module | 81 |
| 4.2.4 Methodology for the solution of the control equations based on MPSO algorithm .. | 85 |
| 4.3 Performance evaluation for the variable cross-sectional TEG module | 88 |
| 4.3.1 Thermoelectric theory for a variable cross-sectional TEG module | 89 |
| 4.3.2 Effects of working conditions on the performance of the variable cross-sectional TEG module | 94 |
| 4.3.3 Effects of geometric structure on the performance of the variable cross-sectional TEG module | 96 |
| 4.4 Optimization the variable cross-sectional TEG module's performances based on the Dual-MPSO algorithm | 98 |
| 4.5 Conclusions | 101 |

| | |
|---|-----|
| <i>Acknowledgments</i> | 103 |
| <i>References</i> | 103 |
| CHAPTER 5 USING A HYPERBOLIC STRUCTURE TO ENHANCE THE DYNAMIC PERFORMANCE OF A THERMOELECTRIC GENERATOR..... | 108 |
| 5.1 Introduction | 108 |
| 5.2 TEG model established in SIMULINK | 110 |
| 5.2.1 Electrical network structure | 110 |
| 5.2.2 Thermal network structure | 115 |
| 5.2.3 Boundary conditions and physical qualities | 118 |
| 5.2.4 Material properties | 119 |
| 5.3 Modelling validation | 120 |
| 5.4 Transient performances of the hyperbolic TEG under the periodic source temperature | 123 |
| 5.5 Conclusions | 133 |
| <i>Acknowledgments</i> | 134 |
| <i>References</i> | 134 |
| CHAPTER 6 CONCLUSIONS AND RECOMMENDATIONS | 138 |
| 6.1 Summary and Conclusions | 138 |
| 6.1.1 Improvement of TEG optimization algorithm | 138 |
| 6.1.2 Hyperbolic shaped design for a TEG | 139 |
| 6.1.3 Limitations | 139 |
| 6.2 Recommendations | 140 |
| <i>References</i> | 140 |
| APPENDICE..... | 142 |
| Appendix A Permissions of the chapters 2 and 3 from the publishers | 142 |
| VITA AUCTORIS | 143 |

LIST OF TABLES

| | |
|--|-----|
| Table 2.1. Material properties of P semiconductor [26] | 13 |
| Table 2.2. Material properties of N semiconductor [26] | 13 |
| Table 2.3. Limits of the search space for the optimization of the output power and efficiency | 22 |
| Table 2.4. The optimal power and efficiency under different seed values | 22 |
| Table 2.5 Optimized working conditions and geometric structure configurations of the TEG module..... | 32 |
| Table 2.6. Optimized working conditions and geometric structure configurations of the TEG module..... | 34 |
| Table 3.1. Cost of semiconductor and ceramic materials [13, 34]..... | 48 |
| Table 3.2. Material properties of P-Bi ₂ Te ₃ and N-Bi ₂ Te ₃ [41] | 49 |
| Table 3.3. Relevant variables and their value ranges | 53 |
| Table 3.4. Parameter selection for optimizations of exergy efficiency and LCOE..... | 59 |
| Table 3.5. The optimized working conditions and geometric structure configurations of the TEG60 | |
| Table 3.6. Analysis results based on TOPSIS method | 65 |
| Table 3.7. TOPSIS ideal working conditions and geometric structure configurations of the TEG module..... | 66 |
| Table 4.1. Material properties of modified bismuth telluride [16, 37]..... | 80 |
| Table 4.2. Expressions of the constant A_i and B_i in the two control equations | 84 |
| Table 4.3. Parameter selections for the MPSO algorithm | 87 |
| Table 4.4. Relevant variables and their value ranges | 100 |
| Table 4.5. Optimized working conditions and geometric structure configurations of the TEG ... | 101 |
| Table 5.1. Material properties of modified bismuth telluride [27, 36]..... | 120 |
| Table 5.2. Comparison between experiment and steady-state model for the TEG ($T_h=423$ K and $T_c= 303$ K)..... | 121 |
| Table 5.3. Comparison between experiment and steady-state model for the pair of TE elements | 123 |
| Table 5.4. Comparison in different time steps for a TEG ($\beta=0$)..... | 124 |

LIST OF FIGURES

| | |
|--|----|
| Figure 2.1. Structural diagram of a TEG module | 11 |
| Figure 2.2. Heat transfer in a TEG module | 11 |
| Figure 2.3. Comparison of thermodynamic model with experimental results for (a) open circuit voltage, and (b) maximum output power | 15 |
| Figure 2.4. Comparison of PSO and M-PSO algorithms (a) the flow diagram for PSO method, and (b) the flow diagram for M-PSO method | 19 |
| Figure 2.5. variations of output power and efficiency with different substrate area ratio and load resistance, (a) variations of output power and (b) variation of efficiency | 20 |
| Figure 2.6. Development of optimal output power using PSO and M-PSO methods..... | 23 |
| Figure 2.7. Development of optimal efficiency using PSO and M-PSO methods..... | 24 |
| Figure 2.8. Rate of convergence for the optimal output power of the TEG under different mutation factors: (a) $\mu = 0.01$, (b) $\mu = 0.02$, (c) $\mu = 0.03$, (d) $\mu = 0.04$, and (e) $\mu = 0.05$ | 26 |
| Figure 2.9. Optimized results for the output power of the TEG under different mutation factors: (a) $\mu = 0.01$, (b) $\mu = 0.02$, (c) $\mu = 0.03$, (d) $\mu = 0.04$, and (e) $\mu = 0.05$ | 28 |
| Figure 2.10. Rate of convergence for the optimal efficiency of the TEG under different mutation factors: (a) $\mu = 0.01$, (b) $\mu = 0.02$, (c) $\mu = 0.03$, (d) $\mu = 0.04$, and (e) $\mu = 0.05$ | 29 |
| Figure 2.11. Optimal results for the efficiency of the TEG under different mutation factors: (a) $\mu = 0.01$, (b) $\mu = 0.02$, (c) $\mu = 0.03$, (d) $\mu = 0.04$, and (e) $\mu = 0.05$ | 30 |
| Figure 2.12. Convergence of the output power and efficiency optimizations | 32 |
| Figure 2.13. Convergence of the multi-objective optimization | 33 |
| Figure 3.1. Cutaway view of a TEG module arrangement and its thermal transfer processes..... | 45 |
| Figure 3.2. Flow chart of the M-PSO method..... | 51 |
| Figure 3.3. Rate of convergence for the optimized exergy efficiency of the TEG, (a) $\mu = 0.01$, (b) $\mu = 0.02$, $\mu = 0.03$, $\mu = 0.04$, and $\mu = 0.05$ | 54 |
| Figure 3.4. Optimized results for exergy efficiency of the TEG, (a) $\mu = 0.01$, (b) $\mu = 0.02$, $\mu = 0.03$, $\mu = 0.04$, and $\mu = 0.05$ | 56 |
| Figure 3.5. Rate of convergence for the optimized LCOE of the TEG, (a) $\mu = 0.01$, (b) $\mu = 0.02$, $\mu = 0.03$, $\mu = 0.04$, and $\mu = 0.05$ | 57 |
| Figure 3.6. Optimized results for the LCOE of the TEG, (a) $\mu = 0.01$, (b) $\mu = 0.02$, $\mu = 0.03$, $\mu = 0.04$, and $\mu = 0.05$ | 58 |
| Figure 3.7. Diagram of ξ -constraint with M-PSO algorithm and TOPSIS method | 61 |
| Figure 3.8. Distribution of Pareto frontier under different values of n, (a) $n=5$, (b) $n=10$, (c) $n=20$, (d) $n=30$ | 62 |

| | |
|---|-----|
| Figure 3.9. Distribution of Pareto frontier and TOPSIS ideal solution point..... | 63 |
| Figure 4.1. Schematic diagram of a variable cross-section TEG module, (a) cutaway view of the TEG module arrangement, and (b) geometric structure of a TE element with variable cross-section shapes | 79 |
| Figure 4.2. Figure of merit of the P&N-type materials..... | 81 |
| Figure 4.3. Thermal transfer processes of a variable cross-section TEG module..... | 82 |
| Figure 4.4. Flow chart of the M-PSO method..... | 87 |
| Figure 4.5. Performances of the TEG with hyperbolic and traditional element shapes under different working conditions, (a) output power of the TEG modules and (b) efficiency of the TEG modules | 90 |
| Figure 4.6. Real temperature difference at the both ends of the TEG with hyperbolic and traditional element shapes under different working conditions | 91 |
| Figure 4.7. Internal thermal resistance and temperature distribution in the two different shapes of the TE couple | 93 |
| Figure 4.8. Variation of the output power and efficiency of the TEG with the load resistance ratio at a temperature ratio of 1.2 | 95 |
| Figure 4.9. Variation of the output power and efficiency of the TEG with the temperature ratio at a resistance ratio of 1.5 | 95 |
| Figure 4.10. Variation of the real temperature at the ends of the TE element with different temperature ratios at a resistance ratio of 1.5..... | 96 |
| Figure 4.11. Variation of the performance of the TEG with different shape parameters and area ratios at $\theta=1.2$ and $r_x=1.5$, (a) variation of the output power, and (b) variation of the efficiency . | 98 |
| Figure 4.12. Flow chart of the M-PSO method..... | 99 |
| Figure 4.13. Convergence of the output power and efficiency optimizations | 101 |
| Figure 5.1. Schematic diagram of a TEG module, (a) cutaway view of a TEG module arrangement, and (b) equivalent circuit diagram of a TEG | 111 |
| Figure 5.2. Schematic diagram of the variable cross-section TE legs, (a) isometric view, and (b) longitudinal section..... | 114 |
| Figure 5.3. Schematic diagram of the thermal model for the TEG in the SIMULINK | 117 |
| Figure 5.4. Schematic diagram of the thermal model for the non-thermoelectric parts in the SIMULINK..... | 117 |
| Figure 5.5. Comparison between previous and present transient TEG models, (a) results from Meng <i>et al.</i> [38], and (b) results from the present TEG model with $n=4$ | 122 |

| | |
|--|-----|
| Figure 5.6. Comparison in the temperature and thermal resistance variations of the hyperbolic and traditional TEG, (a) hot temperature, (b) cold temperature, and (c) thermal resistance | 126 |
| Figure 5.7. Comparison in the temperature difference variations of the hyperbolic and traditional TEGs | 126 |
| Figure 5.8. Comparison in the output power of the hyperbolic and traditional TEGs, (a) output power variations, and (b) mean output power..... | 127 |
| Figure 5.9. Transient performances of the hyperbolic TEG with different shape parameters and resistance ratios, (a) variation of the mean output power, (b) variation of the mean input heat rate, and (c) variation of the overall efficiency | 129 |
| Figure 5.10. Transient performances of the hyperbolic TEG with different source periods and offset distances, (a) variation of the mean output power, (b) variation of the mean input heat rate, and (c) variation of the overall efficiency | 131 |
| Figure 5.11. Comparison in the temperature difference and output power variations of the hyperbolic TEG under different source periods, (a) temperature difference variations, and (b) output power variations..... | 132 |

LIST OF ABBREVIATIONS/SYMBOLS

| | |
|---------------------|--|
| A | Cross sectional area of a TE couple |
| A_{sub} | Substrate area |
| C_1 | Cognitive parameter |
| C_2 | Social parameter |
| CRF | capital recovery factor. |
| d_c | Thickness of a conductor |
| $\dot{E}x_{input}$ | Exergy input rate |
| $\dot{E}x_{output}$ | Exergy output rate |
| F | TE couples to substrate area ratio |
| G_{best} | Global best position vector |
| K | Net thermal conductance of a TE couple |
| k_{air} | Thermal conductivity of air |
| k_N | Thermal conductivity of N semiconductors |
| k_P | Thermal conductivity of P semiconductors |
| L | Length of a TE couple |
| $LCOE$ | Levelized cost of energy |
| $maxgen$ | Maximum number of generations |
| μ | Mutation factor |
| N_{pair} | Number of TE couples |
| P | Output power of a TEG module |
| P_{best} | Local best position vector |
| P_{max} | Maximum output power of a TEG module |
| \dot{Q}_F | Fourier heat |
| \dot{Q}_{input} | Input heat |
| \dot{Q}_J | Joule heat |
| \dot{Q}_L | Heat loss |
| \dot{Q}_P | Peltier heat |
| r_c | Resistance of conductors |
| r_{ct} | Welding resistance |
| R_i | Internal resistance of a TEG module |

| | |
|---------------------|--|
| R_L | Load resistance |
| r_{teg} | Resistance of TE couples |
| S | Net Seebeck coefficient |
| S_N | Seebeck coefficients of N semiconductors |
| S_P | Seebeck coefficients of P semiconductors |
| T_c | Cold side temperature of a TEG module |
| T_h | Hot side temperature of a TEG module |
| TOPSIS | Technique for order preference by similarity ideal solution |
| T_S | Temperature of the thermal source |
| T_∞ | Ambient temperature |
| V | Seebeck voltage |
| V_i | Velocity vector of the i^{th} particle |
| w | Inertia weight |
| X_i | Location vector of the i^{th} particle |
| $Z_{ceramic}$ | Cost of ceramics |
| Z_{inv} | Device investment |
| Z_{om} | Other cost-related maintenance |
| $Z_{semiconductor}$ | Cost of semiconductor material |
| ZT | Figure of merit |
| η | Efficiency of a TEG module |
| ρ_c | Electrical resistivity of conductors |
| ρ_N | Electrical resistivity of N semiconductors |
| ρ_P | Electrical resistivity of P semiconductors |
| ω | Weight factor for the second objective function |
| μ | Ratio of the average cross-sectional areas of the N and P-type semiconductor |
| β | Shape parameter |
| γ | Maintenance factor |
| $\bar{\Delta}$ | Average values of the TE material properties |
| $\delta(T)$ | Equations relating the TE material properties to temperature |
| ψ_c | Thermal resistance at the cold side |
| ψ_h | Thermal resistance at the hot side |
| ψ_{TE} | Thermal resistance of the TE couple |

CHAPTER 1

INTRODUCTION

1.1 Background and Motivation

With modern society developing rapidly, the human lifestyle is increasingly reliant on energy. The global energy demand experienced a dramatic increase over the past decades, from 10 TW in the 1980s to 50 TW in the early twenty-first century [1]. Meanwhile, it is predicted that this figure will increase three-fold by the mid-century [1]. Nowadays, a large amount of energy is still derived from fossil fuel combustion [1]. However, relying on fossil fuel excessively will inevitably put humans in a dire state, due to its finite supply and environmental issues. Exploiting energy-saving technology is one of the effective measures to avoid the dilemma of supplying energy or reducing environmental effects. As an energy recovery technology, the thermoelectric generator (TEG) is considered to have considerable development prospects; thereby, it has become the focus of researchers' concern in recent years.

The TEG is to a kind of solid-state energy convertor, which can produce electrical power under a temperature difference. Compared with traditional energy convertors, TEG technology recovers waste heat, without moving parts [2]. However, in order to popularize the TEG technology, it is crucial to improve its thermoelectrical conversion performance further. There are many factors that determine the thermoelectrical conversion performance. Firstly, a TEG's performance is easy to be affected by its working conditions, especially temperature. According to the relevant literature, some important thermoelectrical properties, such as the Seebeck coefficient, electrical resistivity, and thermal conductivity, vary with temperature [3, 4]. Matching an appropriate working temperature for a TEG can assist in fully using the thermoelectrical conversion performance of the materials [4]. Besides, the thermal source used to drive a TEG may be dynamic. For instance, an oscillating source temperature can be seen in an internal combustion engine or an incineration system [5, 6]. Due to the thermal inertia of TE materials, there is a lag between the variations of the real working temperature of a TEG and the source temperature [5, 6]. This means that the effects of the source temperature variation characteristics, such as the wave form and amplitude of the temperature, on the thermoelectric conversion performance in a transient application should not be ignored.

Additionally, the thermoelectric conversion performance of a TEG is susceptible to its geometric structure, which has been reported in the literature. Some studies have indicated a

TEG's efficiency can be improved by increasing its couple length appropriately [7, 8]. However, with decreasing cross-sectional area of the TE couple, the output power decreases, while the efficiency improves [9, 10]. Besides, some researchers proposed that, compared to traditional TE couples, the variable cross-section is a better design [11-13]. Variable cross-section TEG leg designs, such as trapezoid and parabolic, can be used to improve a TEG's efficiency [12, 13]. Technologies of semiconductor manufacture, such as Additive Manufacture (AM), Selective Laser Sintering/Melting (SLS/SLM), and Spark Plasma Sintering (SPS), have developed at an astounding pace in the past decades, making it possible to produce, and even commercialize, a TE element with complex structural design [21]. Altering geometry to improve a TEG's performance under both steady-state and dynamic operations is one of the main motivations for this research.

However, it is worth noting that the effects of factors, such as temperature and geometry, on the TEG performance are not always monotonic and independent based on the literature review mentioned above. Hence a univariate analysis is not enough to find the optimal state for a TEG. Besides, there are many indices to evaluate a TEG's performance. It is usually necessary to simultaneously consider multiple objectives, such as power output, efficiency, and even cost-effectiveness, for a TEG when optimizing its performance. Generally, the performance optimization for a TEG is to a multiple variable and criteria decision-making problem, which should be solved by an algorithm. Recently, some traditional algorithms, such as genetic algorithm (GA) and simplified conjugate-gradient method (SCGM) have been applied to conduct the TEG optimization [14, 15]. However, during the process of TEG optimization, premature or poor convergence occur for these algorithms [15-17]. Actually, when using an algorithm, such as GA or SCGM to deal with a complicated problem, a large amount of time is always spent on trial-and-error calculations or tuning parameters, such as initial guesses and crossover probability [15, 18]. Therefore, one of the main research areas in TEG optimization is algorithm improvement in order to increase the accuracy and reliability of the TEG optimization. Particle swarm optimization (PSO) is a kind of bionic algorithm. Compared to the traditional algorithms (GA and SCGM), PSO uses a concise program and has excellent convergence. It has been applied in the optimization of power systems, such as a biodiesel engine and a hybrid electric system, in recent years [19, 20]. One of the main innovations in this research is to apply the PSO algorithm for TEG optimization. Meanwhile, it is necessary to improve the PSO method in order to avoid premature convergence and decrease the trial-and-error calculations or parameter tuning processes.

1.2 Objective and Scope

The overall objective in this study is to enhance a TEG's performance through simultaneously optimizing its geometric structure and working conditions. The work can be divided into two different parts. In part one, the particle swarm optimization (PSO) algorithm was used to conduct the TEG optimization. Then, the PSO method was improved further in order to increase its accuracy and reliability. In another part, a novel cross-section function is introduced to the design of the TEG. Finally, the novel shape design is optimized to improve the TEG's performances under the steady-state and transient operations respectively.

The scope of the work is as follows:

1. Utilize a mutation subprogram to improve the traditional PSO method, and apply the mutation PSO (M-PSO) method in multi-variable optimization of the TEG.
2. Use a weighted approach with the M-PSO algorithm to conduct a multi-objective optimization of the TEG. Compare this with the epsilon-constraint method introduced in the M-PSO algorithm in order to acquire a series of acceptable solutions (Pareto solutions), then use the technique for order preference by similarity ideal solution (TOPSIS) to analyze those acceptable results of the multi-objective optimization.
3. Introduce hyperbolic cross-section function to the design of the TE element. Through a comprehensive thermodynamic TEG model, explain the reason why the hyperbolic structure improves the thermoelectric conversion performance is explained.
4. Improve the M-PSO to be a dual-MPSO algorithm, and use the improved algorithm to optimize the hyperbolic TEG based on the comprehensive thermodynamic model.
5. Build a transient model for the hyperbolic TEG under a periodic thermal source. Analyze the difference in the dynamic thermoelectrical conversion performance between the hyperbolic and traditional TEG.

1.3 Thesis Organization

This thesis organizations are as follows:

Chapter 2

In the second chapter, a simplified thermodynamic TEG model was established to calculate two objective performance functions of a TEG. The mutation program was used to improve the accuracy and reliability of the traditional PSO algorithm. The M-PSO method was introduced to optimize the output power and efficiency of the TEG. Some parameters in the M-PSO algorithm, such as mutation factor (μ), cognitive parameter (C_1), and social parameter (C_2), are known to

affect its optimal results. Accordingly, 320 parameter combinations were tested to illustrate the accuracy and reliability of the M-PSO further. Finally, the weighted approach was combined with the M-PSO algorithm to conduct a multi-objective optimization for the TEG's output power and efficiency.

Chapter 3

Although the weighted approach can be used to solve the multi-objective optimization for a TEG (shown in the previous chapter), there are human influences when selecting a weight factor. In this chapter, an ϵ -constraint method was used to improve the multi-objective optimization for two new objective functions, exergy efficiency and levelized cost of energy (LCOE). Again, 320 parameter combinations were tested to illustrate the accuracy and reliability of the M-PSO method in the TEG exergoeconomic optimization. Then, through combining the ϵ -constraint method with the M-PSO algorithm, the multi-objective optimization for the TEG's exergy efficiency and LCOE was conducted, first by acquiring a series of acceptable solutions, named Pareto solutions. Then, a technique for order preference by similarity ideal solution (TOPSIS) method was used to analyze these Pareto solutions to search for a TOPSIS ideal solution.

Chapter 4

In this chapter, a novel cross-section function was introduced to the design of a TEG module. The differences in the thermoelectric conversion performance between the hyperbolic and traditional TEG modules were compared through a comprehensive thermodynamic model. Meanwhile, through comparing the internal temperature and thermal resistance distributions of the two kinds of TE elements, the mechanism was revealed by which the variable cross-section design enhances a TEG's performance. Based on the TEG model, the four non-dimensional parameters (shape parameter (β), area ratio (μ), temperature ratio (θ), and resistance ratio (r_x)) were found to have notable effects on the TEG performance. Optimal parameter combinations for the hyperbolic TEG were determined by an algorithm, which makes the TEG have maximum power output or efficiency. However, differing from the simplified thermodynamic model, the temperatures at the two ends of the TEG in the comprehensive TEG model are unknown. In this chapter, a dual-MPSO algorithm was introduced to optimize the hyperbolic TEG.

Chapter 5

Sometimes, the practical application environments for TEGs may be dynamic. Some heat sources are even characterized by periodic variations, such as a combustion engine and an

incineration system. In this way, it is worthwhile to study the transient characteristics of TEGs. Besides, the TEG designed with a variable cross-section has been verified to have better thermoelectrical conversion performance than the traditional TEG under a steady-state condition; However, research about the variable cross-section TEG leg under transient operation is rarely reported. In this chapter, a transient hyperbolic TEG model was established. Under a sinusoidally varying periodic source temperature, the differences in the transient characteristics of the hyperbolic- and traditional-shaped TEG legs were compared.

Chapter 6

The main research achievements and conclusions of each part were summarized in this chapter. Meanwhile, some suggestions and prospects are presented for future studies.

References

- [1] S. A. Kalogirou. (2014). ‘Solar energy engineering: processes and systems’, 2nd Ed. (Elsevier: Oxford, UK).
- [2] G. Li, S. Shittu, T. M. O. Diallo, M. Yu, X. Zhao, and J. Ji, ‘A review of solar photovoltaic-thermoelectric hybrid system for electricity generation’, *Energy*, vol. 158, pp. 41–58, September 2018.
- [3] E. Kanimba, M. Pearson, J. Sharp, D. Stokes, S. Priya and Z. Tian, “A modeling comparison between a two-stage and three-stage cascaded thermoelectric generator,” *Journal of Power Sources*, vol. 365, pp. 266–272, October 2017.
- [4] Y. Wu, J. Yang, S. Chen and L. Zuo, “Thermo-element geometry optimization for high thermoelectric efficiency,” *Energy*, vol. 147, pp. 672–680, March 2018.
- [5] W. H. Chen, S. R. Huang, X. D. Wang, P. H. Wu and Y. L. Lin, “Performance of a thermoelectric generator intensified by temperature oscillation,” *Energy*, vol. 133, pp. 257–269, May 2017.
- [6] M. Gomez, R. Reid, B. Ohara and H. Lee, “Influence of electrical current variance and thermal resistances on optimum working conditions and geometry for thermoelectric energy harvesting,” *Journal of Applied Physics*, vol. 113, p. 174908, May 2013.
- [7] Y. Mu, G. Chen, R. Yu, G. Li, P. Zhai and P. Li, “Effect of geometric dimensions on thermoelectric and mechanical performance for Mg₂Si-based thermoelectric uncouple,” *Materials Science in Semiconductor Processing*, vol. 17, pp. 21–26, January 2014.
- [8] L. Fan, G. Zhang, R. Wang and K. Jiao, “A comprehensive and time-efficient model for determination of thermoelectric generator length and cross-section area,” *Energy Conversion and Management*, vol. 122 (15), pp. 85–94, August 2016.
- [9] J. Wang, Y. Li, C. Zhao, Y. Chai, L. Zhu, C. Zhang, J. Wang, W. Zhao and P. Cao, “An optimization study of structural size of parameterized thermoelectric generator module on performance,” *Energy Conversion and Management*, vol. 160, pp. 176–181, March 2018.

- [10] B. Jang, S. Han and J. Y. Kim, "Optimal design for micro-thermoelectric generators using finite element analysis," *Microelectronic Engineering*, vol. 88 (5), pp. 775–778, May 2011.
- [11] G. E. Hoyos, K. R. Rao and D. Jerger, "Fast transient response of novel Peltier junctions," *Energy Conversion*, vol. 17 (1), pp. 45–54, February 1977.
- [12] A. Z. Sahin and B. S. Yilbas, "The thermoelement as thermoelectric power generator: Effect of leg geometry on the efficiency and power generation," *Energy Conversion and Management*, vol. 65, pp. 26–32, January 2013.
- [13] Y. Shi, D. Mei, Z. Yao, Y. Wang, H. Liu and Z. Chen, "Nominal power density analysis of thermoelectric pins with non-constant cross sections," *Energy Conversion and Management*, vol. 97, pp. 1–6, June 2015.
- [14] W. H. Chen, P. H. Wu and Y. L. Lin, "Performance optimization of thermoelectric generators designed by multiobjective genetic algorithm," *Applied Energy*, vol. 209 (1), pp. 211–223, January 2018.
- [15] J. H. Meng, X. X. Zhang and X. D. Wang, "Multi-objective and multi-parameter optimization of a thermoelectric generator module," *Energy*, vol. 71 (15), pp. 367–376, July 2014.
- [16] Y. D. Valle, G. K. Venayagamoorthy, S. Mohagheghi, J. C. Hernandez and R. G. Harley, "Particle swarm optimization: Basic concepts, variants and applications in power systems," *IEEE Transactions on Evolutionary Computation*, vol. 12 (2), pp. 171–195, April 2008.
- [17] A. Dener, A. Denchfield and T. Munson, "Preconditioning nonlinear conjugate gradient with diagonalized quasi-newton," *PASC '19: Proceedings of the Platform for Advanced Scientific Computing Conference*, pp. 1–7, June 12–14, 2019.
- [18] Y. J. Gong, J. J. Li, Y. Zhou, Y. Li, H. S-H. Chung, Y. H. Shi and J. Zhang, "Genetic Learning Particle Swarm Optimization," *IEEE Transactions on Cybernetics*, vol. 46 (10), pp. 2277–2290, October 2016.
- [19] Q. Zhang, R. M. Ogren and S. C. Kong, "A comparative study of biodiesel engine performance optimization using enhanced hybrid PSO–GA and basic GA," *Applied Energy*, vol. 165, pp. 676–684, March 2016.
- [20] R. Yang, Y. Yuan, R. Ying, B. Shen, and T. Long, "A Novel Energy Management Strategy for a Ship's Hybrid Solar Energy Generation System Using a Particle Swarm Optimization Algorithm," *Energies*, vol. 13 (6), p. 1380, March 2020.
- [21] M. Guo, D. Gu, L. Xi, H. Zhang, J. Zhang, J. Yang and R. Wang, "Selective laser melting additive manufacturing of pure tungsten: Role of volumetric energy density on densification, microstructure and mechanical properties," *International Journal of Refractory Metals and Hard Materials*, vol. 84, p. 105025, November 2019.

CHAPTER 2

MUTATION PARTICLE SWARM OPTIMIZATION (M-PSO) OF A THERMOELECTRIC GENERATOR IN A MULTI-VARIABLE SPACE

X. Wang, D. S-K Ting, and P. Henshaw, "Mutation particle swarm optimization (M-PSO) of a thermoelectric generator in a multi-variable space," Energy Conversion and Management 224 (2020) 113387

2.1 Introduction

Fossil fuel has played a dominant role in social development over the past decades. However, excessive reliance on fossil fuel creates a dilemma due to energy-related environmental issues, such as global warming and acid rain [1, 2]. Under this situation, many researchers devote themselves to developing energy-saving technology. The application of thermoelectric generators (TEG) is considered a part of the effort to recover more energy from traditional energy systems, such as an Otto cycle system or Rankin cycle system, to improve their overall efficiency [3, 4]. TEG is a kind of semiconductor-based energy converter, producing power from a temperature difference. Due to its highlighted advantages, like compact structure, lack of moving parts, and low noise, TEG technology is increasingly becoming the focus of researchers' concerns [5, 6].

Many researchers dedicate themselves to improve the low efficiency of TEGs (5%-7%), which is considered as the main reason impeding TEGs further development [7]. Apart from the development of advanced TE materials, it is cost-effective to optimize the TEG structure and working conditions. There are two kinds of studies for optimization of the TEG structure and working conditions: single-variable research and multi-variable/objective optimization. As for the former work, Jang *et al.* [8] used the finite element method to analyze independently the effects of geometry on micro-thermoelectric generator performance. The results indicated that a smaller cross-sectional area has a positive effect on efficiency; however, the effect on output power is negative [8]. Meanwhile, a thicker substrate layer can weaken the performance of the TEG due to a higher heat loss from the substrate [8]. A function was derived by Kim [9] to describe the relationship between the internal temperature difference and the load current of a TEG. Also derived from this function was the observation that the internal temperature drop can lead to a TEG output power reduction [9]. Shi *et al.* [10] used normal power density (NPD) and efficiency to evaluate the performance of a pin-shaped TE couple. It was shown that the trapezoid is the preferable cross-section shape of a TE couple due to its higher NPD value and efficiency [10].

Additionally, using a three-dimensional numerical TEG model, Meng *et al.* [11] found that there are two different optimal lengths of the TE couple to maximize the efficiency or output power. Through a thermal resistance model analysis for a TEG, it was verified by Ming *et al.* [12] that the efficiency experiences a dramatic increase with temperature difference growth; meanwhile, the effect of cold junction temperature on the efficiency is linear. Some researchers studied a TEG with complicated pin-shaped TE couples. Karana *et al.* [13] studied a new asymmetrical and segmented TEG. They introduced a new geometric parameter, a , to describe the exponentially varying cross-sectional area of the N-type leg [13]. The results indicated that the maximum efficiency can be improved by 5% when a is 3 for the modified TEG [13].

Currently, the manufacture of TEGs is a complicated process. Normally, it is necessary to consider many factors simultaneously, such as temperature, geometry and load, when designing TEGs. In this way, multi-variable (and even multi-objective) optimization for a TEG has been an increasingly popular topic. Huang *et al.* [14] utilized a simplified conjugate-gradient method to acquire the optimal configuration for a thermoelectric cooler (TEC, which is inverse to a TEG), by varying TE couple length and base area ratio. Through geometric optimization, the TEC cooling rate was improved by 10.21 times [14]. Likewise, Meng *et al.* [15] used the same method to optimize output power and efficiency for a TEG. Based on the results, they made a balance between the output power and efficiency through multi-objective optimization, making both achieve better results simultaneously [15]. In addition, with the development of intelligent algorithms, many researchers have tried to optimize TEGs by different methods. A vehicle-TEG system was optimized by Heghmanns *et al.* [16] through a genetic algorithm, and as a result, can save fuel by 0.5%-0.7%, depending on the driving conditions. Chen *et al.* [17] applied a multi-objective genetic algorithm (MOGA) to acquire optimized results of output power and efficiency for a TEG. The results showed that the output power and efficiency can be improved by 51.9% and 5.4% respectively under a temperature difference of 40 °C [17]. Moreover, based on the non-dominated sorting genetic algorithm (NSGA- II), Ge *et al.* [18] acquired an optimal solution distribution for the semiconductor volume and output power called the Pareto front, using the technique for order preference by similarity to an ideal solution (TOPSIS).

Based on the previous research achievements for TEGs, geometric structure and working conditions have totally different influences on the performance of a TEG. Meanwhile, for some parameters, such as base area ratio and working temperature, their effect on output power and efficiency of a TEG is non-monotonic. Therefore, it is useful to acquire a better parameter combination through an algorithm, improving the performance of a TEG. Additionally, some

continuous functions related to the performance of a TEG have been built as objects by some researchers through a simplified one-dimensional thermal resistance model. Then, the studies about multi-variable/ objective optimization for a TEG can be conducted using an intelligent algorithm, such as a conjugate-gradient method and genetic algorithm.

However, there will be many limitations for a TEG when it is applied to a specific situation, especially working temperature. Therefore, objective functions related to the performance of a TEG are normally discontinuous in the whole search space. In this paper, a constraint condition was utilized - that the temperature difference is below 40 K. In this way, utilizing a comprehensive one-dimensional thermal resistance model, two discrete functions of the relative temperature were established to describe the output power and efficiency of a TEG, respectively. Meanwhile, these functions were validated by the experimental data from Hsu *et al.* [19], and considered as optimization objectives. After optimizing for single-objective functions, a weighting approach was adopted to establish a multi-objective function, and optimized for it through an algorithm, making the TEG module design able to produce better output power and efficiency at the same time. Moreover, although the conjugate-gradient method and genetic algorithms have been mainstream algorithms in optimization, researchers should not lose sight of the limitations of the two methods. Due to excessive reliance on the initial conditions, the conjugate-gradient method will be more complicated and time-consuming when used to solve an optimization problem with more than three variables involved [15]. Despite its better design for search in direction, there are many drawbacks to genetic algorithms, such as poor convergence and some trial-and-error calculations [15, 20]. Particle swarm optimization (PSO) is a kind of bionic algorithm [20-21]. Compared with the other two algorithms, PSO uses a concise program and has excellent convergence, thereby being more suitable for high dimension optimization problems [21]. Additionally, in order to increase the diversity of the population and improve the accuracy of the algorithm, it is beneficial to incorporate some subprograms into the PSO method, such as mutation or differential evolution [21]. Hence, a kind of mutation PSO (M-PSO) algorithm was used to optimize a TEG in this paper. This method can accelerate the convergence procedure. Meanwhile, the mutation can increase randomization for the algorithm, making it possible to improve PSO applicability for discrete problems. Therefore, the main contribution of the paper is that by using a mutation subprogram, the premature convergence when applying a PSO method to conduct the combinatorial optimization for a TEG under a constraint condition can be effectively avoided. Overall, this work demonstrated the combination of algorithm improvement and multi-objective optimization.

2.2 Energy analysis for a TEG

Normally, a TEG is made of many TE couples in series as shown in Figure 2.1. According to the Seebeck effect, when under a temperature difference, TEGs produce a voltage which is directly proportional to the temperature gradient. The Seebeck voltage can be calculated by Eqs. (1) and (2) [22-24].

$$V = S(T_h - T_c)N_{pair} \quad (1)$$

$$S = S_P + |S_N| \quad (2)$$

where S is overall Seebeck coefficient, S_P and S_N are Seebeck coefficients of a P and N semiconductors, T_h and T_c are the hot and cold side temperatures of a TEG, and N_{pair} is the number of TE couples.

When a load resistance connects with the positive and negative terminals of a TEG, there will be power produced from this system. Based on Ohm's law, the output power (P) can be calculated by Eq. (3) [22-24].

$$P = \frac{S^2(T_h - T_c)^2 N_{pair}^2}{(R_i + R_L)^2} R_L \quad (3)$$

in which R_i and R_L are internal and load resistances, respectively. Commonly, the internal resistance is the sum of the resistances of TE couples and conductors. In this way, the calculations for the internal resistance can be shown as the following (Eqs. 4-7) [22].

$$r_{teg} = \left(\frac{\rho_P L_P}{A_P} + \frac{\rho_N L_N}{A_N} \right) N_{pair} \quad (4)$$

where r_{teg} is the resistance of TE couples. ρ_P , ρ_N , L_P , L_N , and A_P , A_N are the electrical resistivity, couple length and cross-sectional area of the P and N semiconductors, respectively. If both P and N components of a TEG have the same cross-sectional area (A) and couple length (L), the TE couple resistance can be derived as Eq. (5).

$$r_{teg} = \frac{L}{A} (\rho_P + \rho_N) N_{pair} = \frac{2N_{pair}L}{FA_{sub}} (\rho_P + \rho_N) N_{pair} \quad (5)$$

$$r_c = \frac{\rho_c \left(1 + \frac{1}{\sqrt{F}}\right)}{d_c} (2N_{pair} + 1) \quad (6)$$

$$R_i = r_{teg} + r_c \quad (7)$$

in which F is the P or N to substrate area ratio, A_{sub} is the substrate area, r_c is conductor resistance, and ρ_c and d_c are the electrical resistivity and thickness of a conductor.

The heat transfer process is displayed in Figure 2.2. Based on the first law of thermodynamics, there are two kinds of energy absorbed by the hot side substrate of a TEG, which are input heat and Joule heat.

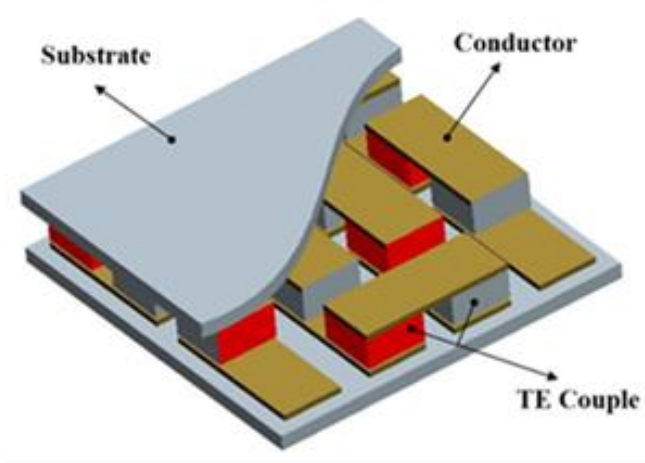


Figure 2.1. Structural diagram of a TEG module

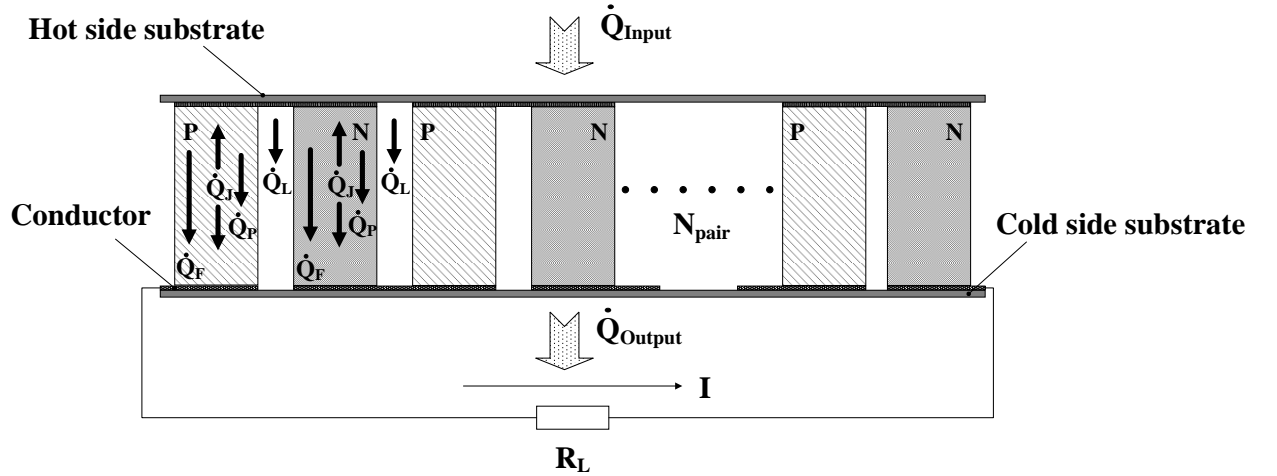


Figure 2.2. Heat transfer in a TEG module

Normally, Joule heat can be transferred to both sides of a TEG when current passes through it. Thus, it was assumed that only half of the Joule heat is absorbed by the upper-temperature side [22-23]. The thickness of a TEG module is very small; hence, the heat transfer from the edge of

the TEG can be ignored. In this way, there are three kinds of energy released from the hot temperature side, which are Fourier heat, Peltier heat, and heat loss. Applying a steady-state energy balance, the input heat (\dot{Q}_{input}) can be calculated by Eq. (8) [22-23].

$$\dot{Q}_{input} = \dot{Q}_F + \dot{Q}_P + \dot{Q}_L - \frac{1}{2} \dot{Q}_J \quad (8)$$

in which \dot{Q}_F is Fourier heat, \dot{Q}_P is Peltier heat, \dot{Q}_L is heat loss, and \dot{Q}_J is Joule heat.

According to Fourier's law of heat conduction and Peltier effect, the Fourier heat and Peltier heat can be calculated using Eqs (9) and (10) [22-23]. Besides, the Joule heat can be displayed as Eq. (11) based on Joule's law [22].

$$\dot{Q}_F = K(T_h - T_c)N_{pair} \quad (9)$$

$$\dot{Q}_P = ST_h IN_{pair} = S^2 T_h \frac{(T_h - T_c) N_{pair}^2}{R_i + R_L} \quad (10)$$

$$\dot{Q}_J = I^2 R_i = \frac{S^2 (T_h - T_c)^2 N_{pair}^2}{(R_i + R_L)^2} R_i \quad (11)$$

where K is the net thermal conductance of a TE couple ($K = \frac{A}{L} (k_P + k_N)$).

The heat loss mainly occurs in the gaps between the TE couples [25]. Normally, the filling material in the gaps is air. In this way, the heat loss can be estimated from the temperature difference-conductive thermal resistance of air ratio [25], *i.e.*,

$$\dot{Q}_L = \frac{T_h - T_c}{R_{gap}} = \frac{(T_h - T_c)}{\frac{L}{A_{sub} k_{air} (1 - F)}} \quad (12)$$

in which R_{gap} is the conductive thermal resistance of the air in the gaps, and k_{air} is the thermal conductivity of air.

According to Eqs. (3) and (8)-(12), the efficiency of a TEG (η) can be shown as Eq. (13) [22-23].

$$\eta = \frac{P}{\dot{Q}_F + \dot{Q}_P + \dot{Q}_L - \frac{1}{2}\dot{Q}_J} \quad (13)$$

$$= \frac{\frac{S^2(T_h - T_c)^2 N_{pair}^2}{(R_i + R_L)^2} R_L}{K(T_h - T_c) N_{pair} + S^2 T_h \frac{(T_h - T_c) N_{pair}^2}{R_i + R_L} + \frac{(T_h - T_c)}{\frac{L}{A_{sub} k_{air} (1 - F)}} - \frac{1}{2} \frac{S^2(T_h - T_c)^2 N_{pair}^2}{(R_i + R_L)^2} R_i}$$

2.3 Modelling validation

In keeping with Hsu *et al.* [19], a TEG module with a 10 cm by 10 cm substrate area was considered in this paper. The TEG module consisted of 199 pairs of cube-shaped couples in series. The initial dimension of couples and conductors was 2 mm × 2 mm × 0.64 mm and 4.5 mm × 2 mm × 0.5 mm, respectively [19]. The properties of TE materials can be seen in Tables 2.1 and 2.2.

Table 2.1. Material properties of P semiconductor [26]

| Properties of P semiconductor | |
|--|--|
| Seebeck coefficient (VK ⁻¹) | $8.3335 \times 10^{-12} T^3 - 1.3273 \times 10^{-8} T^2 + 6.3023 \times 10^{-6} T - 7.0396 \times 10^{-4}$ |
| Thermal conductivity (Wm ⁻¹ K ⁻¹) | $1.5888 \times 10^{-8} T^3 - 3.3157 \times 10^{-6} T^2 - 2.1177 \times 10^{-3} T + 1.5775$ |
| Electrical resistivity (Ωm) | $-7.3559 \times 10^{-13} T^3 + 6.1348 \times 10^{-10} T^2 - 6.3483 \times 10^{-8} T - 1.7788 \times 10^{-6}$ |

Table 2.2. Material properties of N semiconductor [26]

| Properties of N semiconductor | |
|--|--|
| Seebeck coefficient (VK ⁻¹) | $-3.9819 \times 10^{-12} T^3 + 7.3415 \times 10^{-9} T^2 - 3.8211 \times 10^{-6} T + 3.9458 \times 10^{-4}$ |
| Thermal conductivity (Wm ⁻¹ K ⁻¹) | $2.1889 \times 10^{-8} T^3 - 4.5960 \times 10^{-6} T^2 - 4.5182 \times 10^{-3} T + 2.4815$ |
| Electrical resistivity (Ωm) | $-6.8342 \times 10^{-13} T^3 + 6.6613 \times 10^{-10} T^2 - 1.5518 \times 10^{-7} T - 1.8059 \times 10^{-5}$ |

Based on Eq. (3) it was found that the output power of a TEG will reach a maximum value (P_{max}) when the internal resistance equals the load resistance as shown in Eq. (14).

$$P_{max} = \frac{S^2(T_h - T_c)^2 N_{pair}^2}{4R_i} \quad (14)$$

Using the one-dimensional thermodynamic model of a TEG, the maximum output power and open circuit voltage can be calculated from the temperature difference. In Hsu *et al.* [19], the temperature difference ranged from 5 K to 40 K and the hot temperature was fixed at 518 K. Using these conditions, the results were validated by the experimental data from Hsu *et al.* [19].

In this paper, a TEG module was considered through a thermodynamic model under a limited temperature difference (within 40 K). Under this limited temperature difference, the one-dimensional model is acceptable because, under this condition, the effects of the internal temperature field on the TEG performance are limited. In this way, the average values of the related physical parameters were taken into this study in order to solve the influences of the internal temperature field on the TEG performance. The general calculation equation for the average values of the related physical parameters can be shown as in Eq. (15):

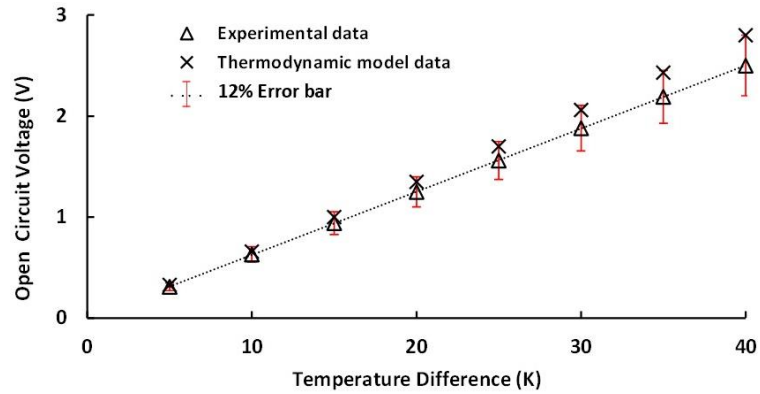
$$\bar{\Delta} = \frac{\int_{T_c}^{T_h} \delta(T) \cdot dT}{(T_h - T_c)} \quad (15)$$

where $\bar{\Delta}$ represents the average value of the Seebeck coefficient, thermal conductivity, or electrical resistivity. $\delta(T)$ represents the equation related temperature of the physical parameter. T_h and T_c are the hot and cold temperatures.

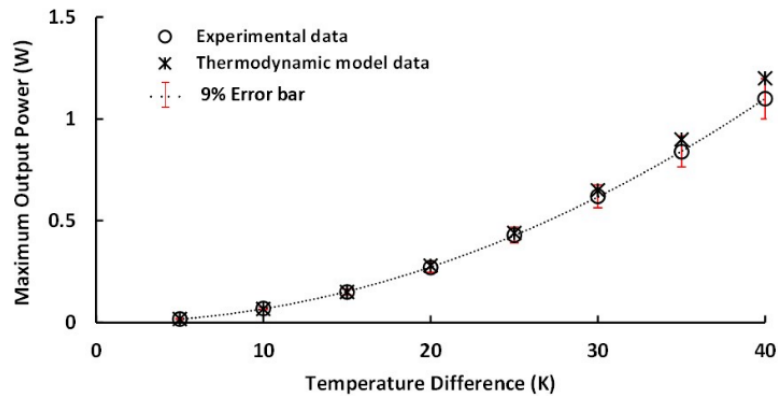
Based on the results for open circuit voltage (Figure 2.3-(a)), it was found that there was a similar tendency in both the experiment and thermodynamic model. Namely, the open circuit voltage experienced a dynamic increase linearly with the temperature difference growth. The values of the thermodynamic model are higher than those from the experiment. However, the largest error is 12% (when the temperature difference is 40 K) and the average error is about 8%. Likewise, the maximum output power increased non-linearly with the temperature difference rise, as shown in Figure 2.3-(b). The maximum error is about 9% at a temperature difference of 40 K, and the average error is around 4%. Error bars in Figures 2.3-(a) and (b) illustrate the 12% and 9% error, respectively.

The thermodynamic model was established based on some simplifying assumptions. In this paper, the contact thermal resistance and welding resistance were ignored, which is the main reason for the calculated values being higher than the experimental data. Additionally, the average values of TE material properties were used into the model. Moreover, as temperature difference increases, the error will increase when using the average values to simulate the actual behavior of the TE material [27]. That is a reason why the largest error happens at the largest temperature difference (40 K).

However, some references indicate that the thermodynamic model is acceptable under a limited working temperature difference (in this paper the temperature difference was below 40 K) [27-28]. Since this work mainly focused on the effectiveness of the M-PSO algorithm to optimize the performance of the TEG, the errors can be considered as within the acceptable range [29-30].



(a)



(b)

Figure 2.3. Comparison of thermodynamic model with experimental results for (a) open circuit voltage, and (b) maximum output power

2.4 Single-objective optimization for the TEG via M-PSO method

The PSO was developed mainly for applications in social science and computer science [21]. As a kind of bionic algorithm, the PSO imitates the food searching process of bird flocks. Through interacting locally with the environment, the particles (birds) can change their velocity continuously to find the best location [21]. The updated equations for the velocity vector (V) and location vector (X) of the i^{th} generation particle are shown in Eqs. (16) and (17) [21,31-32].

$$V_{i+1} = wV_i + C_1R_1(P_{best} - X_i) + C_2R_2(G_{best} - X_i) \quad (16)$$

$$X_{i+1} = X_i + V_{i+1} \quad (17)$$

where, w is the inertia weight, which can adjust the effect of the velocity of the previous generation. C_1 and C_2 are positive acceleration constants known as the cognitive and the social parameters. P_{best} is the local best position, and G_{best} is the global best position. R_1 and R_2 are two random numbers ranging from 0 to 1.

Equation (16), the velocity updating equation, has three terms. The first is wV_i which represents momentum, describing the tendency of each particle to maintain its movement habit. Using the swarm of bird analogy, it is the tendency for an individual bird to maintain its velocity vector. Term two, $C_1R_1(P_{best} - X_i)$, is the cognitive term. It can be interpreted to mean the particle memory influence which describes the difference between the current position and its individual best position. In the bird analogy, it quantifies how much an individual bird is influenced by its own previous experience in terms of finding food. The last term is $C_2R_2(G_{best} - X_i)$, representing the swarm information sharing which is the difference between the position of the i^{th} particle and the global best position of all particles. This relates to how well the bird listens to other bird's reports of food found.

Therefore, the physical significances of the C_1 and C_2 are the level of individual cognition and social information sharing in and between the birds of the swarm. The value of C_1 and C_2 can be used to adjust the relative contribution of the cognitive and information sharing term, governing the extent to which the particle moves to the individual and global best position [33]. The particle population ($Popsiz$ e) defines the number of simultaneous participants in the searching process.

The calculation process of a PSO method is shown in Figure 2.4-(a). After defining the objective function and related constants, the initial particle population was created. Then, the objective function was used to evaluate the fitness for each particle, which was compared with the local best and global best. Moreover, the velocity and position of the particles was adjusted by

Eqs. (16) and (17). This cycle of calculation continued until the convergence criterion was satisfied.

However, a shortage of enough diversity can potentially make the PSO method hard to converge to the global optimum, especially for discrete optimizing problems [34-35]. The M-PSO method (as shown in Figure 2.4-(b)) is an effective way to tackle this problem. Differing from the traditional PSO method, the subprogram, mutation, can increase randomization for the algorithm, making it possible to improve its search direction. During the mutation process, a threshold condition was set up as shown in Eq. (18):

$$threshold\ value = (1 - (i - 1)/(maxgen - 1))^{\frac{1}{mu}} \quad (18)$$

where, *maxgen* is the maximum number of generations, and *mu* is the mutation factor.

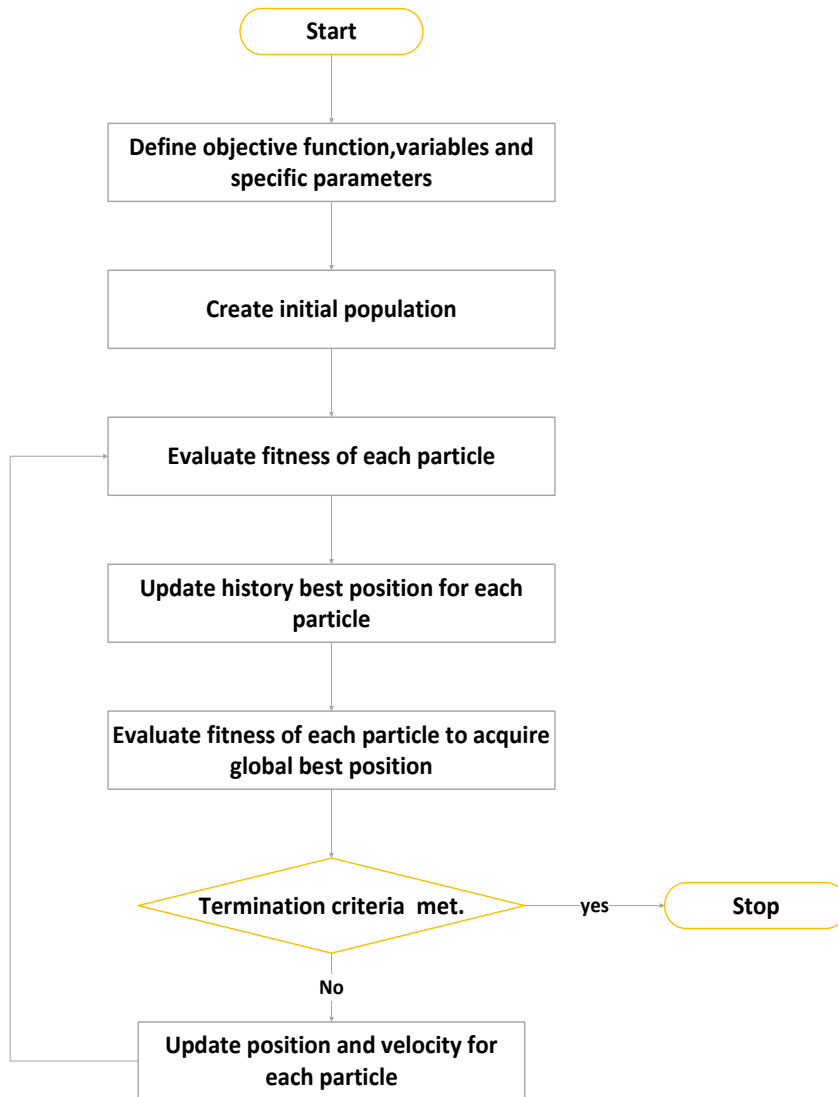
Once a random number was below the threshold value, the mutation program was invoked. In this way, a new position was created randomly between a lower boundary (*lb*) and upper boundary (*ub*). The value of the boundary was calculated by Eqs. (19)-(22). Meanwhile, the new position remained if its fitness was better than that of the old position.

$$\delta x = threshold\ value \times (X_{max} - X_{min}) \quad (19)$$

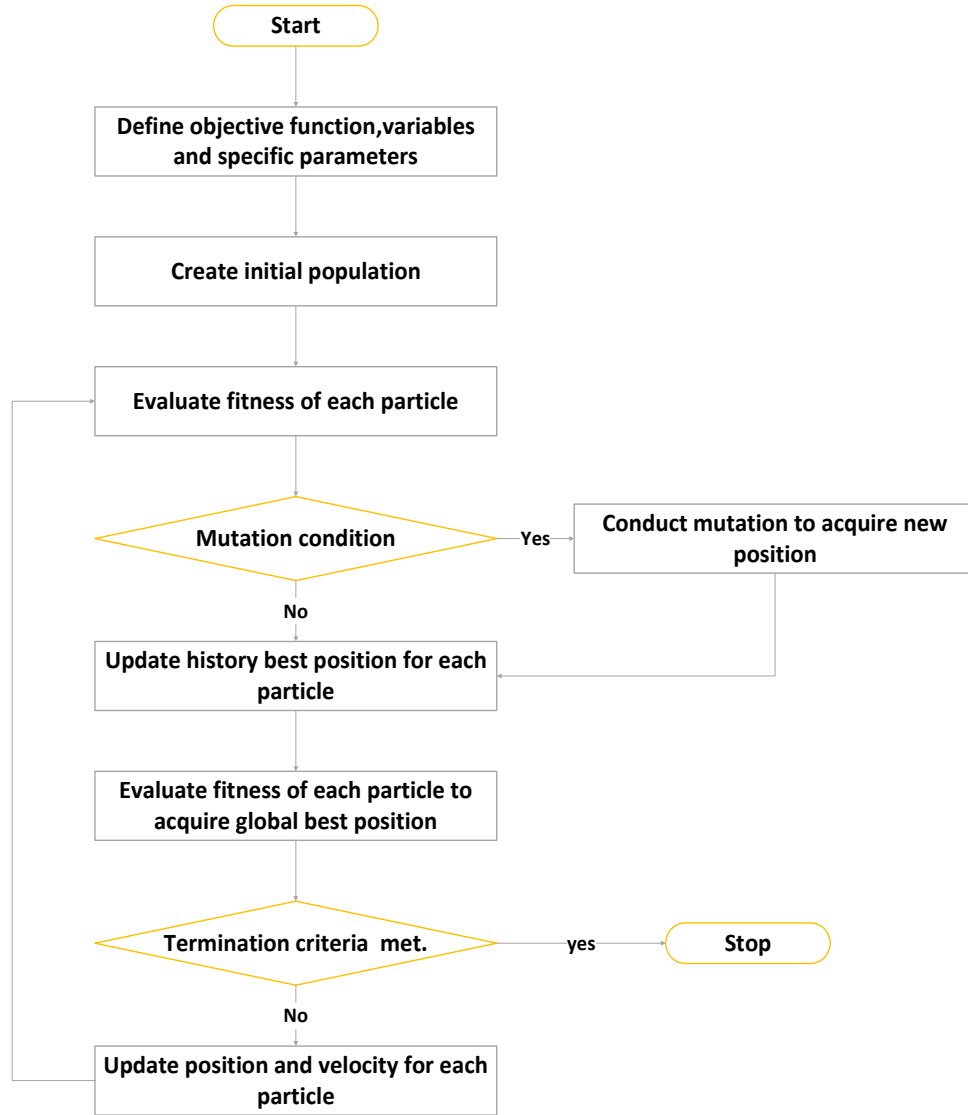
$$lb = X_i - \delta x \quad (20)$$

$$ub = X_i + \delta x \quad (21)$$

$$[lb\ ub] \in [X_{min}\ X_{max}] \quad (22)$$



(a)



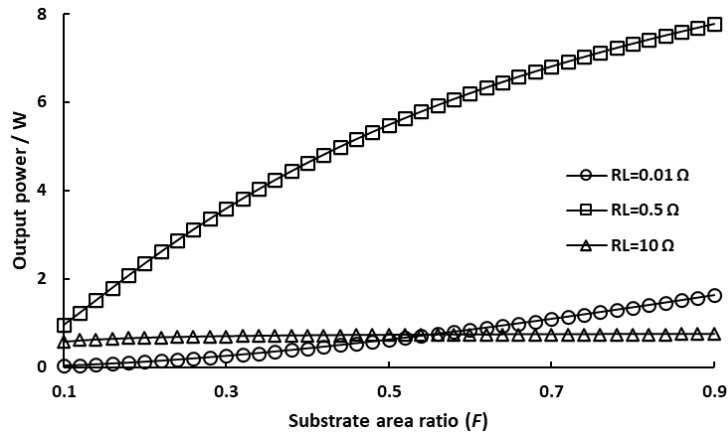
(b)

Figure 2.4. Comparison of PSO and M-PSO algorithms (a) the flow diagram for PSO method, and (b) the flow diagram for M-PSO method

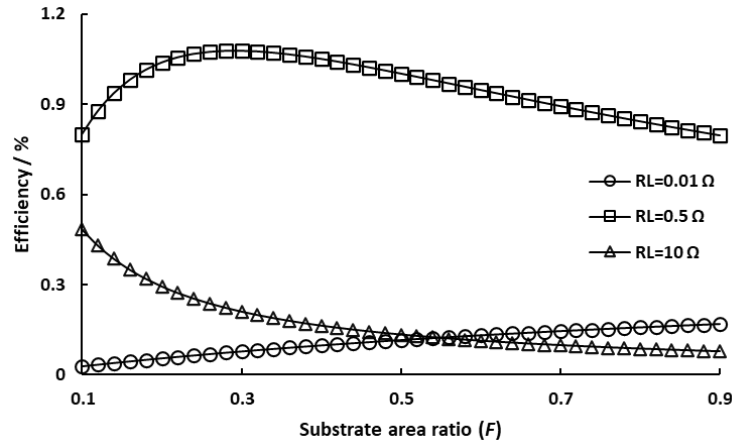
2.4.1 Variables and dimension in the searching space

Before performing the optimization for the TEG, it is necessary to confirm variables and dimensions of the searching space. The thermodynamic model for the TEG mentioned before has indicated that its performance is closely related to its geometric structure and working conditions. Thus, the effects of load resistance and substrate area ratio on the output power and efficiency of the TEG were analyzed. In the analysis, all other parameters were kept at the default values and the temperature difference was 40 K. The results for the output power are shown in Figure 2.5-

(a). Over the studied load resistance, its effect on the output power is non-monotonic. Although the influence of substrate area ratio on the output power is monotonic, the variation was affected by the load resistance. The same can be said about efficiency as shown in Figure 2.5-(b). In other words, the load resistance significantly affects the linear relationship between the efficiency and substrate area ratio. When the load resistance was 0.01Ω , the efficiency increased roughly linearly with increasing substrate area ratio. Under a load resistance of 0.5Ω , the efficiency increases, reaches a maximum and decreases, when the substrate area ratio is increased from 0.1 to 0.9. However, with the load resistance rising to 10Ω further, the efficiency experiences a moderate decrease with the substrate area ratio growth.



(a)



(b)

Figure 2.5. variations of output power and efficiency with different substrate area ratio and load resistance, (a) variations of output power and (b) variation of efficiency

Additionally, the previous research about the TEG module reported by our group indicated that there was an opposite effect of the couple length on the output power and efficiency [36]. Although the effect of the working temperature on the output power is linear, its effect on the efficiency is not [36]. Meanwhile, changes in the working temperature and TE couple structure can lead to a variation of the internal resistance, which also is an important factor in TEG optimal performance [36].

Overall, it is inadequate to optimize TEG performance in a single variable space as there are coupling effects between different variables. Therefore, it is necessary to conduct the optimizations for the TEG module in the 5-dimensional searching space made by hot temperature (T_h), cold temperature (T_c), load resistance (R_L), TE couple length (L), and substrate area ratio (F).

2.4.2 Comparison of PSO and M-PSO algorithm in optimizing problem

Before solving an optimizing problem, it is necessary to establish an objective function and search space. The objective functions in this study were output power and efficiency and the variables considered in the objective functions were: hot temperature, cold temperature, load resistance, couple length, and base area ratio. The problem descriptions are as follows, and the searching space is shown in Table 2.3.

The objective function (1) for the output power is:

$$f_1(T_h, T_c, R_L, L, F) = \begin{cases} \frac{S^2(T_h - T_c)^2 N_{pair}^2}{(R_i + R_L)^2} R_L, & T_h - T_c \leq 40 \text{ K} \\ 0, & T_h - T_c > 40 \text{ K} \end{cases} \quad (23)$$

The objective function (2) for the efficiency is:

$$f_2(T_h, T_c, R_L, L, F) = \begin{cases} \frac{S^2(T_h - T_c)^2 N_{pair}^2}{(R_i + R_L)^2} R_L, & T_h - T_c \leq 40 \text{ K} \\ \frac{\dot{Q}_F + \dot{Q}_P + \dot{Q}_L - \frac{1}{2}\dot{Q}_J}{\dot{Q}_F + \dot{Q}_P + \dot{Q}_L - \frac{1}{2}\dot{Q}_J}, & T_h - T_c > 40 \text{ K} \end{cases} \quad (24)$$

Table 2.3. Limits of the search space for the optimization of the output power and efficiency

| Variable | Value range |
|-----------------------------|---|
| Hot temperature (T_h): | $273\text{ K} \leq T_h \leq 573\text{ K}$ |
| Cold temperature (T_c): | $273\text{ K} \leq T_c \leq 573\text{ K}$ |
| Load resistance (R_L): | $0.01\ \Omega \leq R_L \leq 10\ \Omega$ |
| Couple length (L): | $0.0005\text{ m} \leq L \leq 0.0009\text{ m}$ |
| Based area ratio (F): | $0.1 \leq F \leq 0.9$ |

In this paper, the PSO and M-PSO methods, compiled through MATLAB, were used to optimize the output power and efficiency of the TEG. In the PSO or MPSO algorithm, some random numbers are generated in MATLAB. In MATLAB, random numbers are generated through the Mersenne Twister generator, which generates a pseudo-random number [37]. The random number is deterministic and depends on the value of the seed selected. The seed value with 0 is the default in MATLAB, and “shuffle” is a kind of dynamic seed value, which is related to the clock system in the computer. Before doing PSO and MPSO optimizations, seven kinds of seed values were tested. The results indicate (as shown in Table 2.4) that the optimal power output and efficiency were the same when using the different seed values. Hence, the seed value was set to *default* for the random number generator in this study.

Table 2.4. The optimal power and efficiency under different seed values

| Seed value | Output power (W) | Efficiency (%) |
|-------------|------------------|----------------|
| 0 (default) | 23.6 | 4.05 |
| 1 | 23.6 | 4.05 |
| 2 | 23.6 | 4.05 |
| 3 | 23.6 | 4.05 |

| | | |
|----------------|------|------|
| 4 | 23.6 | 4.05 |
| 5 | 23.6 | 4.05 |
| shuffle | 23.6 | 4.05 |

During the optimizing process, the inertia weight was kept the same (0.4) for the two methods. Additionally, the largest value of the mutation factors considered in this paper was 0.05, which is the highest probability of mutation occurring, which leads to the greatest randomization in the algorithm and potentially the best chance of finding the optimum value. In this way, the biggest difference between the M-PSO and traditional PSO algorithms should occur when $\mu = 0.05$. Meanwhile, there were three groups of constants, involving the cognitive parameter (C_1), the social parameter (C_2), and the particle population ($Popsiz$), which were utilized in the two methods. The optimized results are shown as Figures 2.6 and 2.7.

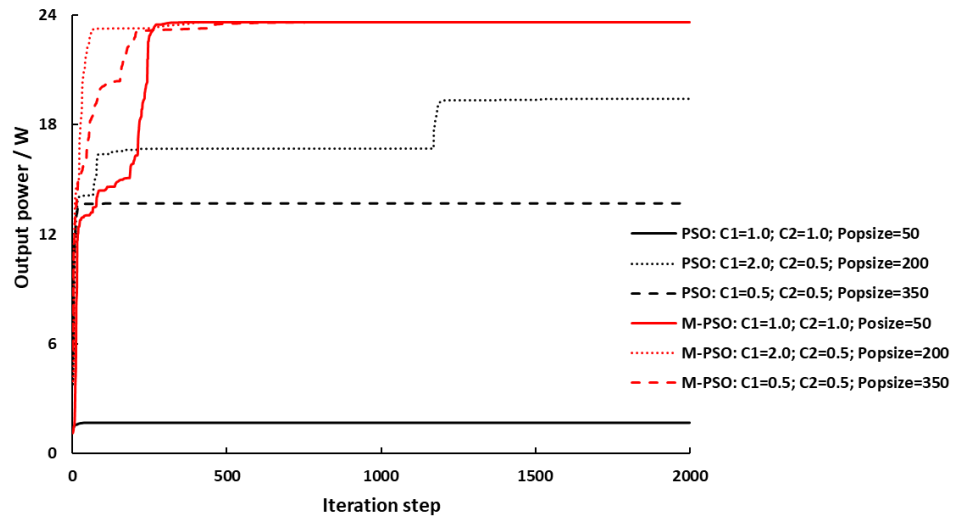


Figure 2.6. Development of optimal output power using PSO and M-PSO methods

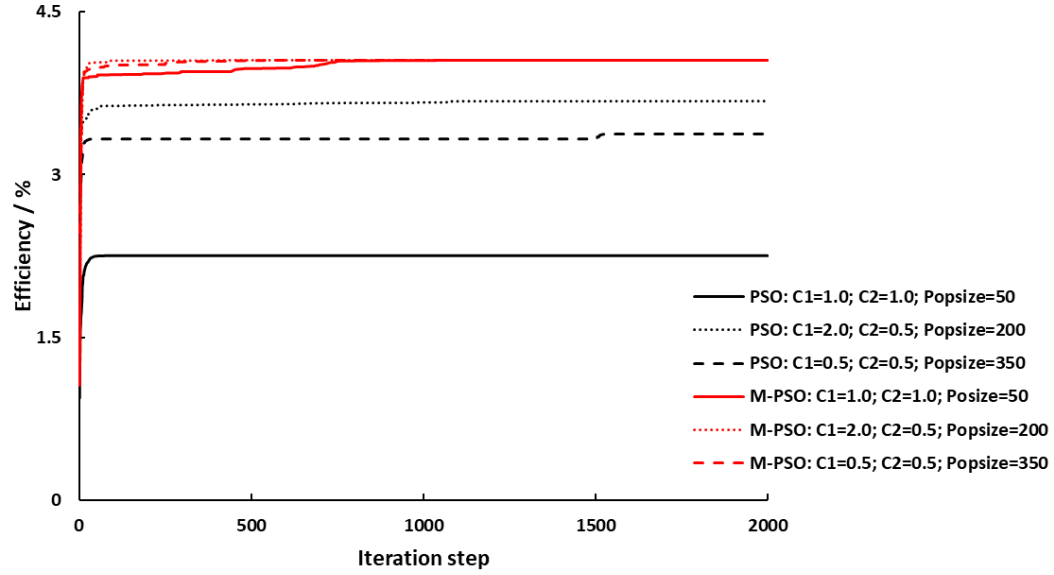


Figure 2.7. Development of optimal efficiency using PSO and M-PSO methods

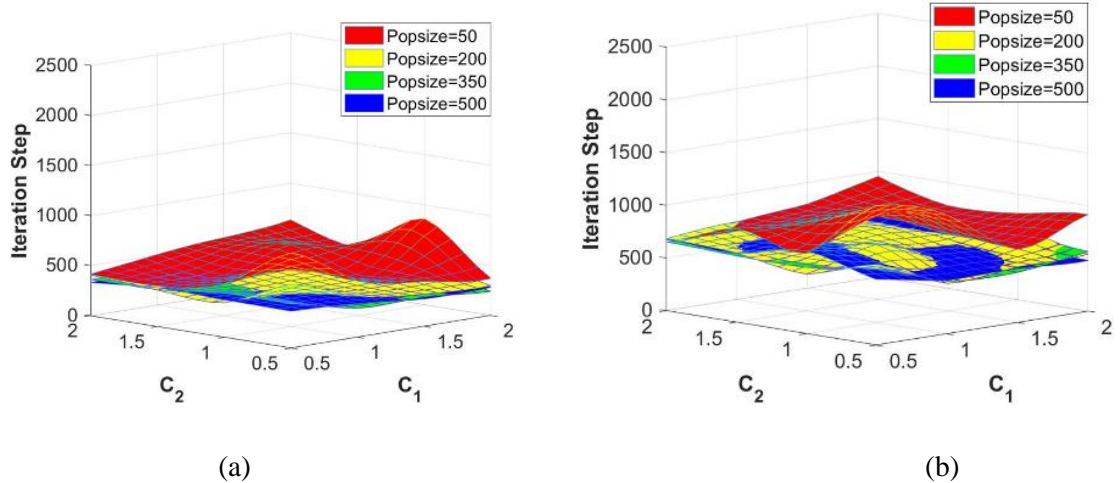
According to the results for the output power, the optimized result based on the PSO method varied dramatically across the values of related parameters. Conversely, the result acquired by the M-PSO algorithm was most repeatable. However, one should not lose sight of the important influence of the related parameters on the rate of convergence (inverse of the necessary number of iteration steps). Moreover, the optimized result of the M-PSO algorithm was better than that of the PSO method. When $C_1 = 2.0$, $C_2 = 0.5$, and $Popsiz = 200$, the optimal output power of the TEG using the M-PSO method is about 17.8% higher than that of the PSO method. Additionally, there were similar tendencies for the optimal efficiency of the TEG. When $C_1 = 2.0$, $C_2 = 0.5$, and $Popsiz = 200$, the optimal efficiency of the M-PSO method is about 9.3% higher than that of the PSO method.

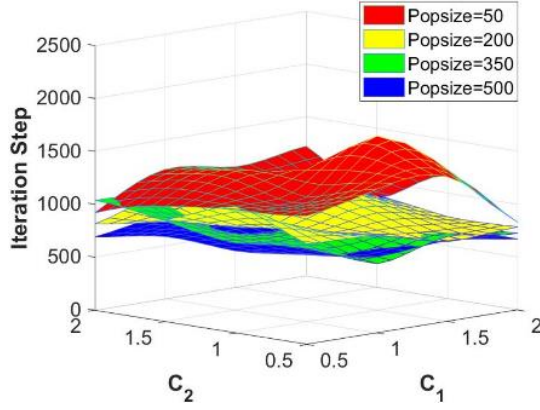
The figures also illustrate that it was easy to drop into a local best value using the PSO method due to its poorer randomness. Therefore, the PSO method was not suitable for solving this discrete optimizing problem for the TEG. Meanwhile, no matter whether optimizing output power or efficiency for the TEG, the M-PSO was an effective method to impede acquiring incorrect results since the mutation subprogram increased randomization for the algorithm.

2.4.3 The influence of parameters in the M-PSO method on the optimization of results

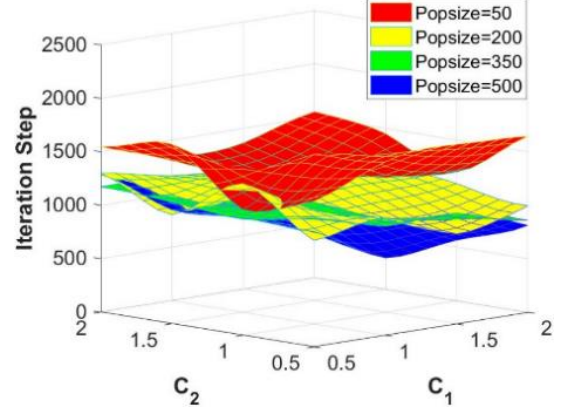
Based on the results mentioned above, it was found that the parameters in the M-PSO method have non-ignorable effects on the optimization of results, especially on the rate of convergence and precision. In this way, there were 320 parameter combinations considered for the output power and efficiency optimization in this paper. Thereinto, the mutation factor was [0.01, 0.02, 0.03, 0.04, 0.05], and the particle population was [50, 200, 350, 500]. Meanwhile, there were four values for the cognitive and social parameters, which were [0.5, 1.0, 1.5, 2.0].

Figure 2.8 displays the rate of convergence for optimizing output power under different set-up parameters. Under a specific mutation factor, increasing the particle population (when *Popsiz*e was below 200) improved the rate of convergence. When the *Popsiz*e was more than 200 and μ was more than 0.02, however, the rate of convergence was not only decided by the particle population, but also acceleration constants (C_1 and C_2). As for a bionic algorithm, the result is consistent with its biological root. When having more population, the bird flock can search for the location of food more rapidly. However, when the population of the bird flock is sufficient, the information sharing mechanism also plays a dominant role in the group working efficiency. Moreover, the rate of convergence experienced an obvious decline when the mutation factor increased from 0.01 to 0.05 under a specific particle population. The main reason is that the searching characteristics of the M-PSO with a lower mutation factor is much closer to that of the standard PSO method.

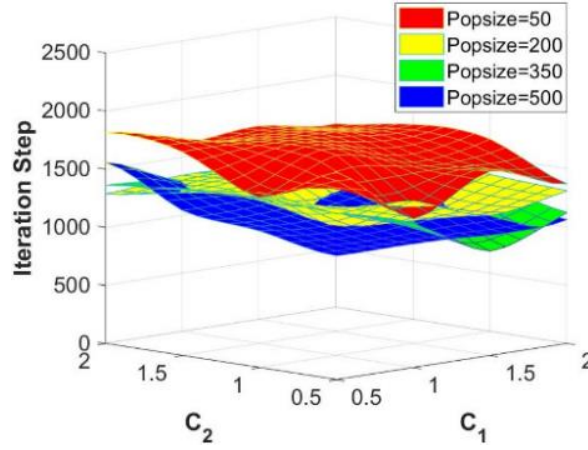




(c)



(d)



(e)

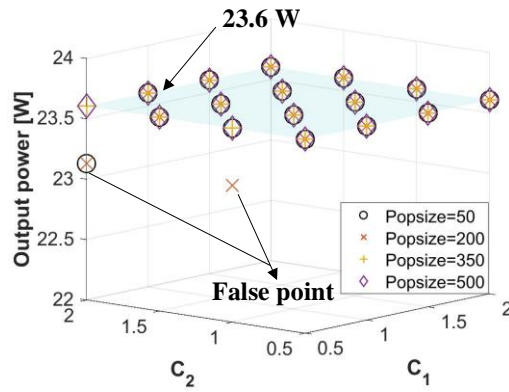
Figure 2.8. Rate of convergence for the optimal output power of the TEG under different mutation factors: (a) $\mu = 0.01$, (b) $\mu = 0.02$, (c) $\mu = 0.03$, (d) $\mu = 0.04$, and (e) $\mu = 0.05$

The optimization results for the output power are shown in Figure 2.9. Overall, the optimized results for the output power were repeatable through the M-PSO algorithm under most situations. Those points, lower than the optimal value, were defined as false points. There were 64 combinations for each specific mutation factor. Based on the results, it was found that the false point rates for the mutation factors 0.01 and 0.02 were the highest, which were both about 4.7%. That for mutation factor 0.03 ranked in the middle, which was about 3.1%. The lowest false point rate was found for the cases of mutation factors of 0.04 and 0.05, which were both about 1.6%. Therefore, the accuracy of the optimized result for the output power with a higher mutation factor was better than that with a lower mutation factor. A higher mutation factor can increase the

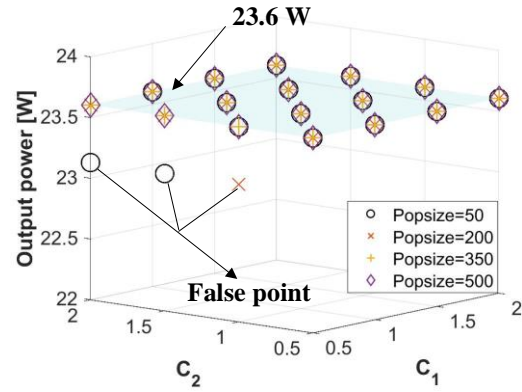
randomization for the algorithm dramatically, making it more likely to converge at an optimal value.

Likewise, there were 80 combinations for each *Popsiz*e. The false point rate for the *Popsiz*e with 50 topped the group, at 7.5%. The figure for *Popsiz*e with 200 was 5%. When the *Popsiz*e was higher than 200, the false point rate was 0. In this way, the accuracy of the optimized result can also be improved by increasing the particle population. It is easy to understand that a bird flock with more population can locate the position of food more accurately.

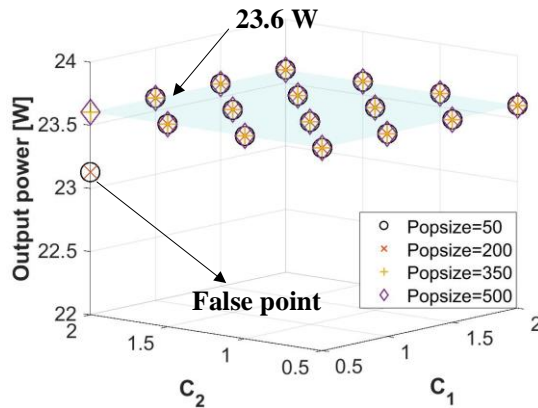
Overall, there were 320 combinations tested in total for the output power optimization through the M-PSO algorithm. The standard deviation of the means associated with the algorithm for the output power optimization was 0.00463 W.



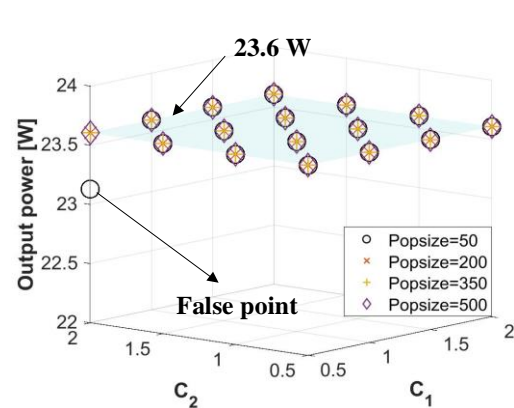
(a)



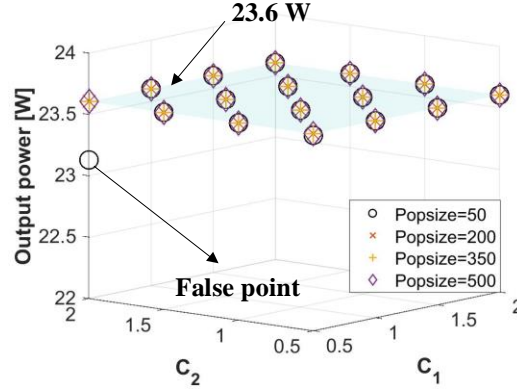
(b)



(c)



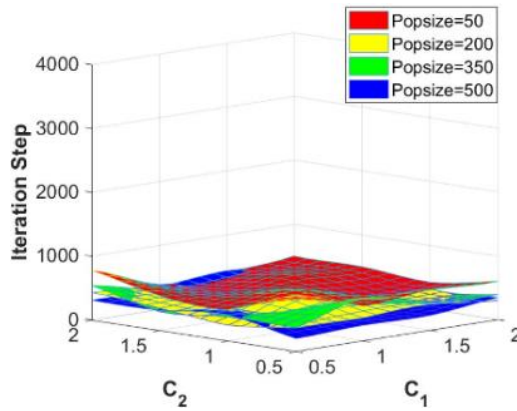
(d)



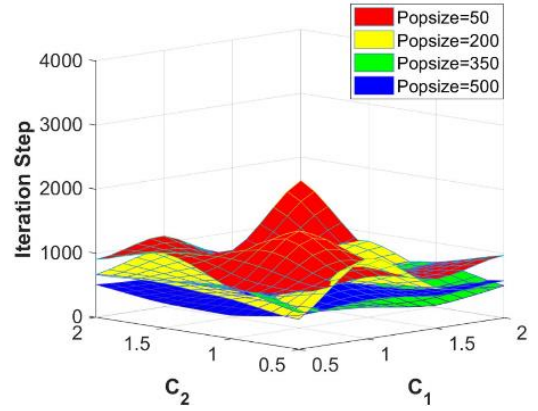
(e)

Figure 2.9. Optimized results for the output power of the TEG under different mutation factors: (a) $\mu = 0.01$, (b) $\mu = 0.02$, (c) $\mu = 0.03$, (d) $\mu = 0.04$, and (e) $\mu = 0.05$

There were similar tendencies found in the optimized results of efficiency. The rate of convergence for optimal efficiency is shown in Figure 2.10. More iteration steps were needed for the result to converge under a higher mutation factor. Meanwhile, increasing the particle population was an effective method to accelerate the calculation to converge when the $Popsiz$ was below 200. However, even under a higher particle population ($Popsiz$ more than 200), the influence of acceleration constant on the rate of convergence cannot be ignored.



(a)



(b)

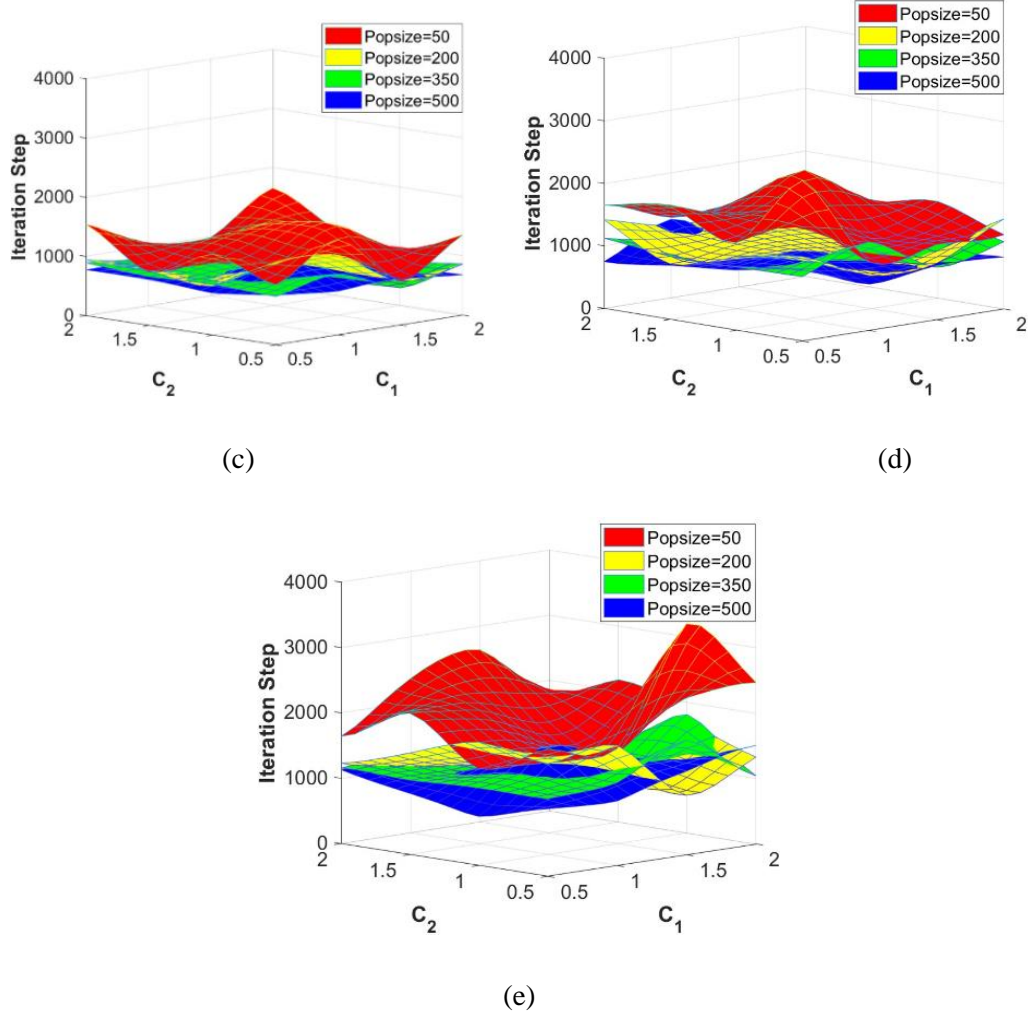
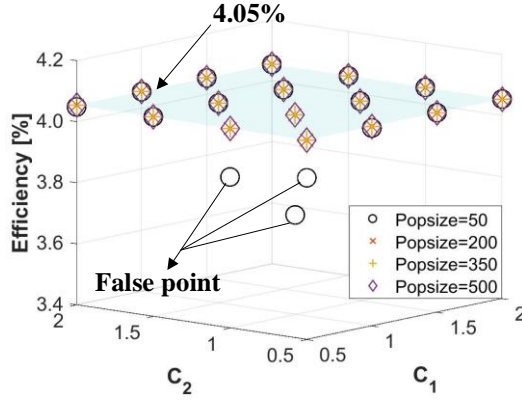


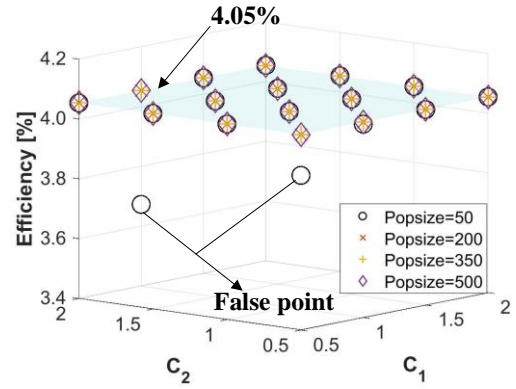
Figure 2.10. Rate of convergence for the optimal efficiency of the TEG under different mutation factors: (a) $\mu = 0.01$, (b) $\mu = 0.02$, (c) $\mu = 0.03$, (d) $\mu = 0.04$, and (e) $\mu = 0.05$

The optimized results for the efficiency are displayed in Figure 2.11. Similar to the optimal output power, the false point rates for the cases with mutation factors of 0.01 and 0.02 were 4.7% and 3.1%, respectively. When the mutation factor was more than 0.02, the false point rate was 0. Moreover, the false point rate for the case of a *Popsiz* of 50 was about 6.3%. When the *Popsiz* was more than 50, the false point rate was 0. Therefore, the mutation factor and particle population had a positive correlation with the accuracy of the optimized result for the efficiency using the M-PSO method.

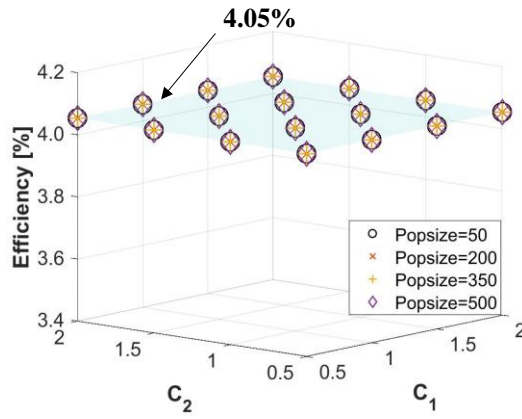
Overall, there were 320 combinations tested in total for the efficiency optimization through the M-PSO algorithm. The standard deviation of the means associated with the algorithm for the efficiency optimization was 0.00174%.



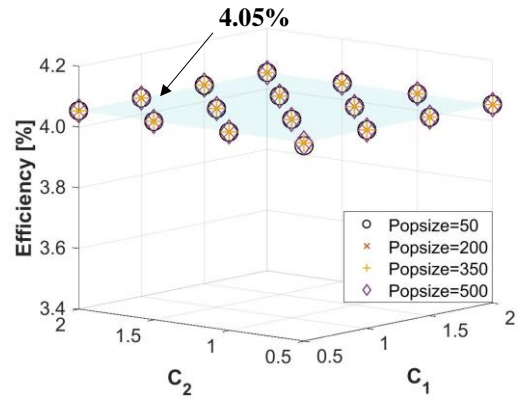
(a)



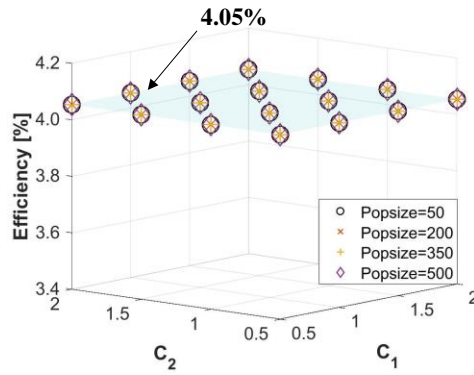
(b)



(c)



(d)



(e)

Figure 2.11. Optimal results for the efficiency of the TEG under different mutation factors: (a) $\mu = 0.01$, (b) $\mu = 0.02$, (c) $\mu = 0.03$, (d) $\mu = 0.04$, and (e) $\mu = 0.05$

2.4.4 The optimized results for the output power and efficiency of the TEG module

Through analysis of convergence rate and stability of the M-PSO method mentioned above, two different parameter combinations emerged to optimize the output power and efficiency (shown in Table 2.5), making it possible to converge. The iterative processes are displayed in Figure 2.12.

Table 2.5. Parameters selected for optimizations of the output power and efficiency

| Parameter | Output power | Efficiency |
|-------------------------------------|----------------------------------|----------------------------------|
| cognitive parameter (C_1) | 2.0 | 1.5 |
| social parameter (C_2) | 0.5 | 1.0 |
| Particle population ($Popsiz$) | 350 | 500 |
| Mutation factor (μ) | 0.01 | 0.01 |
| Inertia weight (w) | Random number in [0.4 to 0.9] | Random number in [0.4 to 0.9] |
| Dimensionality (D) | 5 | 5 |

It was found that the optimization of output power and efficiency converged separately after 242 and 184 steps, respectively, under the two parameter combinations in Table 2.4. After the optimization for the TEG module through the M-PSO method, the output power and efficiency were to 23.6 W and 4.05%, respectively. The related configurations of working conditions and geometric structures for these optimal TEGs are shown in Table 2.5.

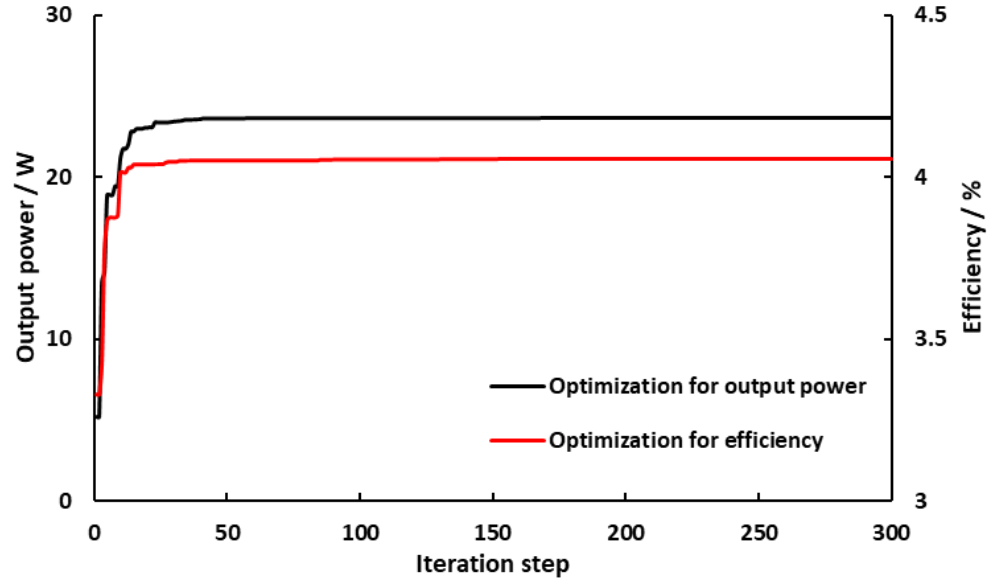


Figure 2.12. Convergence of the output power and efficiency optimizations

Table 2.5 Optimized working conditions and geometric structure configurations of the TEG module

| Objective function | T_h (K) | T_c (K) | R_L (Ω) | L (m) | F |
|--------------------|--------------|--------------|-----------------------|------------|--------|
| Output power | 335.9 | 295.9 | 0.1237 | 0.0005 | 0.9 |
| Efficiency | 315.5 | 275.5 | 0.5678 | 0.0009 | 0.1998 |

2.5 Multi-objective Optimization for the TEG Via M-PSO Method

Through the single-objective optimizations, it was found that there were totally different configurations for the working conditions and geometric structures of the TEG when optimizing maximum output power or efficiency in the search space. However, both the efficiency and output power are significant objects to be considered in the TEG design. Therefore, it is meaningful to take into account both the output power and efficiency for a TEG. In this paper, a multi-objective function relating to the output power and efficiency of the TEG module was built through a weighted approach. Then, the multi-objective optimization was conducted under the same search space by the M-PSO method. The multi-objective function is shown in Eq. (25).

$$f_3(T_h, T_c, R_L, L, F) = \begin{cases} (1 - \omega) \frac{f_1}{f_{1,opt}} + \omega \frac{f_2}{f_{2,opt}}, & T_h - T_c \leq 40 \text{ K} \\ 0, & T_h - T_c > 40 \text{ K} \end{cases} \quad (25)$$

where, ω is the weight factor for the second objective function (here, it is for the efficiency); $f_{1,opt}$ and $f_{2,opt}$ are the optimized results for the output power and efficiency, which were 23.6 W and 4.05% in this study.

Actually, the weight factor can be changed from 0 to 1 based on the design goals of the TEG [15]. The value of the weight factor represents the relative significance of the corresponding single-objective function [15]. The single-objective optimization indicated that the TEG module has a poor efficiency. In practice, power can be increased by using multiple cells, but efficiency cannot be increased in this way. Therefore, to emphasize an increase in efficiency, a higher weight factor (0.8) was allocated to the efficiency of the TEG. In addition, the related parameters in the M-PSO method were kept the same as those used to optimize efficiency. The iteration process is displayed in Figure 2.13, and the configuration for the working conditions and geometric structures of the TEG is shown in Table 2.6.

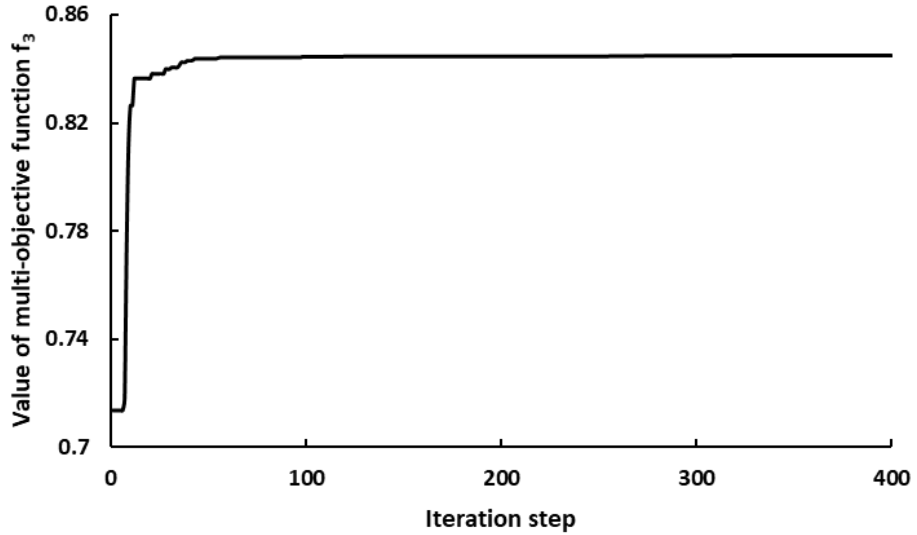


Figure 2.13. Convergence of the multi-objective optimization

Table 2.6. Optimized working conditions and geometric structure configurations of the TEG module

| f_3 | f_2 (%) | f_1 (W) | T_h (K) | T_c (K) | R_L (Ω) | L (m) | F |
|--------|--------------|--------------|--------------|--------------|-----------------------|------------|--------|
| 0.8448 | 3.99 | 6.69 | 316 | 276 | 0.3841 | 0.0009 | 0.3082 |

Based on the optimization results, after 334 iteration steps, the multi-objective function (f_3) converged at 0.8448. Under the multi-objective optimal configuration for the TEG, the output power and efficiency were about 6.69 W and 3.99%, respectively. A short sensitivity test of the results indicates that the efficiency can be increased from 3.46% to 3.99% by increasing the weight factor from 0.7 to 0.8. When increasing the weight factor further to 0.9, there was less increase in the efficiency, from 3.99% to 4.04%, an absolute gain of only 1.25%. However, the output power declined 24.3%, from 6.69 W to 5.07 W. Therefore, the weight factor choice of 0.8 was a good one.

2.6 Conclusions

In this paper, a steady-state thermodynamic model was used to analyze a TEG module with 199 pairs of couples. Two discrete functions, for the output power and the efficiency of the TEG module, were the optimization objectives. Then, it was demonstrated that the M-PSO algorithm is an effective method to acquire accurate optimized results for the output power and efficiency when the temperature difference was below 40 K. Meanwhile, a weighted approach was used to build a multi-objective function for the output power and efficiency. The multi-objective optimization was executed by the same algorithm, making it possible to acquire better output power and efficiency for the TEG simultaneously. The main conclusions are as follows:

- 1) Compared with the traditional PSO method, the M-PSO can improve the randomization for the algorithm, which makes the discrete optimization converge to a global best more easily. Through single-objective optimizations using the M-PSO method, the output power and efficiency of the TEG module can reach 23.6 W and 4.05%, respectively, for a maximum temperature difference of 40 K.
- 2) The effects of parameters in the M-PSO method mainly affected the rate of convergence and accuracy. The research indicated that a higher mutation factor can improve the accuracy of the optimized result, while having a negative effect on the convergence rate. Additionally, when the particle population is low, the optimizing process can be accelerated to converge at an optimized result by increasing the population. At a higher

population level, the acceleration constants play a significant role in the convergence speed.

- 3) The weighted optimization approach is a kind of trade-off analysis, which is an effective method to convert a multi-objective optimization into a single optimization. When the weight factor for the efficiency was 0.8, the output power and efficiency of the TEG module reached 6.69 W and 3.99%, respectively.

Acknowledgments

This work was made possible by funding from the Natural Sciences and Engineering Research Council of Canada.

References

- [1] S. A. Kalogirou, *Solar Energy Engineering: Processes and Systems*, 2nd Ed. Elsevier, UK: Oxford, 2014.
- [2] A. Vassel and D. S.-K. Ting, *Advances in Sustainable Energy*. Springer, Switzerland: Cham, 2019.
- [3] C. Zhang, G. Shu, H. Tian, H. Wei and X. Liang, "Comparative study of alternative ORC-based combined power systems to exploit high temperature waste heat," *Energy Conversion and Management*, vol. 89, pp. 541–554, January 2015.
- [4] T. Y. Kima, J. Kwak and B. Kim, "Energy harvesting performance of hexagonal shaped thermoelectric generator for passenger vehicle applications: An experimental approach," *Energy Conversion and Management*, vol. 160, pp. 14–21, March 2018.
- [5] M. Sajid, I. Hassan and A. Rahman, "An overview of cooling of thermoelectric devices," *Renewable and Sustainable Energy Reviews*, vol. 78, pp. 15–22, October 2017.
- [6] S. M. Pourkiaei, M. H. Ahmadi, M. Sadeghzadeh, S. Moosavi, F. Pourfayaz, L. Chen, M. A. P. Yazdi and R. Kumar, "Thermoelectric cooler and thermoelectric generator devices: A review of present and potential applications, modeling and materials," *Energy*, vol. 186, pp. 115849-1–115849-17, November 2019.
- [7] O. H. Ando Junior, A. L. O. Maran and N. C. Henao, "A Review of the development and applications of thermoelectric microgenerators for energy harvesting," *Renewable and Sustainable Energy Reviews*, vol. 91, pp. 376–393, August 2018.
- [8] B. Jang, S. Han and J. Y. Kim, "Optimal design for micro-thermoelectric generators using finite element analysis," *Microelectronic Engineering*, vol. 88 (5), pp. 775–778, May 2011.

- [9] S. Kim, "Analysis and modeling of effective temperature differences and electrical parameters of thermoelectric generators," *Applied Energy*, vol. 102, pp. 1458–1463, February 2013.
- [10] Y. Shia, D. Mei, Z. Yao, Y. Wang, H. Liu and Z. Chen, "Nominal power density analysis of thermoelectric pins with non-constant cross sections," *Energy Conversion and Management*, vol. 97, pp. 1–6, June 2015.
- [11] J. H. Meng, X. X. Zhang and X. D. Wang, "Characteristics analysis and parametric study of a thermoelectric generator by considering variable material properties and heat losses," *International Journal of Heat and Mass Transfer*, vol. 80, pp. 227–235, January 2015.
- [12] T. Ming, W. Yang, Y. Wu, X. Xiang and X. Huang, "Numerical analysis on the thermal behavior of a segmented thermoelectric generator," *International Journal of Hydrogen Energy*, vol. 42 (5), pp. 3521–3535, February 2017.
- [13] D. R. Karana and R. R. Sahoo, "Characteristics analysis and parametric study of a thermoelectric generator by considering variable material properties and heat losses," *Energy*, vol. 179 (15), pp. 90–99, July 2019.
- [14] Y. X. Huang, X. D. Wang, C. H. Cheng and D. T. W. Lin, "Geometry optimization of thermoelectric coolers using simplified conjugate-gradient method," *Energy*, vol. 59 (15), pp. 689–697, September 2013.
- [15] J. H. Meng, X. X. Zhang and X. D. Wang, "Multi-objective and multi-parameter optimization of a thermoelectric generator module," *Energy*, vol. 71 (15), pp. 367–376, July 2014.
- [16] A. Heghmanns, S. Wilbrecht, M. Beitel Schmidt and K. Geradts, "Parameter Optimization and Operating Strategy of a TEG System for Railway Vehicles," *Journal of Electronic Materials*, vol. 45 (3), pp. 1633–1643, November 2015.
- [17] W. H. Chen, P. H. Wu and Y. L. Lin, "Performance optimization of thermoelectric generators designed by multiobjective genetic algorithm," *Applied Energy*, vol. 209 (1), pp. 211–223, January 2018.
- [18] Y. Ge, Z. Liu, H. Sun and W. Liu, "Optimal design of a segmented thermoelectric generator based on three-dimensional numerical simulation and multi-objective genetic algorithm," *Energy*, vol. 147 (15), pp. 1060–1069, March 2018.
- [19] C. T. Hsu, G. Y. Huang, H. S. Chu, B. Yu and D. J. Yao, "Experiments and simulations on low-temperature waste heat harvesting system by thermoelectric power generators," *Applied Energy* 88 (4), pp. 1291–1297, April 2011.
- [20] Y. J. Gong, J. J. Li, Y. Zhou, Y. Li, H. S-H. Chung, Y. H. Shi and J. Zhang, "Genetic Learning Particle Swarm Optimization," *IEEE Transactions on Cybernetics*, vol. 46 (10), pp. 2277–2290, October 2016.

- [21] Y. D. Valle, G. K. Venayagamoorthy, S. Mohagheghi, J. C. Hernandez and R. G. Harley, "Particle Swarm Optimization: Basic Concepts, Variants and Applications in Power Systems," *IEEE Transactions on Evolutionary Computation*, vol. 12 (2), pp. 171–195, April 2008.
- [22] S. Valea, L. Heber, P. J. Coelho and C. M. Silva, "Parametric study of a thermoelectric generator system for exhaust gas energy recovery in diesel road freight transportation," *Energy Conversion and Management*, vol. 133, pp. 167–177, February 2017.
- [23] X. Lu, X. Yu, Z. Qu, Q. Wang and T. Ma, "Experimental investigation on thermoelectric generator with non-uniform hot-side heat exchanger for waste heat recovery," *Energy Conversion and Management*, vol. 150, pp. 403–414, October 2017.
- [24] S. Shittu, G. Lia, X. Zhao, X. Ma, Y. G. Akhlaghi and Y. Fan, "Comprehensive study and optimization of concentrated photovoltaic/thermoelectric considering all contact resistances," *Energy Conversion and Management*, vol. 205, pp. 112422-1–112422-17, February 2020.
- [25] E. Kanimba, M. Pearson, J. Sharp, D. Stokes, S. Priya and Z. Tian, "A comprehensive model of a lead telluride thermoelectric generator," *Energy*, vol. 142, pp. 813–821, October 2017.
- [26] X. Hu, H. Takazawa, K. Nagase, M. Ohta and A. Yamamoto, "Three-dimensional finite-element simulation for a thermoelectric generator module," *Journal of Electronic Materials*, vol. 44 (10), pp. 3637–3645, July 2015.
- [27] X. Jia and Y. Gao, "Optimal design of a novel thermoelectric generator with linear-shaped structure under different operating temperature conditions" *Applied Thermal Engineering* 78, pp. 533–542, December 2014.
- [28] S. Vostrikov, A. Somov and P. Gotovtsev, "Low temperature gradient thermoelectric generator: Modelling and experimental verification," *Applied Energy* 255, pp. 113786-1–113786-8, August 2019.
- [29] T. H. Kwan, X. Wu and Q. Yao, "Thermoelectric device multi-objective optimization using a simultaneous TEG and TEC characterization" *Energy Conversion and Management* 168, pp. 85–97, April 2018.
- [30] A. Rezanian, L. A. Rosendahl and H. Yin, "Parametric optimization of thermoelectric elements footprint for maximum power generation" *Journal of Power Sources* 255, pp. 151–156, April 2014.
- [31] R. Dwivedi and O. Dikshit, "A comparison of particle swarm optimization (PSO) and genetic algorithm (GA) in second order design (SOD) of GPS networks," *Journal of Applied Geodesy*, vol. 7 (2), pp. 135–145, May 2013.

- [32] G. Xu, Q. Cui, X. Shi, H. Ge, Z. H. Zhan, H. P. Lee, Y. Liang, R. Tai and C. Wu, “Particle swarm optimization based on dimensional learning strategy,” *Swarm and Evolutionary Computation*, vol. 45, pp. 33–51, March 2019.
- [33] F. Marini and B. Walczak, “Particle swarm optimization (PSO). A tutorial” *Chemometrics and Intelligent Laboratory Systems* 149, pp. 153–165, August 2015.
- [34] Q. Zhang, R. M. Ogren and S. C. Kong, “A comparative study of biodiesel engine performance optimization using enhanced hybrid PSO–GA and basic GA,” *Applied Energy*, vol. 165, pp. 676–684, March 2016.
- [35] F. Salajegheh and E. Salajegheh, “PSOG: Enhanced particle swarm optimization by a unit vector of first and second order gradient directions,” *Swarm and Evolutionary Computation*, vol. 46, pp. 28–51, May 2019.
- [36] X. Wang, D. S.-K. Ting, and P. Henshaw, “The Effects of Geometry and Substrate Material on Thermoelectric Generator Performance,” in *Complementary Resources for Tomorrow*, AG, Switzerland: Springer, 2020, pp. 93–110.
- [37] C. Moler, *Numerical Computing with MATLAB*, the Society for Industrial and Applied Mathematics, USA: Philadelphia, 2004.

CHAPTER 3

EXERGOECONOMIC ANALYSIS FOR A THERMOELECTRIC GENERATOR USING MUTATION PARTICLE SWARM OPTIMIZATION (M-PSO)

X. Wang, P. Henshaw, and D. S-K Ting, "Exergoeconomic analysis for a thermoelectric generator using mutation particle swarm optimization (M-PSO)," Applied Energy 294 (2021) 116952

3.1 Introduction

The development of modern civilization increasingly excessively relies on energy supply, especially electricity. The global population consumed about 20-terawatt hour (TWh) electricity in 2010 [1]. It is predicted that the electricity demand will experience nearly a two-fold increase to 34 TWh in 2035 [1]. Thereinto, the majority of electricity supply also was contributed by fossil fuel [1]. It is estimated that the daily oil consumption will increase sharply from 87.4 million barrels in 2011 to 123 million barrels in 2025 [2]. Despite the fact that fossil fuels are the industrial energy source for maintaining continuous social development, excessive reliance on fossil fuels is detrimental to the environment [3]. The relevant research has verified the carbon dioxide (CO₂), mainly released from fossil fuel consumption, leads to at least two-thirds of the greenhouse effect enhancement [2]. To prevent further deterioration of the environment, the energy sector must strive toward greater efficiency. To this end, thermoelectric generator (TEG) technology is positioned to play an important role, harnessing otherwise wasted, and/or readily-available heat into electricity. This potential has spurred TEG materials development and other aspects of TEG at an astounding pace in recent years, leading to progressively competitive TEG technology. In spite of this, there is still an obvious gap between the poor performance of TEG and the level of performance which would lead to its widespread utilization.

Therefore, the study of performance improvement for TEG devices is always an important topic in this field. Differing from the TE materials development is the improvement of TEG performance through internal structure optimization. Many researchers were attracted, initially, by the output power and efficiency optimization for a TEG device, for those indices are the most direct characteristics to evaluate the performance. Mu *et al.* [4] utilized a three-dimensional model to study the effects of geometric structure on a Mg₂Si-based TEG. They found that the TEG efficiency increases with couple length and the inverse of couple width. A comprehensive mathematical model developed by Fan *et al.* [5] confirmed that the maximum output power of a

TEG can be optimized at the appropriate couple length and cross-sectional area under a convective thermal boundary condition. Wang *et al.* [6] studied different shapes of TE couples. Their results indicated that the electrical properties of a TEG are not sensitive to the TE couple shape, but the cross-sectional area. The output power decreases, while the efficiency improves, with decreasing cross-sectional area [6]. Moreover, some research related to multi-stage TEGs has increasingly become a hot topic due to the huge influence of temperature on TE material performance. A modelling study for two-stage and three-stage TEGs was conducted by Kanimba *et al.* [7]. They found that the output power of the three-stage TEG is 21% more than that of the two-stage under a heat input of 505 W [7]. Wu *et al.* [8] also tried to analyze the performance of a multi-stage TEG module using a three-dimensional model. They selected three kinds of TE materials for each TE pin, which are $\text{Bi}_2(\text{TeSe})_3$, SnSe , and SiGe for N-type pin; $(\text{BiSb})_2\text{Se}_3$, PbTe , and FeNbSB for P-type pin. through changing the cross-sectional area for each local thermoelectric segment, the efficiency of the N-type pin can be improved from 12.2% to 21.7%, and that of the P-type pin can be increased from 22.9% to 25.7%, with a working temperature range of 300 -1100 K [8].

However, the commercialization of an energy system is not only decided by measures of physical performance, such as output power and efficiency, but also its energy quality and cost-effectiveness play a significant role. Meanwhile, thermodynamic irreversibility is always significant and difficult to eliminate for an energy conversion system [9]. In this way, studies about optimization based on exergoeconomic analysis have been the focus of researchers' concern. Using a one-dimensional model, Xiao *et al.* [10] made an analysis of the irreversible transfer process of a TEG. The results indicated that the irreversible convective heat process can lead to a large exergy loss. Thus, decreasing the irreversible heat loss is one of the research directions for the optimization of TEG performance [10]. In addition, Xiao *et al.* [10] found that the internal and load resistances should be matched during the process of TEG optimization, as the internal exergy loss is derived from the irreversible consumption of the TEG resistance. Through establishing an irreversible thermodynamic model for a two-stage TEG (TTEG), Manikandan and Kaushik [11] confirmed that the exergy efficiency of a TEG can be improved through optimizing the number of TE couples. After the optimization of a TEG, they determined the optimal number of TE couples as 30 when the hot side temperature was 450 K and that of the cold was 300 K, which can increase the TEG exergy efficiency to 13.1% [11]. Feng *et al.* [12] utilized an irreversible thermodynamic model to optimize a combined TE device which is a thermoelectric generator-driven thermoelectric heat pump (TEG-TEH). The results indicated that

the exergy efficiency of the system can be improved through increasing the TEG hot junction temperature appropriately [12]. Besides, when allocated more TE elements on the TEG, the device can achieve a higher exergy efficiency [12]. Asaadi *et al.* [13] analyzed the effects of geometric structure, involving height ratio and angle ratio, on the exergoeconomic performance of a two-stage TEG module through a three-dimensional model. The exergoeconomic performance of the two-stage TEG module was better than that of the single-stage except for its cost-effectiveness under the same conditions [13]. As for the two-stage TEG module, its exergoeconomic performance reached the maximum when the angle ratio was 1; however, the optimal height ratio was decided by the working temperature conditions [13].

From the literature [3-13], the researchers analyzed some design factors which may affect a TEG's performance, such as cross-sectional area, working temperature, *etc.* The results indicate that the geometric structures and working conditions of a TEG module have considerable influence on its performance, in either power, energy or exergoeconomic aspects. Meanwhile, through optimizing a TEG's performance based on single-objective function (output power or efficiency), they found that those influences on the performance of a TEG module are normally coupled, which makes it difficult to reach an optimal state for different performance indices simultaneously, especially for the exergoeconomic aspect. For example, a higher temperature difference can increase exergy output (higher output power), which has a positive effect on the cost-effectiveness of a TEG. However, with the temperature increasing further, the irreversible loss is more severe for a TEG system, making it possible to decrease the exergy efficiency while still increasing the power output and cost-effectiveness. Therefore, in order to break through the limitation for a TEG optimization, it is necessary to consider multiple objectives simultaneously, such as exergy efficiency and cost effectiveness, making it possible to achieve a balanced design.

With regard to multi-objective optimization for a TEG, it is a type of combinatorial problem, which can be addressed by an algorithm, normally. Meng *et al.* [14] utilized a conjugate-gradient with a weighted approach to conduct a multi-objective optimization for a TEG to balance its performances in output power and efficiency. A few recent studies were focused on applying a genetic algorithm (GA) to solve a multi-objective optimization for TEGs. Chen *et al.* [15] applied a multi-objective genetic algorithm to optimize the output power and efficiency of a TEG. The results indicated that the power and efficiency can be increased by 51.9% and 5.4% under a temperature difference of 40°C. In addition, a GA method was applied by Ge *et al.* [16] to optimize power and efficiency for a segment of a TEG module. Through the multi-objective optimization, they acquired an assembly of acceptable results named Pareto solutions [16]. After

analyzing the Pareto solutions through the TOPSIS method, an ideal optimized power and efficiency was acquired. However, the recent research about multi-objective optimization of exergoeconomic performance of a TEG is rarely reported. Based on the previous studies [10-13], it can be found that energy quality and cost-effectiveness are significant for the application of TEG technology. Meanwhile, there are important effects of geometric structures and working conditions of a TEG on its exergoeconomic performance. Thus, one of the main purposes of this study is to conduct a multi-objective optimization for a TEG based on exergoeconomic analysis. Noticeably, the heat loss between the gaps of the TE couples can be considered as an important source of the internal irreversibility for a TEG. Hence, unlike the recent research related to multi-objective optimization, the heat loss was considered in this exergoeconomic model of a TEG, making the study more accurate.

Additionally, in the existing literature related to multi-objective optimization for TEGs, most reported research ignored the influence of parameters in the algorithms on the optimized results. Inaccurate and premature convergence are the main challenges for algorithms, especially in complicated optimization problems [14, 17-18]. For example, due to excessive reliance on the initial conditions, the conjugate-gradient method will be more complicated and time-consuming when used to solve an optimization problem with more than three variables involved [14]. Also, the main challenge of GA is the poor convergence and some trial-and-error calculations [14, 19]. In order to solve this problem, it is normally necessary to spend lots of time on parameter tuning for algorithms, such as initial guesses and crossover probability. In this way, one of the main aims of this study is to provide a more effective method to optimize TEG performance. Meanwhile, this method can make the optimal results independent with the parameters of the algorithm. Firstly, compared with other algorithms, such as genetic algorithms, the particle swarm optimization (PSO) method has excellent convergency and concise programming [18]. The increasing number of researchers paid more attention to applying the PSO algorithm to engineering systems. Zhang *et al.* [20] utilized a hybrid PSO algorithm to optimize performance and emissions for a biodiesel engine. The result indicated that compared with GA, the hybrid PSO method can accelerate the converging process and acquire a superior optimum. The PSO algorithm can also be used to manage energy systems. Through a PSO method, Yang *et al.* [21] optimized the proportion of solar power generation in a hybrid electric system, making it possible to balance the hybrid system's economy and efficiency under different electrical loads. In addition, the algorithm engineers confirmed that combined with a subprogram, such as mutation, can increase randomization for the algorithm, which is an effective method to alleviate the

premature convergence problem of traditional PSO algorithm [18, 22]. It is also verified in the study from Zhang *et al.* [20]. Therefore, the mutation particle swarm (M-PSO) algorithm was used to optimize a TEG module. Meanwhile, in order to test the independence of the optimal results, the influences of the main parameters in the M-PSO (involving social and cognitive constant, population size, and mutation factor) on the optimizing results were analyzed through testing a large number of parameter combinations. This work also can provide a reference for parameter selection of the M-PSO method, making it possible to simplify the parameter tuning process when solving a similar optimization problem for a TEG. Hence, the combination of these performance and algorithm parameters and the M-PSO algorithm applied to optimize a TEG is the unique feature of this work.

In this study, under a steady-state condition, exergy analysis was conducted for a TEG with 199 cascaded TE couples using a one-dimensional thermodynamic model. Based on the results, two objective functions related to the exergy efficiency and levelized cost of energy (LCOE) were established. Firstly, the exergy efficiency and LCOE were optimized separately through the M-PSO method. In the process, 320 parameter combinations were tested in order to analyze the effects of these values on the convergence rate and optimized result. Then, a ξ -constraint with the M-PSO algorithm was used to conduct the multi-objective optimization for the TEG exergoeconomic performance, making it possible to acquire a series of alternatives, named Pareto solutions. Finally, these alternatives were evaluated by the TOPSIS method to obtain an ideal solution.

3.2 Thermodynamic Analysis for a TEG

In this paper, a one-dimensional steady-state thermodynamic model was used to analyze a TEG module. Through the energy and exergoeconomic analysis, there were two equations related to exergy efficiency and cost-effectiveness derived to be the objective functions, which is an important basis of optimization.

3.2.1 Analysis based on the 1st law of thermodynamics for a TEG module

Commonly, a TEG module consists of three different parts, which are cascading semiconductors, conductors, and ceramics (Figure 3.1). Based on the Seebeck effect, a voltage can be produced by a TEG module under a temperature difference, and the value of the voltage is proportional to the temperature gradient. The open circuit voltage of a TEG module can be calculated by Eqs. (1) and (2) [23]:

$$V = S(T_h - T_c)N_{pair} \quad (1)$$

$$S = S_p + |S_n| \quad (2)$$

where, S_p and S_n are the Seebeck coefficients of P and N semiconductors. The overall Seebeck coefficient is represented as S . T_h and T_c are the hot and cold temperatures. N_{pair} is the number of TE couples.

If a load is connected at its positive and negative, the TEG module will produce electrical power from this system. According to Ohm's law, Eq. (3) can be used to calculate the output power [24]:

$$P = \frac{S^2(T_h - T_c)^2 N_{pair}^2}{(R_i + R_L)^2} R_L \quad (3)$$

where, P is the output power; the internal and load resistance are represented as R_i and R_L . The internal resistance can be calculated by Eqs. (4-7), as it can be considered as the sum of the resistance of TE couples and conductors [25]:

$$r_{teg} = \left(\frac{\rho_P L_P}{A_P} + \frac{\rho_N L_N}{A_N} \right) N_{pair} \quad (4)$$

in which, ρ_P and ρ_N are the electrical resistivities of the P and N semiconductors. A_P , A_N , L_P and L_N represent the cross-sectional areas and couple lengths of the P and N semiconductors, respectively. In this paper, the cross-sectional area (A) and couple length (L) of the P and N semiconductor are kept the same; thereby, Eq. (4) can be written as Eq. (5) [25-26]:

$$r_{teg} = \frac{L}{A} (\rho_P + \rho_N) N_{pair} = \frac{2N_{pair}L}{FA_{sub}} (\rho_P + \rho_N) N_{pair} \quad (5)$$

$$r_c = \frac{\rho_c \left(1 + \frac{1}{\sqrt{F}}\right)}{d_c} (2N_{pair} + 1) \quad (6)$$

$$R_i = r_{teg} + r_c \quad (7)$$

in which F is the base area ratio which describes a proportion of TE couples' area in the substrate area (as shown in Figure 3.1); A_{sub} is the ceramic substrate area; ρ_c and d_c are the electrical resistivity and thickness of the conductor.

Figure 3.1 shows the thermal transfer process of a TEG module. According to the first law of thermodynamics, there are two kinds of energy coming into the hot temperature side of a TEG module: the input heat and Joule heat. The rates of these energy transfers are expressed as \dot{Q}_{input} and \dot{Q}_J , respectively.

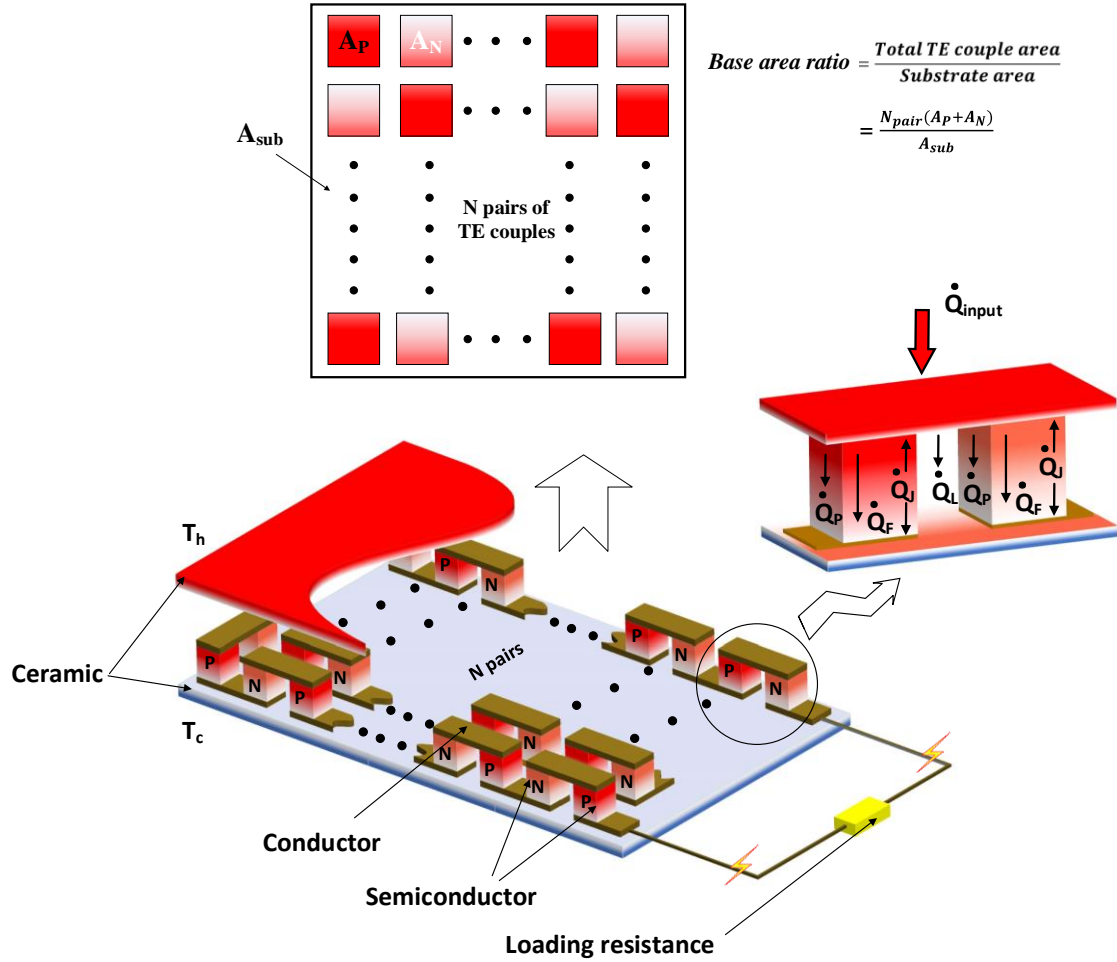


Figure 3.1. Cutaway view of a TEG module arrangement and its thermal transfer processes

Commonly, the Joule heat can be transferred to both sides of a TEG when the current passes it. In this way, an assumption that only half of Joule heat is absorbed by the hot temperature side of a TEG module was made [26-27]. Meanwhile, there are three kinds of energy leaving the hot temperature side: Fourier heat (\dot{Q}_F), Peltier heat (\dot{Q}_P), and heat loss from the gap between the semiconductors (\dot{Q}_L). Therefore, Eq. (8) can be used to calculate the input heat [26-28]:

$$\dot{Q}_{input} = \dot{Q}_F + \dot{Q}_P + \dot{Q}_L - \frac{1}{2}\dot{Q}_J \quad (8)$$

where, the relative thermal transfer rate can be calculated by Eqs. (9-12):

$$\dot{Q}_F = K(T_h - T_c)N_{pair} \quad (9)$$

$$\dot{Q}_P = S^2 T_h \frac{(T_h - T_c)N_{pair}^2}{R_i + R_L} \quad (10)$$

$$\dot{Q}_L = \frac{(T_h - T_c)A_{sub}k_{air}(1 - F)}{L} \quad (11)$$

$$\dot{Q}_J = \frac{S^2(T_h - T_c)^2 N_{pair}^2}{(R_i + R_L)^2} R_i \quad (12)$$

in which K is the net thermal conductance of a TE couple ($K = \frac{A}{L}(k_P + k_N)$), and k_{air} is the thermal conductivity of air.

3.2.2 Analysis based on the 2nd law of thermodynamics for a TEG module

Sometimes, irreversibility is important for improving the operation of an energy system [9]. In this way, the second thermodynamic law can provide a better understanding for an energy system than the first law. Based on the second thermodynamic law, exergy analysis is an effective method to identify the location and source of irreversible losses for an energy system [9]. Hence, the optimization of exergy efficiency can provide an energy system with an excellent direction to decrease its irreversibility. In this paper, the exergy efficiency was used as an index to evaluate the performance of a TEG module.

According to the exergy analysis for an energy system under a steady state, its balanced equation can be written as Eq. (13).

$$\sum Ex_{in} = \sum Ex_{out} + Irreversibility \quad (13)$$

For a TEG system, the irreversibility can be divided into two different parts: internal and external [13]. The internal irreversibility is induced by the welding resistance and material properties. According to the basic assumptions in this paper, the irreversibility caused by the welding resistance and contact thermal resistance can be ignored. Although the assumptions lead to some errors, some references indicate that within a limited temperature difference (the limitation of temperature difference is 40 K in this paper), the errors for an analytical model are acceptable [13, 29]. Besides, the effects of the errors on the effectiveness of algorithms can be neglected. Normally, ignoring welding resistance and contact thermal resistance can be found in

the research related optimization [29-30]. In this way, the internal irreversibility is mainly produced by the material properties. Moreover, the irreversible thermal transfer can be considered as the main factor causing external irreversibility. The exergy input rate of a TEG module can be defined by Eq. (14) [13]:

$$\dot{Ex}_{input} = \dot{Q}_{input} \left(1 - \frac{T_0}{T_h}\right) \quad (14)$$

in which T_0 is ambient temperature, assumed as 293 K in this paper.

Meanwhile, the exergy output rate of the system is actually the output power [9]. Therefore, the exergy efficiency (ψ) of a TEG module can be defined as in Eqs. (15-16), which is one of the objective functions in this study.

$$\dot{Ex}_{output} = P = \frac{S^2(T_h - T_c)^2 N_{pair}^2}{(R_i + R_L)^2} R_L \quad (15)$$

$$\psi = \frac{\dot{Ex}_{output}}{\dot{Ex}_{input}} = \frac{\frac{S^2(T_h - T_c)^2 N_{pair}^2}{(R_i + R_L)^2} R_L}{\dot{Q}_{input} \left(1 - \frac{T_0}{T_h}\right)} \quad (16)$$

3.2.3 Cost-effectiveness analysis for a TEG module

The commercialization of an energy system is decided by its cost-effectiveness. The exergoeconomic analysis was defined by Tsatsaronis *et al.* [9, 31]. This method makes it possible to analyze exergy and cost-effectiveness simultaneously, which can provide an important index for optimizing design and economic feasibility and profitability of an energy system. According to the economic balance, the cost calculation for a TEG module involves two different parts, which are device investment (Z_{inv}) and other cost-related maintenance (Z_{om}) as shown in Eq. (17) [9].

$$cost\ generation = Z_{inv} + Z_{om} \quad (17)$$

As for a solid energy convertor, it is equipped with high reliability and long lifetime [32]. A manufacture claims that their TEG modules can be continuously operated for more than 100000 hours [33]. In this analysis, the cost-related maintenance was ignored. Meanwhile, the costs of ceramics and semiconductors were considered in the device investment. Based on the market for materials, the cost of ceramics ($Z_{ceramic}$) is mainly a function of the machined surface area. Also,

the cost of semiconductor material ($Z_{semiconductor}$) is related to both the machined surface and volume. The relative calculations are shown in Eqs. (18-20) [13].

$$Z_{ceramic} = Z'' A_{cr} \quad (18)$$

$$Z_{semiconductor} = Z''' V_s + Z'' A_s \quad (19)$$

$$Z_{inv} = Z_{ceramic} + Z_{semiconductor} \quad (20)$$

in which, Z'' and Z''' are surface cost (\$US/mm²) and volumetric cost (\$US/mm³).

In this paper, a Bi₂Te₃ based TEG with 199 cascade couples was simulated. The information about cost is shown in Table 3.1.

Table 3.1. Cost of semiconductor and ceramic materials [13, 34]

| Material | Z'' (\$/mm ²) | Z''' (\$/mm ³) |
|---------------|-----------------------------|------------------------------|
| Semiconductor | 0.0008896 | 0.0001682 |
| Ceramic | 0.001 | — |

As for an index of exergoeconomic analysis, the levelized cost of energy (LCOE, \$US/kWh·m²) was considered as an objective function (as defined in Eqs. (21-22)):

$$CRF = \frac{i(1+i)^n}{(1+i)^n - 1} \quad (21)$$

$$LCOE = \frac{Z_{inv} \times CRF \times \phi}{N \times \dot{E}x_{output} \times A_{cr}} \quad (22)$$

where, CRF is capital recovery factor. i is interest rate, and n is system life, which is normally 20 years [13]. ϕ is the maintenance factor, which is assumed equal to 1 because of free-maintenance [13]. N is the total operating hours in a whole year.

According to the information from American Express, the average interest rate for a business loan in 2021 is 6.98% - 19.97% [35]. Meanwhile, referring to the study from Asaadi *et al.* [13], the interest rate is assumed 10%. Besides, the study considered the TEG application scenario as vehicle engine exhaust recovery. In this way, it is impossible for the energy recovery system to be operated in a whole year as it is necessary to spend time on engine maintenance. Based on an

engine test made by Mohammadkhani *et al.* [36], the total operating hours in a whole year can be assumed to be 7500 h [13, 36].

3.2.4 Model establishment for a TEG module

In this paper, a 10 cm by 10 cm Bi₂Te₃ based TEG module was considered, which is manufactured by Wise Life Technology, Taiwan. This TEG module is widely applied in waste heat recovery technology [37-38]. The TEG consists of 199 pairs of cube-shaped couples of which dimensions are 2 mm × 2 mm × 0.64 mm. Besides, the study considered the TEG application scenario as vehicle engine exhaust recovery. The relative research indicates that the end gas from an engine has a wide temperature distribution in the exhaust system, normally ranging from 300 K to 900 K [39-40]. In this way, when building a thermodynamic model for the TEG, it is necessary to the effect of temperature on the properties of TE materials rather than using constant parameters. The properties of TE materials can be shown in Table 3.2.

Table 3.2. Material properties of P-Bi₂Te₃ and N-Bi₂Te₃ [41]

| Material properties | P-Bi ₂ Te ₃ | N-Bi ₂ Te ₃ |
|---|---|---|
| Seebeck coefficient (VK ⁻¹) | $-1.3 \times 10^{-10}T^2 + 1.17 \times 10^{-6}T - 8.8 \times 10^{-5}$ | $2.31 \times 10^{-9}T^2 - 1.65 \times 10^{-6}T + 6.89 \times 10^{-5}$ |
| Thermal conductivity (Wm ⁻¹ K ⁻¹) | $3.11 \times 10^{-5}T^2 - 0.02413T + 5.902$ | $1.19 \times 10^{-5}T^2 - 0.00577T + 2.004$ |
| Electrical conductivity (S/m) | $1.802T^2 - 2102T - 686700$ | $0.8963T^2 - 860.8T - 262900$ |

Additionally, many references indicated that the one-dimensional TEG model is effective under a limited temperature gradient [42-43]. In this way, the optimizations for the TEG exergoeconomic performance were conducted when the temperature gradient was below 40 K. Meanwhile, the average values of the TE material properties were taken into the model to reflect the effects of the internal temperature field on the TEG performances. Equation (23) represents a general formula for the average values of TE material properties:

$$\bar{\Delta} = \frac{\int_{T_c}^{T_h} \delta(T) \cdot dT}{(T_h - T_c)} \quad (23)$$

where $\bar{\Delta}$ means the average value of the Seebeck coefficient, thermal conductivity, or electrical conductivity. $\delta(T)$ is the formula related temperature of these properties. T_h and T_c are the hot and cold temperatures.

3.3 Single-objective Optimization for a TEG Using M-PSO Algorithm

In this paper, a M-PSO method developed from the PSO algorithm was used to conduct the optimizations. The PSO algorithm is a kind of bionic algorithm, imitating how a bird flock locates food. The birds' velocities can be updated continuously through interacting with their surroundings locally to find the best position [34]. The updating equations for the velocity (V_i) and position (X_i) of i^{th} generation particle are displayed in Eqs. (24) and (25) [44-46]:

$$V_{i+1} = wV_i + C_1R_1(P_{best} - X_i) + C_2R_2(G_{best} - X_i) \quad (24)$$

$$X_{i+1} = X_i + V_{i+1} \quad (25)$$

where, w is the inertia weight, utilized to adjust the influence of the velocity of the previous generation particle. C_1 and C_2 are the cognitive and social parameters which are positive acceleration constants. R_1 and R_2 are random numbers ranging from 0 to 1. The local and global best positions are marked with P_{best} and G_{best} , respectively.

The updated equation of the velocity (as shown in Eq. (24)) can be divided into three different parts. The first part, wV_i , is called a momentum item, which represents the movement habit of the previous generation particles. Analogy to a bird swarm, the momentum item describes the birds' inertia. The second part is $C_1R_1(P_{best} - X_i)$, also named as a cognitive item, which is actually a gap between the current position and its individual best position. Likewise, analogy to a bird, this item quantifies the tendency that a bird identifies the food location based on its own previous experience. $C_2R_2(G_{best} - X_i)$ is the third part, describing a gap between the i^{th} particle's position and the global best position in whole parties. It represents a level of food location information interaction in a bird's swarm, thereby, named as a social information sharing item. Therefore, the parameters C_1 and C_2 represent the level of individual cognition and social information sharing in the bird's swarm. Through changing the value of C_1 and C_2 , the relative contribution of the cognitive and information sharing item can be adjusted, making it possible to govern the extent to which the particles look for the individual and global best position. Besides, during the searching process, the number of participants is defined by the particle population (*Popsi*ze). Finally, within unit time, the birds can update the position based on their velocity and original location (as shown in Eq. (25)).

The flow diagram of the M-PSO calculation method is displayed in Figure 3.2. The main sequence is similar to the traditional PSO algorithm. As shown in the flow chart, it is necessary to create an objective function firstly and make sure the direction for the optimization (looking for maximum value or minimum value?). The PSO theory indicates that in order to search for optimal position, the particles adjust their velocity based on the individual cognitive and social sharing. In this way, before conducting the iterations, the relevant parameters of the algorithm should be defined appropriately, such as C_1 and C_2 , *etc.* For the next step, the initial particle swarm will be created involving their position and velocity vectors. After that, the fitness for each particle can be evaluated by the objective function, making it possible to acquire the local best and global best position in later generations. Besides, a mutation position will generate when the mutation condition ($Rand. < threshold\ value$) is triggered. Finally, if the maximum generation number criterion is not satisfied (namely, the iteration step is bigger than the maximum step), each new generation particles' position and velocity will be created by the updating equations.

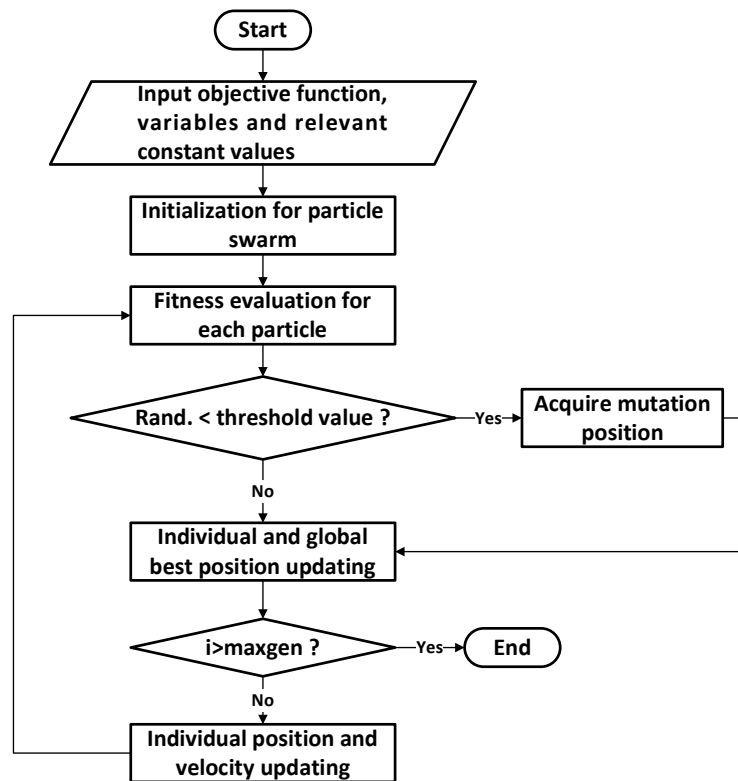


Figure 3.2. Flow chart of the M-PSO method

The difference between the MPSO and PSO method is the subprogram named mutation. Although the traditional PSO method has an excellent performance in terms of convergence, the shortage of enough diversity can allow the PSO method to converge to a local optimum, and not

the global optimum [47]. The subprogram, mutation, can be considered as an effective method to tackle this problem, for it can increase the randomization of the algorithm. In the mutation program, a threshold condition was set up as shown in Eq. (26):

$$threshold\ value = (1 - (i - 1)/(maxgen - 1))^{\frac{1}{mu}} \quad (26)$$

where, $maxgen$ is the maximum generations of particles and the mutation factor is marked as mu .

The mutation program will be triggered when a random number is lower than the threshold value. Therefore, a new position will be generated from a lower boundary (lb) and an upper boundary (ub) randomly. Equations (27)-(30) display how to acquire the upper and lower boundary. Meanwhile, the new position will remain if its fitness is better than that of the old position.

$$\delta x = threshold\ value \times (X_{max} - X_{min}) \quad (27)$$

$$lb = X_i - \delta x \quad (28)$$

$$ub = X_i + \delta x \quad (29)$$

$$[lb\ ub] \in [X_{min}\ X_{max}] \quad (30)$$

3.3.1 The influence of related parameters in the M-PSO method on the optimized results

The top priority for an optimizing problem is to establish an objective function. In this paper, through exergoeconomic analysis, two functions were chosen to be optimization objects: exergy efficiency and LCOE. Meanwhile, these functions involve five variables ranging from working conditions to geometric structures. The objective functions and searching space are displayed in Eqs. (31) and (32) and Table 3.3.

The objective function (1) for the exergy efficiency:

$$f_1(T_h, T_c, R_L, L, F) = \begin{cases} \frac{S^2(T_h - T_c)^2 N_{pair}^2 R_L}{(R_i + R_L)^2}, & T_h - T_c \leq 40\ K \\ \dot{Q}_{input}(1 - \frac{T_0}{T_h}), & \\ 0, & T_h - T_c > 40\ K \end{cases} \quad (31)$$

The objective function (2) for the LCOE:

$$f_2(T_h, T_c, R_L, L, F) = \begin{cases} \frac{Z_{inv} \times CRF \times \emptyset}{N \times \dot{E}x_{output} \times A_{cr}}, & T_h - T_c \leq 40 \text{ K} \\ 0, & T_h - T_c > 40 \text{ K} \end{cases} \quad (32)$$

Table 3.3. Relevant variables and their value ranges

| Variable | Value range |
|-----------------------------|---|
| Hot temperature (T_h): | $300 \text{ K} \leq T_h \leq 900 \text{ K}$ |
| Cold temperature (T_c): | $300 \text{ K} \leq T_c \leq 900 \text{ K}$ |
| Load resistance (R_L): | $0.01 \Omega \leq R_L \leq 10 \Omega$ |
| Couple length (L): | $0.0005 \text{ m} \leq L \leq 0.0009 \text{ m}$ |
| Based area ratio (F): | $0.1 \leq F \leq 0.9$ |

The objective functions mainly involve five kinds of variables. In this way, the dimensionality of the searching space is five. Some research from algorithm engineers indicated that the recommendation for the inertia weight (w) ranges from 0.4 to 0.9, which can allow the particle to move enough freely [18, 22]. Additionally, according to the theory of the M-PSO algorithm, the influences of algorithm parameters in Eq. (24) on convergence speed and accuracy cannot be ignored. In order to illustrate the effectiveness of the M-PSO method in this study, 320 parameter combinations were considered for each optimization: exergy efficiency and LCOE. Accordingly, the mutation factor was [0.01, 0.02, 0.03, 0.04, 0.05], the particle population ($Popsiz$) was [50, 200, 350, 500], and there are four values for the cognitive and social parameters: [0.5, 1.0, 1.5, 2.0].

The number of iterations to convergence for optimized exergy efficiency under different parameters is displayed in Figure 3.3. The rate convergence is the inverse of the number of iterations, and can be improved by increasing the particle population appropriately under a specific mutation factor. However, when the $Popsiz$ was more than 200, the convergence speed was associated with both the particle population and the acceleration constants (C_1 and C_2). The phenomenon can be illustrated through the analogy of a biological system. The bird flock equipped more individuals can find the location of food more quickly. However, with an excessive population of the bird flock, the effects of information communication within the group cannot be ignored. Additionally, at a specific particle population, there was a moderate decline in

the rate of convergence with the mutation factor growth. The main reason is that the diversity of the values increased under a higher mutation factor, requiring more iterative steps to acquire convergence.

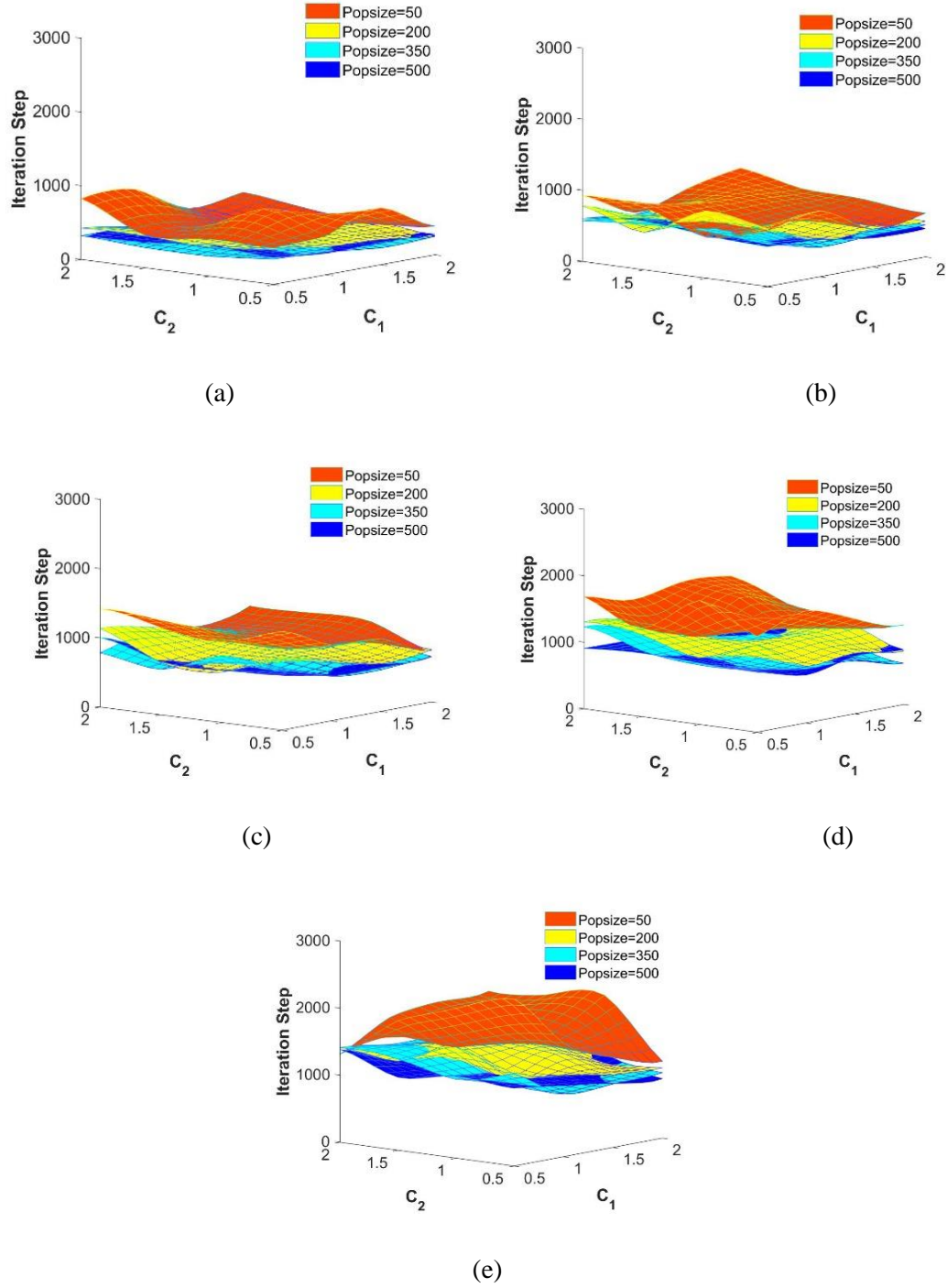
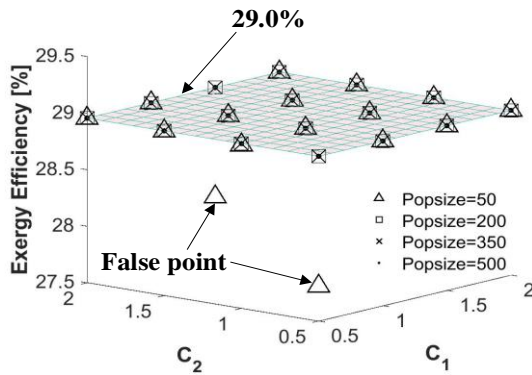


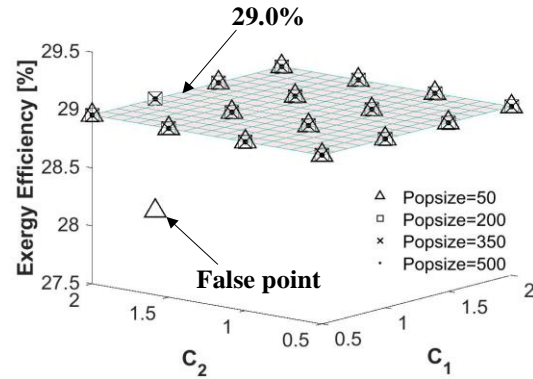
Figure 3.3. Rate of convergence for the optimized exergy efficiency of the TEG, (a) $\mu = 0.01$, (b) $\mu = 0.02$, $\mu = 0.03$, $\mu = 0.04$, and $\mu = 0.05$

The optimized results for the exergy efficiency can be found in Figure 3.4. As a whole, a reliable optimized result for the exergy efficiency can be acquired through the M-PSO algorithm under most situations. Those points lower than the optimal value, were defined as false points. In this paper, 64 combinations were tested for each specific mutation factor. The results indicated that the false point rate for mutation factors of 0.01 and 0.02 were about 3.1% and 1.6%, respectively. The figure was 0% when the mutation factor was more than 0.02. Therefore, increasing the mutation factor can be considered as an effective method to improve the accuracy of the optimized result for the exergy efficiency.

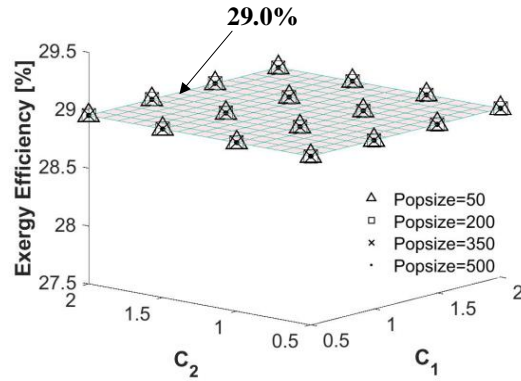
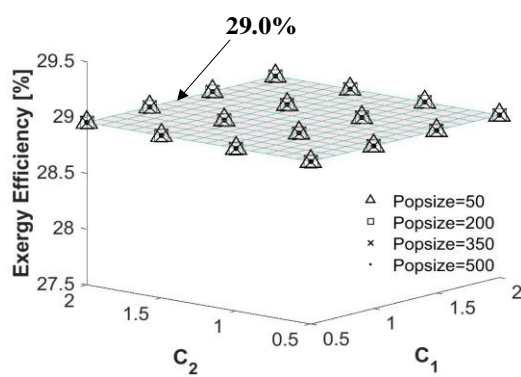
Likewise, 80 combinations were tested for each *Popsiz*e. The false point rate for the *Popsiz*e with 50 topped the group, with about 3.8%. When the *Popsiz*e was more than 50, the false point rate was 0%. In this way, the accuracy of the optimized result can also be improved through increasing the particle population. By analogy, it is easy to understand that a bird flock with more population can locate the position of food more accurately.



(a)

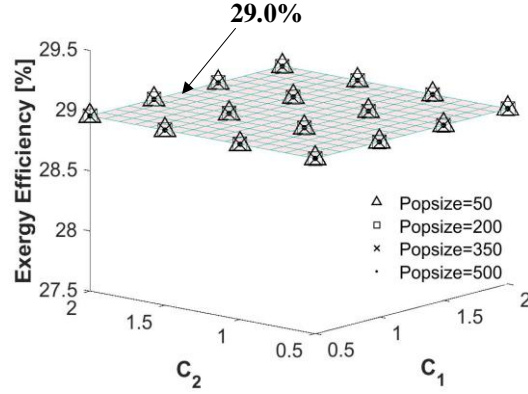


(b)



(c)

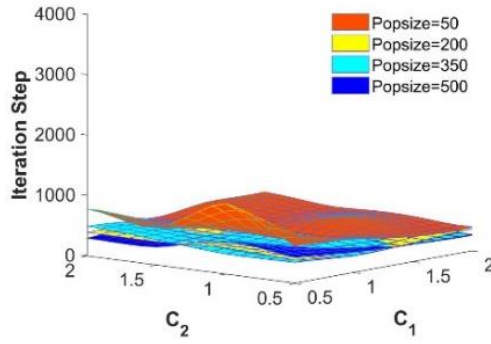
(d)



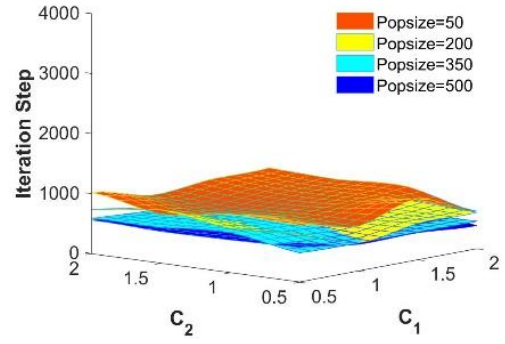
(e)

Figure 3.4. Optimized results for exergy efficiency of the TEG, (a) $\mu = 0.01$, (b) $\mu = 0.02$, $\mu = 0.03$, $\mu = 0.04$, and $\mu = 0.05$

In addition, similar tendencies can be found in the optimized results for the LCOE. Figure 3.5 indicates that more iteration steps were needed to converge to a result under a higher mutation factor. Meanwhile, increasing *Popsiz* can accelerate the convergence speed for the LCOE optimization. Nevertheless, it is necessary to consider the effect of the acceleration constants on the convergence speed when the particle population is more than 200.



(a)



(b)

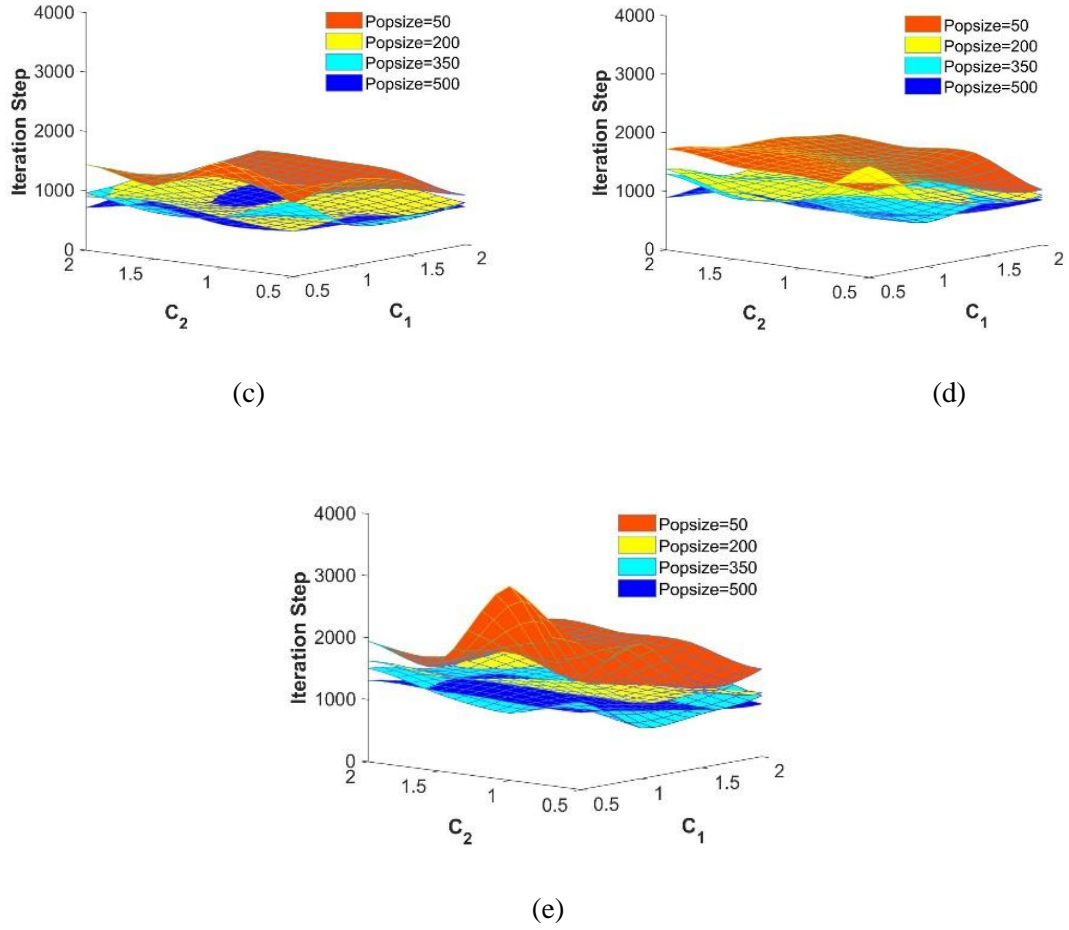
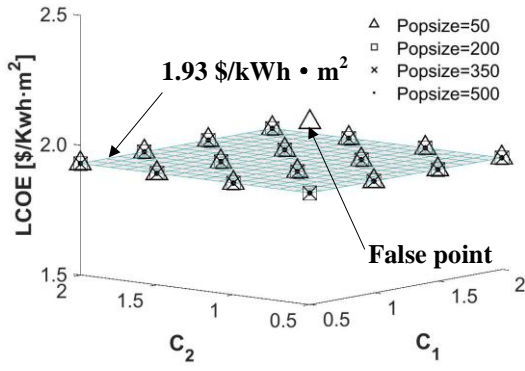
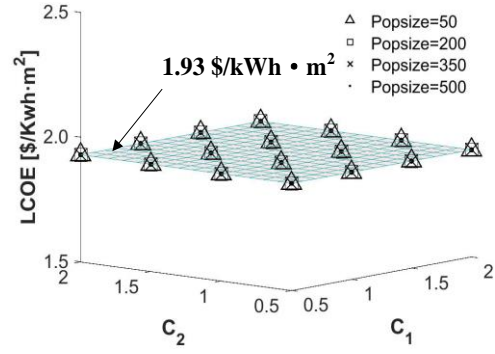


Figure 3.5. Rate of convergence for the optimized LCOE of the TEG, (a) $\mu = 0.01$, (b) $\mu = 0.02$, $\mu = 0.03$, $\mu = 0.04$, and $\mu = 0.05$

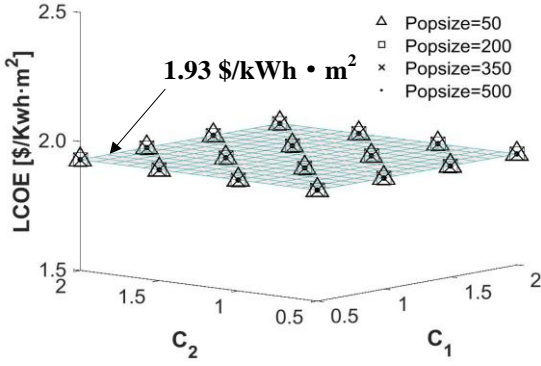
The optimized results for the LCOE are displayed in Figure 3.6. Differing from the exergy efficiency optimization, the false point was defined as those which are higher than the optimal value. Accordingly, the false point rate for the case of a mutation factor of 0.01 was around 1.6%. When the mutation factor was more than 0.01, the false point rate was 0%. Moreover, the false point rate for the case of the *Popsiz* with 50 was about 1.3%. When the *Popsiz* was more than 50, the false point rate was 0%. Therefore, the mutation factor and particle population had a positive correlation with the accuracy of optimized results for the LCOE using the M-PSO method.



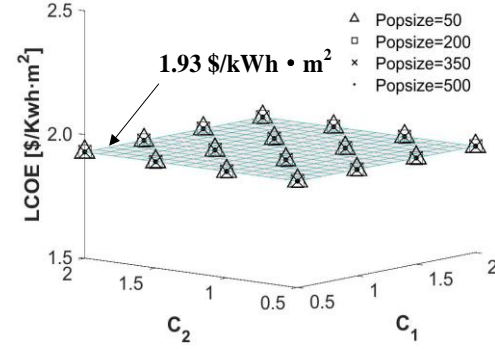
(a)



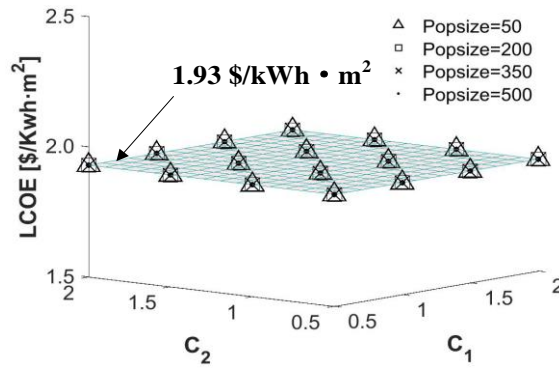
(b)



(c)



(d)



(e)

Figure 3.6. Optimized results for the LCOE of the TEG, (a) $\mu = 0.01$, (b) $\mu = 0.02$, $\mu = 0.03$, $\mu = 0.04$, and $\mu = 0.05$

3.3.2 The optimized results for the exergy efficiency and LCOE of the TEG module

According to the research mentioned before, two different parameter combinations were chosen for the exergy efficiency and LCOE optimizations, making it possible to converge at optimal results more rapidly and accurately. The parameter combinations were displayed in Table 3.4.

Table 3.4. Parameter selection for optimizations of exergy efficiency and LCOE

| Parameter | Exergy efficiency | LCOE |
|----------------------------------|----------------------------------|----------------------------------|
| cognitive parameter (C_1) | 1.5 | 2.0 |
| social parameter (C_2) | 0.5 | 0.5 |
| Particle population($Popsiz$ e) | 350 | 500 |
| Mutation factor (μ) | 0.01 | 0.01 |
| Inertia weight (w) | Random number in [0.4 to 0.9] | Random number in [0.4 to 0.9] |
| Dimensionality (D) | 5 | 5 |

The result indicates that the optimization for the exergy efficiency and LCOE converged at the relevant optimal result after 229 and 260 steps, respectively. In terms of the optimal values, the exergy efficiency and LCOE were about 29.0% and 1.93 \$US/kWh·m², respectively. The related configurations of working conditions and geometric structures for the TEG are shown in Table 3.5.

Table 3.5. The optimized working conditions and geometric structure configurations of the TEG

| Optimization objective | Exergy efficiency (%) | LCOE (\$/kWh·m ²) | T_h (K) | T_c (K) | R_L (Ω) | L (m) | F |
|---------------------------|--------------------------|----------------------------------|--------------|--------------|-----------------------|------------|--------|
| Exergy efficiency | 29 | 12.9 | 340 | 300 | 0.6723 | 0.0009 | 0.2044 |
| LCOE | 2.05 | 1.93 | 740.7 | 700.7 | 0.134 | 0.0005 | 0.9 |

3.4 Multi-objective Optimization for a TEG using ξ -constraint combined with M-PSO algorithm

The single-objective optimization indicated that there were totally different optimal configurations for a TEG when considering the exergy efficiency and LCOE. Besides, it is highly unlikely to achieve the optimal state for both exergoeconomic indices simultaneously. Table 3.5 indicates that when the TEG reached the optimum conditions for the exergy efficiency or LCOE, the corresponding exergoeconomic index was 12.9 \$US/kWh·m² and 2.05%, respectively. However, designers have to consider exergy efficiency and LCOE for a TEG simultaneously.

The optimization for the TEG system with more than two objectives is a multiple criteria decision-making problem [48]. Normally, when tackling the problem, it is possible to acquire an infinite number of solutions known as Pareto points rather than a unique one due to the competition between the objectives [48]. In this paper, the Pareto solutions can be acquired through a hybrid algorithm which is a combination of the M-PSO and ξ -constraint methods. Figure 3.7 displays the flow diagram of the ξ -constraint M-PSO algorithm. The basic strategy is that one objective can be considered as an inherent part of the original problem, and another is introduced as a penalty condition. In this way, the multi-objective optimization can be defined as follows:

The objective function:

$$\max [f_1(T_h, T_c, R_L, L, F)] \quad (33)$$

The penalty condition:

$$f_2(T_h, T_c, R_L, L, F) \leq \xi_k \quad (34)$$

in which ξ can be calculated by Eq. (34)

$$\xi_k = f_2(\mu_2) + k \times \frac{f_2(\mu_1) - f_2(\mu_2)}{n} \quad (34)$$

where, μ_1 and μ_2 are anchor points of the Pareto frontier which can be acquired by single-objective optimization for the exergy efficiency and LCOE of the TEG module. According to Table 3.5, the value of $f_2(\mu_1)$ and $f_2(\mu_2)$ were 12.9 \$US/kWh·m² and 1.93 \$US/kWh·m², respectively. n is the number of equal intervals between points μ_1 and μ_2 .

As for a multiple criteria decision-making problem, the basic strategy for the problem is to acquire the Pareto frontier made by the Pareto points [48]. the results (as shown in Figure 3.8) indicate that the frontier curve is enough stable when n is 20. With the n increasing further, the Pareto points become denser; however, the Pareto frontier made by these points is almost unchanged. In this way, n was set up as 20 in the study.

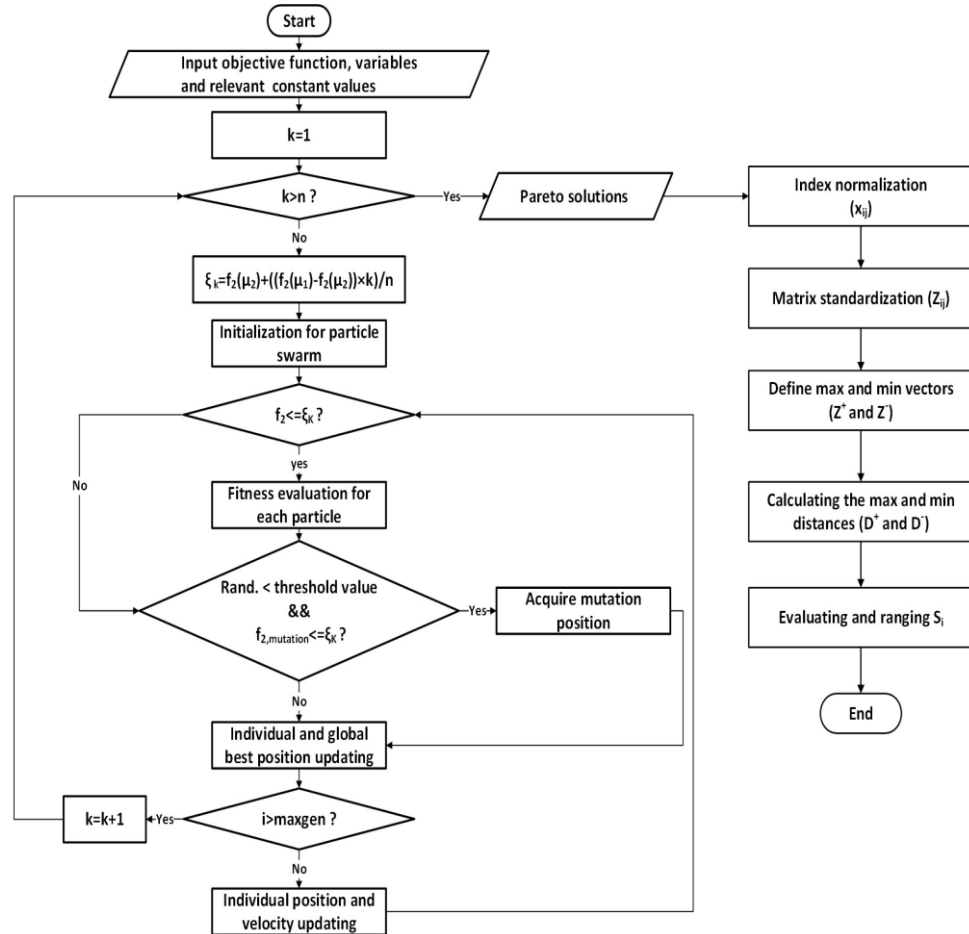


Figure 3.7. Diagram of ξ -constraint with M-PSO algorithm and TOPSIS method

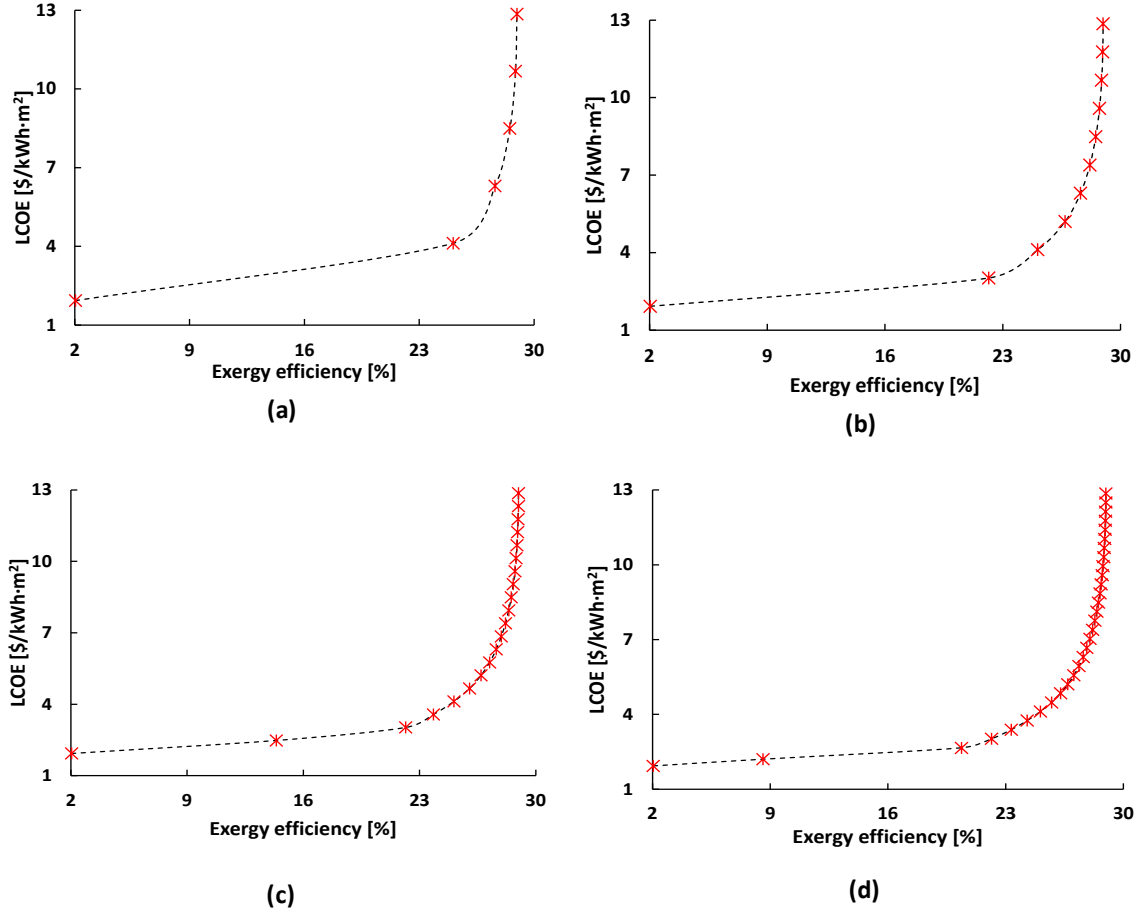


Figure 3.8. Distribution of Pareto frontier under different values of n , (a) $n=5$, (b) $n=10$, (c) $n=20$, (d) $n=30$

Based on the ξ -constraint M-PSO algorithm, a Pareto frontier of the multi-objective optimization for the TEG exergoeconomic performances can be acquired as shown in Figure 3.9. Although all the Pareto solutions are acceptable, there is a priority to evaluate these optimal results. In this research, a technique for order preference by similarity ideal solution (TOPSIS) was used to rank for these solutions, and then to acquire a TOPSIS ideal solution.

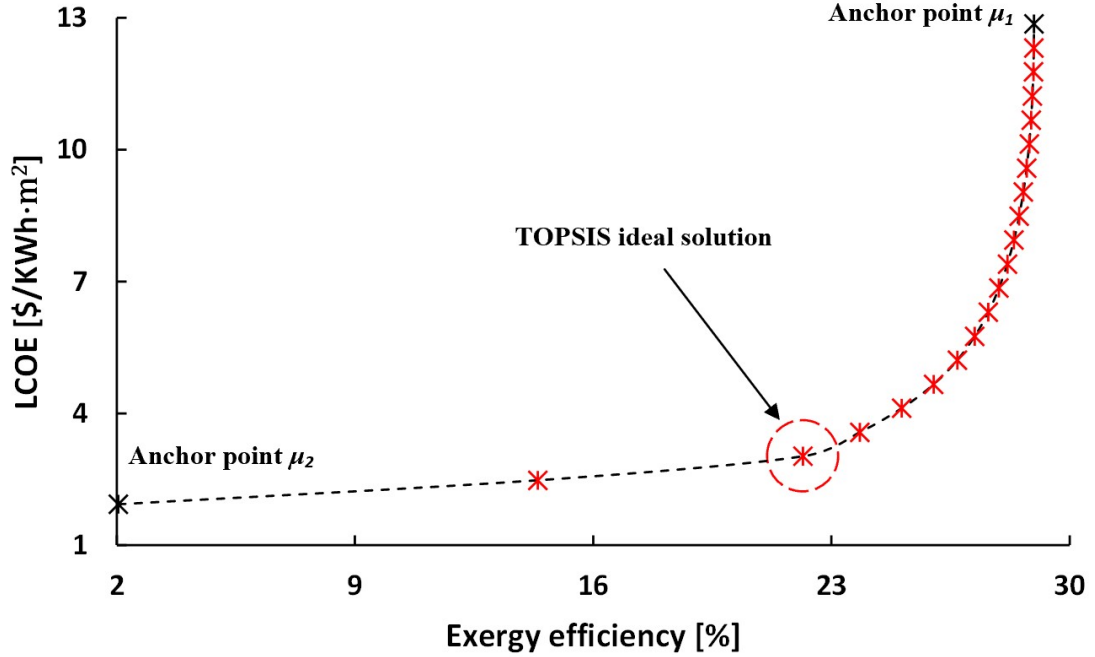


Figure 3.9. Distribution of Pareto frontier and TOPSIS ideal solution point

TOPSIS is an effective method to deal with decision making problem based on multi-criteria, making it possible to acquire an ideal solution from numerous alternatives [49]. The basic principle of TOPSIS method is that the ideal solution should have the shortest distance from the positive ideal solution, meanwhile, having the farthest distance from the negative ideal solution [49].

In this study, there were two inverse optimization problems, which are maximum exergy efficiency and minimum LCOE. In this way, before analyzing the solutions through TOPSIS method, it is necessary to change the minimum problem to a maximum one. Then, the solutions should be normalized in order to avoid the effects from dimensions. Finally, a TOPSIS ideal solution can be acquired through ranking for all of the alternatives based the scores of the distance from the positive and negative ideal solutions. The main steps of TOPSIS are as follows:

1) *Problem conversion*

$$LCOE_i^+ = LCOE_{max} - LCOE_i \quad (35)$$

where $LCOE_{max}$ is the maximum value of the LCOE in the all solutions.

2) *The normalization for the decision matrix*

$$z_{ij} = x_{ij} / \sqrt{\sum_{i=1}^p x_{ij}^2} \quad (36)$$

where, p is number of the alternatives, and here, based on the results of the ξ -constraint method, the value is 21.

3) *Definition for the positive (Z^+) and negative (Z^-) ideal solution*

$$\begin{aligned} Z^+ &= [Z_1^+, Z_2^+, \dots, Z_m^+] \\ &= [\max(z_{11}, z_{21} \dots z_{p1}), \max(z_{12}, z_{22} \dots z_{p2}), \dots, \max(z_{1m}, z_{2m} \dots z_{pm})] \end{aligned} \quad (37)$$

$$\begin{aligned} Z^- &= [Z_1^-, Z_2^-, \dots, Z_m^-] \\ &= [\min(z_{11}, z_{21} \dots z_{p1}), \min(z_{12}, z_{22} \dots z_{p2}), \dots, \min(z_{1m}, z_{2m} \dots z_{pm})] \end{aligned} \quad (38)$$

In this study, there were two criteria, which are exergy efficiency and LCOE, respectively. Therefore, the value of m is 2.

4) *Separation calculation of each alternative from the positive (d^+) and negative (d^-) ideal solution based on the Euclidean distance*

$$d_i^+ = \sqrt{\sum_{j=1}^m (Z_j^+ - z_{ij})^2} \quad (39)$$

$$d_i^- = \sqrt{\sum_{j=1}^m (Z_j^- - z_{ij})^2} \quad (40)$$

5) *Relative closeness calculation (S_i)*

$$S_i = \frac{d_i^-}{d_i^+ + d_i^-} \quad (41)$$

6) *Ranking for the all alternatives based on their value of S_i from the minimum to the maximum*

The results analyzed by the TOPSIS method are displayed in Table 3.6. According to the rank of S_i , the TOPSIS ideal solution can be obtained. The TOPSIS ideal solution and the configuration relating the working conditions and geometrical structure of the TEG can be found in Table 3.7.

Table 3.6. Analysis results based on TOPSIS method

| η_x | LCOE | LCOE _{max} - | Normalized | Normalized | d^+ | d^- | S_i | Rank |
|----------|-----------------------|-----------------------|--------------|-------------|-------|-------|-------|------|
| % | \$/kWh·m ² | LCOE | N_{η_x} | N_{LCOE+} | | | | |
| | | \$/kWh·m ² | | | | | | |
| 2.05 | 1.93 | 11.0 | 0.017 | 0.373 | 0.223 | 0.373 | 0.626 | 10 |
| 14.4 | 2.48 | 10.4 | 0.119 | 0.354 | 0.122 | 0.368 | 0.751 | 5 |
| 22.2 | 3.02 | 9.88 | 0.183 | 0.336 | 0.067 | 0.375 | 0.848 | 1 |
| 23.8 | 3.57 | 9.33 | 0.197 | 0.317 | 0.070 | 0.364 | 0.838 | 2 |
| 25.1 | 4.12 | 8.78 | 0.207 | 0.298 | 0.081 | 0.354 | 0.814 | 3 |
| 26 | 4.66 | 8.24 | 0.215 | 0.280 | 0.096 | 0.343 | 0.781 | 4 |
| 26.7 | 5.21 | 7.69 | 0.221 | 0.261 | 0.113 | 0.331 | 0.746 | 6 |
| 27.2 | 5.76 | 7.14 | 0.225 | 0.243 | 0.131 | 0.319 | 0.709 | 7 |
| 27.6 | 6.3 | 6.60 | 0.228 | 0.224 | 0.149 | 0.308 | 0.674 | 8 |
| 27.9 | 6.85 | 6.05 | 0.231 | 0.206 | 0.167 | 0.296 | 0.639 | 9 |
| 28.2 | 7.4 | 5.50 | 0.233 | 0.187 | 0.186 | 0.286 | 0.606 | 11 |
| 28.4 | 7.94 | 4.96 | 0.235 | 0.169 | 0.204 | 0.275 | 0.574 | 12 |
| 28.5 | 8.49 | 4.41 | 0.236 | 0.150 | 0.223 | 0.265 | 0.543 | 13 |
| 28.6 | 9.04 | 3.86 | 0.236 | 0.131 | 0.242 | 0.256 | 0.514 | 14 |
| 28.7 | 9.58 | 3.32 | 0.237 | 0.113 | 0.260 | 0.247 | 0.488 | 15 |
| 28.8 | 10.1 | 2.80 | 0.238 | 0.095 | 0.278 | 0.241 | 0.464 | 16 |
| 28.9 | 10.7 | 2.20 | 0.239 | 0.075 | 0.298 | 0.234 | 0.440 | 17 |
| 28.9 | 11.2 | 1.70 | 0.239 | 0.058 | 0.315 | 0.229 | 0.421 | 18 |
| 28.9 | 11.8 | 1.10 | 0.239 | 0.037 | 0.335 | 0.225 | 0.402 | 19 |
| 29 | 12.3 | 0.60 | 0.240 | 0.020 | 0.352 | 0.224 | 0.388 | 20 |
| 29 | 12.9 | 0.00 | 0.240 | 0.000 | 0.373 | 0.223 | 0.374 | 21 |

Table 3.7. TOPSIS ideal working conditions and geometric structure configurations of the TEG module

| <i>Exergy efficiency</i> (%) | <i>LCOE</i> (\$/kWh·m ²) | <i>T_h</i> (K) | <i>T_c</i> (K) | <i>R_L</i> (Ω) | <i>L</i> (m) | <i>F</i> |
|---------------------------------|---|-----------------------------|-----------------------------|-----------------------------|-----------------|----------|
| 22.3 | 3.02 | 340 | 300 | 0.142 | 0.000595 | 0.9 |

According to the TOPSIS ideal solution, the exergy efficiency and LCOE of the TEG are 22.2%, and 3.02 \$US/kWh·m², respectively.

3.5 Conclusions

In this paper, an exergoeconomic analysis was completed for a TEG module with 199 pairs of couples through a one-dimensional steady-state thermodynamic model. After that, two objective functions were established, which are the exergy efficiency and LCOE. Meanwhile, many parameter combinations were tested for the algorithm in order to demonstrate its effectiveness for the optimization problem. Additionally, the Pareto solutions can be acquired through the ξ -constraint with M-PSO algorithm when conducting the multi-objective optimization of the exergy efficiency and LCOE. Finally, these alternatives were ranked by the TOPSIS method to get an ideal solution. The conclusions of this work are as follows:

- 1) The relevant research indicated that the MPSO algorithm is an effective method to optimize the exergy efficiency and LCOE of a TEG module. The effects of parameters mainly focus on the convergence speed and accuracy. A higher mutation factor has a positive effect on the accuracy, however, slowing down the convergence speed. Moreover, the accuracy can be improved through increasing particle numbers.
- 2) Through the single-objective optimizations under a constrain condition: the optimal exergy efficiency and LCOE of the TEG module were 29.0% and 1.93 \$US/kWh·m², respectively, under a maximum temperature difference of 40 K.
- 3) As a kind of multi-criteria decision-making strategy, the ξ -constraint with the M-PSO algorithm can be used to conduct the multi-objective optimization, making it possible to obtain a series of Pareto solutions for the exergoeconomic performances of the TEG module. Then, the TOPSIS method was adopted to rank these alternatives, and an ideal solution was determined. As for the TOPSIS ideal solution, the corresponding exergy

efficiency and LCOE of the TEG module reached 22.2% and 3.02 \$US/kWh·m², respectively.

Acknowledgments

This work was made possible by funding from the Natural Sciences and Engineering Research Council of Canada.

References

- [1] M. W. Shahzad, M. Burhan, L. Ang, and K. C. Ng, “Energy-water-environment nexus underpinning future desalination sustainability,” *Desalination*, vol. 413, pp. 52-64, July 2017.
- [2] S. A. Kalogirou, *Solar energy engineering: processes and systems*, 2nd Ed. Elsevier, UK: Oxford, 2014.
- [3] A. Vasel and D. S.-K. Ting, *Advances in Sustainable Energy*. Springer, Switzerland: Cham, 2019.
- [4] Y. Mu, G. Chen, R. Yu, G. Li, P. Zhai and P. Li, “Effect of geometric dimensions on thermoelectric and mechanical performance for Mg₂Si-based thermoelectric uncouple,” *Materials Science in Semiconductor Processing*, vol. 17, pp. 21–26, January 2014.
- [5] L. Fan, G. Zhang, R. Wang and K. Jiao, “A comprehensive and time-efficient model for determination of thermoelectric generator length and cross-section area,” *Energy Conversion and Management*, vol. 122 (15), pp. 85–94, August 2016.
- [6] J. Wang, Y. Li, C. Zhao, Y. Chai, L. Zhu, C. Zhang, J. Wang, W. Zhao and P. Cao, “An optimization study of structural size of parameterized thermoelectric generator module on performance,” *Energy Conversion and Management*, vol. 160, pp. 176–181, March 2018.
- [7] E. Kanimba, M. Pearson, J. Sharp, D. Stokes, S. Priya and Z. Tian, “A modeling comparison between a two-stage and three-stage cascaded thermoelectric generator,” *Journal of Power Sources*, vol. 365, pp. 266–272, October 2017.
- [8] Y. Wu, J. Yang, S. Chen and L. Zuo, “Thermo-element geometry optimization for high thermoelectric efficiency,” *Energy*, vol. 147, pp. 672–680, March 2018.
- [9] I. Dinçer and M. Rosen, *Exergy - Energy, Environment, and Sustainable Development*. 2nd Edition, Elsevier, Netherlands: Amsterdam, 2013.
- [10] H. Xiao, X. Gou and S. Yang, “Detailed modeling and irreversible transfer process analysis of a multi-element thermoelectric generator system,” *Journal of Electronic Materials*, vol. 40 (5), pp. 1195–1201, May 2011.

- [11] S. Manikandan and S. C. Kaushik, "The influence of Thomson effect in the performance optimization of a two-stage thermoelectric generator," *Energy*, vol. 100 (1), pp. 227–237, April 2016.
- [12] Y. Feng, L. Chen and F. Meng, "Influences of the Thomson effect on the performance of a thermoelectric generator-driven thermoelectric heat pump combined device," *Entropy*, vol. 20 (1), pp. 1–18, January 2018.
- [13] S. Asaadi, S. Khalilarya and S. Jafarmadar, "A thermodynamic and exergoeconomic numerical study of two-stage annular thermoelectric generator," *Applied Thermal Engineering*, vol. 156, pp. 371–381, April 2019.
- [14] J. H. Meng, X. X. Zhang and X. D. Wang, "Multi-objective and multi-parameter optimization of a thermoelectric generator module," *Energy*, vol. 71, pp. 367–376, July 2014.
- [15] W. H. Chen, P. H. Wu and Y. L. Lin, "Performance optimization of thermoelectric generators designed by multiobjective genetic algorithm," *Applied Energy*, vol. 209, pp. 211–223, January 2018.
- [16] Y. Ge, Z. Liu, H. Sun and W. Liu, "Optimal design of a segmented thermoelectric generator based on three-dimensional numerical simulation and multi-objective genetic algorithm," *Energy*, vol. 147, pp. 1060–1069, March 2018.
- [17] A. Dener, A. Denchfield and T. Munson, "Preconditioning nonlinear conjugate gradient with diagonalized quasi-newton," *PASC '19: Proceedings of the Platform for Advanced Scientific Computing Conference*, pp. 1–7, June 12–14, 2019.
- [18] Y. D. Valle, G. K. Venayagamoorthy, S. Mohagheghi, J. C. Hernandez and R. G. Harley, "Particle swarm optimization: Basic concepts, variants and applications in power systems," *IEEE Transactions on Evolutionary Computation*, vol. 12 (2), pp. 171–195, April 2008.
- [19] Y. J. Gong, J. J. Li, Y. Zhou, Y. Li, H. S-H. Chung, Y. H. Shi and J. Zhang, "Genetic Learning Particle Swarm Optimization," *IEEE Transactions on Cybernetics*, vol. 46 (10), pp. 2277–2290, October 2016.
- [20] Q. Zhang, R. M. Ogren and S. C. Kong, "A comparative study of biodiesel engine performance optimization using enhanced hybrid PSO–GA and basic GA," *Applied Energy*, vol. 165, pp. 676–684, March 2016.
- [21] R. Yang, Y. Yuan, R. Ying, B. Shen, and T. Long, "A Novel Energy Management Strategy for a Ship's Hybrid Solar Energy Generation System Using a Particle Swarm Optimization Algorithm," *Energies*, vol. 13 (6), p. 1380, March 2020.
- [22] H. Cui, M. Shu, M. Song, and Y. Wang, "Parameter Selection and Performance Comparison of Particle Swarm Optimization in Sensor Networks Localization," *Sensors*, vol. 17 (3), p. 487, March 2017.

- [23] J. Dongxu, W. Zhongbao, J. Pou, S. Mazzoni, S. Rajoo and A. Romagnoli, "Geometry optimization of thermoelectric modules: Simulation and experimental study," *Energy Conversion and Management*, vol. 195, pp. 236–243, September 2019.
- [24] R. Rodriguez, J. Guo, M. Preindl, J. S. Cotton and A. Emadi, "High frequency in jection maximum power point tracking for thermoelectric generators," *Energy Conversion and Management*, vol. 198, pp. 111832-1–111832-9, October 2019.
- [25] S. Zou, E. Kanimba, T. E. Diller, Z. Tian and Z. He, "Modeling assisted evaluation of direct electricity generation from waste heat of wastewater via a thermoelectric generator," *Science of the Total Environment*, vol. 635, pp. 1215–1224, September 2018.
- [26] E. Kanimba, M. Pearson, J. Sharp, D. Stokes, S. Priya and Z. Tian, "A comprehensive model of a lead telluride thermoelectric generator," *Energy*, vol. 142, pp. 813–821, October 2017.
- [27] D. Patil, R. Arakerimath and P. Walke, "Thermoelectric materials and heat exchangers for power generation – A review," *Renewable and Sustainable Energy Reviews*, vol. 95, pp. 1–22, July 2018.
- [28] M. Saufi Sulaiman, B. Singh and W. A. N. W. Mohamed, "Experimental and theoretical study of thermoelectric generator waste heat recovery model for an ultra-low temperature PEM fuel cell powered vehicle," *Energy*, vol. 179 (15), pp. 628–646, July 2019.
- [29] T. H. Kwan, X. Wu and Q. Yao, "Thermoelectric device multi-objective optimization using a simultaneous TEG and TEC characterization" *Energy Conversion and Management* 168, pp. 85–97, April 2018.
- [30] A. Rezanian, L. A. Rosendahl and H. Yin, "Parametric optimization of thermoelectric elements footprint for maximum power generation" *Journal of Power Sources* 255, pp. 151–156, April 2014.
- [31] A. Lazzaretto and G. Tsatsaronis, "SPECO: A systematic and general methodology for calculating efficiencies and costs in thermal systems," *Energy*, vol. 31, pp. 1257–1289, July 2006.
- [32] N. Jaziri, A. Boughamoura, J. Müller, B. Mezghani, F. Tounsi, and M. Ismail, "A comprehensive review of Thermoelectric Generators: Technologies and common applications," *Energy Reports*, vol. 6, pp. 264-287, December 2020.
- [33] TEG POWER INFO (2017), [Online], Converting heat to electricity worldwide with TEG power, <http://www.tegpower.com/>. Accessed 10, March 2021.
- [34] S. L. Blanc, S. K. Yee, M. L. Scullin, C. Dames and K. E. Goodson, "Material and manufacturing cost considerations for thermoelectrics," *Renewable and Sustainable Energy Reviews*, vol. 32, pp. 313–327, January 2014.

- [35] ValuePenguin (updated 15, January 2021) [Online], Average Small Business Loan Interest Rates in 2021: Comparing Top Lenders, <https://www.valuepenguin.com/average-small-business-loan-interest-rates#:~:text=The%20average%20interest%20rate%20on,on%20business%20loans%20since%20201.> Accessed 10, March 2021.
- [36] F. Mohammadkhani, S. Khalilarya, and I. Mirzaee, “Exergy and exergoeconomic analysis and optimisation of diesel engine based Combined Heat and Power (CHP) system using genetic algorithm,” *International Journal of Exergy*, vol. 12 (2), pp. 139-161, April 2013.
- [37] G. Y. Huang and D. J. Yao, “Two-dimensional thermal resistance analysis of a waste heat recovery system with thermoelectric generators,” *Journal of Electronic Materials*, vol. 42, pp. 1982–1987, February 2013.
- [38] G. Y. Huang, C. T. Hsu, C. J. Fang, and D. J. Yao, “Optimization of a waste heat recovery system with thermoelectric generators by three-dimensional thermal resistance analysis,” *Energy Conversion and Management*, vol. 126 (15), pp. 581-594, October 2016.
- [39] K. T. Wojciechowski, M. Schmidt, R. Zybala, J. Merkisz, P. Fuć, and P. Lijewski, “Comparison of Waste Heat Recovery from the Exhaust of a Spark Ignition and a Diesel Engine,” *Journal of Electronic Materials*, vol. 39, pp. 2034–2038, December 2009.
- [40] H. Lu, T. Wu, S. Bai, K. Xu, Y. Huang, and W. Gao et al., “Experiment on thermal uniformity and pressure drop of exhaust heat exchanger for automotive thermoelectric generator,” *Energy*, vol. 54 (1), pp. 372-377, June 2013.
- [41] H. Sun, Y. Ge, W. Liu and Z. Liu, “Geometric optimization of two-stage thermoelectric generator using genetic algorithms and thermodynamic analysis,” *Energy*, vol. 171, pp. 37–48, January 2019.
- [42] X. Jia and Y. Gao, “Optimal design of a novel thermoelectric generator with linear-shaped structure under different operating temperature conditions” *Applied Thermal Engineering* 78, pp. 533–542, December 2014.
- [43] S. Vostrikov, A. Somov and P. Gotovtsev, “Low temperature gradient thermoelectric generator: Modelling and experimental verification,” *Applied Energy* 255, pp. 113786-1–113786-8, August 2019.
- [44] H. Han, W. Lu, L. Zhang and J. Qiao, “Adaptive gradient multi-objective particle swarm optimization,” *IEEE Transactions on Cybernetics*, vol. 48 (11), pp. 3067–3079, November 2018.
- [45] G. G. Yen and W. F. Leong, “Dynamic multiple swarms in multi-objective particle swarm optimization,” *IEEE Transactions on Systems, Man and Cybernetics*, vol. 39 (4), pp. 890–911, July 2009.

- [46] P. Hou, W. Hu and Z. Chen, "Optimisation for offshore wind farm cable connection layout using adaptive particle swarm optimisation minimum spanning tree method," *IET Renewable Power Generation*, vol. 10 (5), pp. 694–702, January 2016.
- [47] G. Xu, Q. Cui, X. Shi, H. Ge, Z. H. Zhan, H. P. Lee, Y. Liang, R. Tai and C. Wu, "Particle swarm optimization based on dimensional learning strategy," *Swarm and Evolutionary Computation*, vol. 45, pp. 33–51, January 2019.
- [48] K. Chircop and D. Zammit-Mangion, "On ξ -constraint based methods for the generation of Pareto frontiers," *Journal of Mechanics Engineering and Automation*, vol. 3, pp. 279–289, May 2013.
- [49] G. R. Jahanshahloo, F. Hosseinzadeh Lotfi and M. Izadikhah, "An algorithmic method to extend TOPSIS for decision-making problems with interval data," *Applied Mathematics and Computation*, vol. 175 (2), pp. 1375–1384, April 2006.

CHAPTER 4

USING DUAL MUTATION PARTICLE SWARM METHOD TO OPTIMIZE THE VARIABLE CROSS-SECTION OF A THERMOELECTRIC GENERATOR BASED ON A COMPREHENSIVE THERMODYNAMIC MODEL

X. Wang, P. Henshaw, and D. S-K Ting, "Using dual mutation particle swarm method to optimize the variable cross-section of a thermoelectric generator based on a comprehensive thermodynamic model," Cleaner Engineering and Technology, Under Review

4.1 Introduction

In the past decades, rapid economic development has created an increasing demand for energy. The energy demand experienced a surge from 5,519 million tons of oil equivalent (Mtoe) in 1971 to 14,282 Mtoe in 2018 [1]. Fossil fuels continue to play a dominant role in modern society despite recent increases in renewable energy such as solar and wind power. According to the statistics from the International Energy Agency (IEA) [1], in 2018, the energy produced from fossil fuels (oil, coal, and natural gas) made up around 80% of the world's total energy supply. The carbon dioxide (CO₂) produced from fossil fuel combustion has become a severe global issue, which is linked to global warming [2-3]. Therefore, it is necessary to take measures to curb carbon emission. Increasing energy efficiency is a potent means to decrease CO₂ emissions. A report from IEA [4] indicated that the global energy-related emissions were reduced by 3.5 gigatons (Gt) during the period between 2015 and 2018 due to the technical efficiency improvements. To this end, thermoelectric generators (TEGs), a kind of solid-state energy convertor, are becoming the focus of researchers' concern as they can convert wasted, and/or readily available heat into electricity, making it possible to improve the overall efficiency of energy systems. Compared with traditional energy systems, the superiority of TEG technology is due to zero-emissions while working [5]. Overall, with the continuous advancement of TE materials, TEG technology will have wide developmental prospects.

Theoretically, there is a huge potential to improve TEG performance, which has attracted many researchers' attention in recent years. Other than exploiting advanced TE materials and heat transfer technology, a reasonable geometric design plays an important role in the improvement of TEG performance. Limited by the processing technology, the design of the constant cross-sectional TE semiconductor element can be seen in common commercial TEG modules [6]. In

this way, the early studies were mainly focused on the effects of the traditional TE element structure on its performance. Du *et al.* [7] used a thermodynamic model to analyze the effect of the aspect ratio (ratio of the cross-sectional area of TE element and its length) on a TEG's performance under a temperature difference of 200 K. The results indicated that with the increase of the aspect ratio, there was an obvious improvement in the output power while the efficiency experienced a slow decrease [7]. In addition, through a three-dimensional TEG model, Jang *et al.* [8] found that there is a positive effect on the power output as the cross-sectional area of the TE element was enlarged [8]. A similar result can be found in the research from Wang *et al.* [9]. Meanwhile, by comparing the performances of rectangle-TEG (R-TEG) and circle-TEG (C-TEG), they verified the TEG performances are affected by cross-sectional area, rather than shape [9].

The effect of a variable cross-sectional area along the length of the TE semiconductor element was first studied by Hoyos *et al.* [6, 10]. Their study indicated that compared with a traditional constant cross-section TE element, the TEG with variable cross-sectional area design has better thermoelectric conversion. In the following decades, technologies of semiconductor manufacture, such as Additive Manufacture (AM), Selective Laser Sintering/Melting (SLS/SLM), and Spark Plasma Sintering (SPS), have been developed, making it possible to produce and even commercialize a TE element with complexed structural design [11]. In this way, an increasing number of researchers paid more attention to exploit TE materials' potential further through a variable cross-sectional area structural design. Sahin *et al.* [12] made a simulation for a TEG with a linearly variable cross-sectional area. They found that increasing the shape parameter, describing the changing rate of the cross-sectional area, can improve the TEG efficiency [12]. Additionally, Shi *et al.* [13] utilized nominal power density analysis to compare the effects of three kinds of variable cross-sectional area functions: linear, quadratic, and exponential on a TEG's performance. The results indicated that both the power generation and efficiency of the linear variable TE element was top among the three [13]. Moreover, the non-constant cross-sectional area TE element can be used to improve multi-stage TEG modules. Through a three-dimensional model, Wu *et al.* [14] analyzed the performance of a three-stage TE element with variable cross-sectional design. The TE element consisted of three kinds of segmented TE materials and worked at a temperature range of 300 K-1000 K [14]. Through changing the cross-sectional area for each local thermoelectric segment, the efficiency of the N-type pin was improved from 12.2% to 21.7%, and that of the P-type pin was increased from 22.9% to 25.7% [14]. Liu *et al.* [15] utilized COMSOL Multiphysics to analyze a two-stage TEG. They found that the variable cross-section asymmetric design had a positive effect on the TEG power generation.

Compared to taking a linear variable cross-section design for the P-type pin, the overall output power increased 4.21% by introducing the segmented design [15]. Similarly, Karana *et al.* [16] analyzed a two-stage TE element with an exponentially varying cross-section. They verified that the influence of the geometric parameter ‘a’ (which are the coefficients of the exponential cross-section equation) on the TEG performances cannot be ignored. When the parameter ‘a’ is 3, the overall efficiency of the two-stage TEG module was improved by 5% [16].

However, the manufacture of TEGs is a complicated process. Normally, many factors, such as geometry, working temperature, and loading resistance, should be considered in designing a TEG module in order to exploit its performance fully. Besides, the effects of these factors on the TEG performance are not always monotonic and independent. For instance, through analyzing for a segmented TEG with exponential area variation in the element, Ali *et al.* [17] verified that there is an optimal exponential function making the TEG reach the maximum efficiency. Meanwhile, the specific optimal exponential function may vary across the load resistance [17]. In this way, some researchers consider the TEG optimization a combinatorial problem and try to use an algorithm to solve it. Meng *et al.* [18] applied a simplified conjugate-gradient method (SCGM) to adjust semiconductor element number, length, and filling factor for a TEG module simultaneously, improving the power generated from 0.14 W to 1.39 W at a current of 0.5 A [18]. Likewise, the SCGM algorithm was used to optimize a two-stage TEG module by Liu *et al.* [19]. The algorithm found an optimal combination of geometric structure (element length of the lower stage and cross-sectional area ratio of P&N pins in the lower and upper stages), making the output power increase by 30.6% under a temperature of 680 K [19]. Under a temperature difference of 500 K, Ranjan *et al.* [20] applied Taguchi and ANOVA methods to search for the optimal combination of the element length, cross-sectional area, and load resistance for a TEG module, which improved its efficiency to 12.8% [20]. One of the popular algorithms, the genetic algorithm (GA), also has become the focus of researchers’ concern. Zhu *et al.* [21] optimized a two-stage TE couple in a five-dimensional variable searching space (including geometric structure and load resistance). The result indicated that the optimum efficiency can reach 9.15% under a temperature difference of 350 K [21]. Yusuf *et al.* [22] ran a GA program to deal with a discrete optimization problem. When the TEG was operated in the temperature range of 300 K-800 K, they acquired a maximum output power of 30.1 W in a four-dimensional searching space related to element number and its geometric structure [22].

Numerous algorithms have been utilized in TEG optimization; meanwhile, premature or poor convergence are the main challenges for these methods [18, 23-24]. In particular, when using an

algorithm, such as GA or SCGM to deal with a complicated problem, it is normally necessary to spend lots of time on trial-and-error calculations or parameter tuning for algorithms, such as initial guesses and crossover probability [18, 25]. As a kind of bionic algorithm, particle swarm optimization (PSO) is equipped with outstanding performances in convergence and conciseness [25-26]. Meanwhile, through adding a subprogram, like mutation or differential evolution, the premature convergence for the PSO algorithm can be avoided effectively [26]. Due to the distinctive advantages of the PSO algorithm, many researchers tried to apply it to engineering systems. In order to balance the hybrid system's economy and efficiency under different electrical loads, Yang *et al.* [27] utilized the PSO method to optimize the proportion of power generation from solar input to the system. Using a hybrid PSO algorithm, the performances and emissions of a biodiesel engine were optimized by Zhang *et al.* [26]. They also verified the optimum and converging processes of the hybrid PSO algorithm are better than that of the GA method [26]. Therefore, the PSO algorithm was taken as a basic tool to analyze and optimize a TEG module in this study.

In this paper, a new variable cross-sectional function, which is a kind of hyperbolic function, was introduced to design a TE element. Based on a comprehensive thermodynamic model, the reason why the performances of variable cross-sectional TEG are better than that of traditional were determined. Meanwhile, the main non-dimensional design parameters (cross-sectional changing rate, loading resistance ratio, and temperature ratio, *etc.*) were taken to be a multi-variable searching space of the TEG performance optimization. Moreover, the review in most of the previous literature related to the TEG optimization took a simplified thermodynamic model to be an objective function. Namely, the temperature difference across the sides of a TE element remained constant during the optimizing process. In practice, affected by the variation of Joule heat and Peltier heat, the temperature difference is unlikely to remain unchanged [27]. Besides, through an experimental validation, Gomez *et al.* [27] verified the results of a comprehensive thermodynamic model (considering effects of Joule heat and Peltier heat) are closer to the real working performances of a TEG compared to that of the simplified model. In this way, one of the motivations in this paper is to apply an algorithm to conduct the optimization for a TEG based on a comprehensive thermodynamic model, making it possible for the optimal scheme to be suitable for real working conditions. In order to conduct the optimization for the TEG based on the comprehensive thermodynamic model, an improved PSO method, named Dual-PSO, was introduced into this study. First, using the PSO algorithm, the governing equations for the TEG were solved, which determined the exact temperature difference between the ends of the TE

element. After that, the TEG's output power and efficiency were optimized through running the PSO method for the second time. Meanwhile, in order to avoid premature convergence, a subprogram, mutation, was embedded into the PSO program, which increased the randomization in the algorithm.

4.2 Thermodynamic Analysis for a TEG

Based on the 1st law of thermodynamics, two control equations can be established for a TEG module consisting of 199 pairs of variable cross-sectional couples. These equations can be solved by an MPSO algorithm to acquire the real temperature difference across the semiconductor elements. The evaluation and optimization for the TEG's performances can be conducted after the working temperature is calculated.

The thermodynamic model was established based on some simplifying assumptions. In this paper, the total volume of the TE elements keeps constant in different shape designs, which means that there is no obvious difference in the volume of the gap between the TE elements. Meanwhile, the air, which is the filling material in the gaps, is always equipped with a high thermal resistance [19]. In this way, the heat loss in the gaps was ignored in this TEG model. Besides, in order to simplify the model, the substrate and contact thermal resistance were ignored, which can be also found in other studies about TEG optimization [16-18].

4.2.1 Thermoelectric theory for a variable cross-sectional TEG module

A TEG module typically consists of three basic elements: cascaded TE couples (semiconductor elements in P-N pairs), conductors, and substrates, as shown in Figure 4.1-(a). The Seebeck effect indicates that the voltage produced by TE couples is proportional to the temperature difference at its ends. In this way, the open-circuit voltage of a TEG can be calculated from Eq. (1) [29].

$$V = S(T_h - T_c)N_{pair} \quad (1)$$

where N_{pair} is the number of cascaded TE couples, T_h and T_c are the hot and cold temperatures. The overall Seebeck coefficient, S , is related to the Seebeck coefficients of P and N semiconductors, S_P and S_N , as

$$S = S_P + |S_N| \quad (2)$$

When a TEG's positive and negative anodes are connected to a load resistance, the output power can be generated from the system. The output power (P) can be calculated through Ohm's law [30], that is,

$$P = \frac{S^2(T_h - T_c)^2 N_{pair}^2}{(R_i + R_L)^2} R_L = \frac{S^2(T_h - T_c)^2 N_{pair}^2}{R_i \times (1 + r_x)^2} r_x \quad (3)$$

where, R_i and R_L represent the internal and load resistance. r_x is the ratio of load resistance (R_L) to internal resistance (R_i).

The internal resistance is the sum of the resistance of the TE couples (r_{teg}) and conductors (r_c) [31], that is,

$$R_i = r_{teg} + r_c \quad (4)$$

According to the mathematical nature of resistance, the resistance of the P and N elements is proportional to their lengths and inversely proportional to their cross-sectional areas. For an infinitesimal length for a TE couple, dx , its electrical resistance can be calculated as in Eq. (5) [13, 16].

$$dr_{teg} = \left[\frac{1}{\sigma_P A_P(x)} + \frac{1}{\sigma_N A_N(x)} \right] dx \quad (5)$$

where A , and σ represent the cross-sectional area and electrical conductivity. The subscripts P and N represent the P-type and N-type semiconductors, respectively.

The resistance of the entire TE elements can be obtained via integration along with the length of the element (L), as shown in Eq. (6) [13, 16],

$$r_{teg} = N_{pair} \int_0^L \left[\frac{1}{\sigma_P A_P(x)} + \frac{1}{\sigma_N A_N(x)} \right] dx \quad (6)$$

The resistance of the conductors can be calculated in a similar manner. Meanwhile, conductors are connected to semiconductors by welding balls. Hence, considering the resistance of the welding balls, the total conductors' resistance can be deduced from Eq. (7).

$$r_c = \left(\frac{L_c}{\sigma_c A_c} \right) (2N_{pair} + 1) + r_{ct} \times 4N_{pair} \quad (7)$$

where, A_c , L_c , and σ_c represent the conductor's cross-sectional area, length, and electrical conductivity, respectively. r_{ct} is the welding resistance. A low value for the welding resistance is desirable, for it can decrease the negative effects of the welding resistance on the power generation of a TEG. Moreover, the welding resistance may vary across to the geometric structure and manufacturing technique. In this way, a low value can decrease the source of uncertainty

from the changing welding resistance in the geometric optimization for a TEG to some extent. Referring to the research from Gomez *et al.* [28], a welding resistance of $3.41 \times 10^{-10} \Omega \cdot \text{m}$ was used in this paper.

A new cross-sectional function (a kind of hyperbolic function) was introduced in this study. In order to make the research results comparable, it is necessary to keep the total volume of a TE couple the same (the total volume of a TE couple is $A_0 L$) for both the traditional and new design shapes. Therefore, two hyperbolic functions were established (as shown Eqs. (8)-(9)) to control the variation of the cross-sectional area for the P and N-type semiconductors respectively. Defined by the two equations, the volume of a pair of the hyperbolic elements can remain the constant at $A_0 L$.

$$A_P(x) = \frac{A_0}{1+\mu} + \frac{2\beta A_0 \ln 2}{1+\mu} - \frac{2\beta A_0 L}{(x+L)(1+\mu)} \quad (8)$$

$$A_N(x) = \frac{\mu A_0}{1+\mu} + \frac{2\beta \mu A_0 \ln 2}{1+\mu} - \frac{2\beta \mu A_0 L}{(x+L)(1+\mu)} \quad (9)$$

where, β is the shape parameter (a ratio of the subtraction between the maximum and minimum areas in a TE element to the average area). The shape parameter describes the cross-sectional area gradient in a TE element ($\beta > 0$ means the cross-sectional area decreases from the hot side to cold; $\beta = 0$ means the cross-sectional area is constant; $\beta < 0$ means the cross-sectional area decreases from the cold side to hot). μ represents the ratio of the average cross-sectional areas of the N and P-type semiconductor. A_0 is the total average cross-sectional area of the P and N-type semiconductor. In this study, A_0 was kept constant of 8 mm^2 .

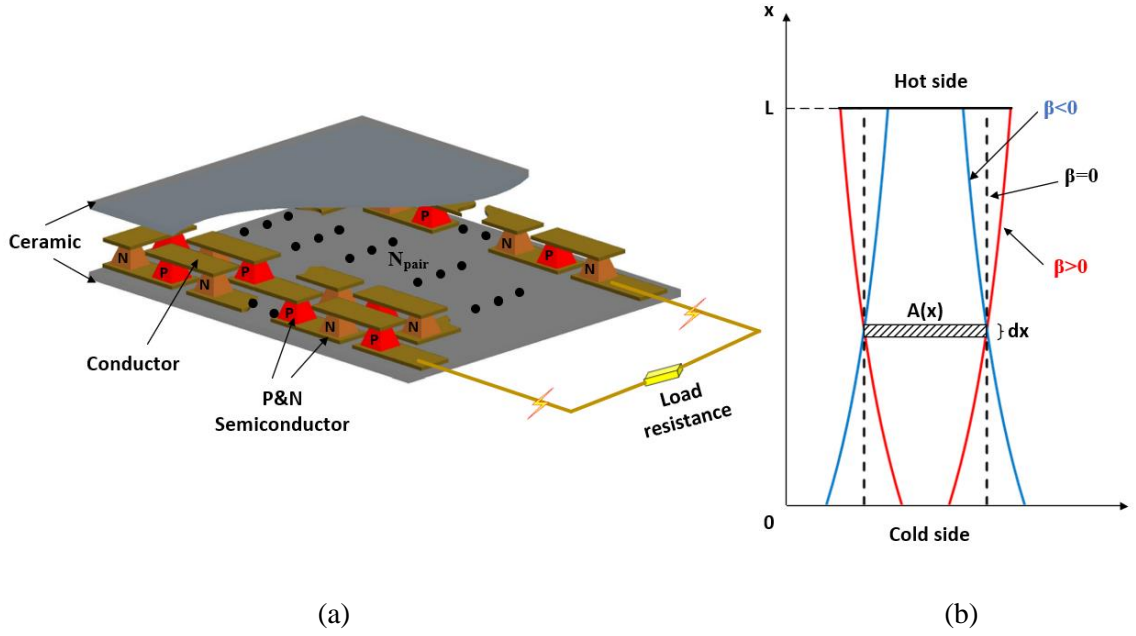


Figure 4.1. Schematic diagram of a variable cross-section TEG module, (a) cutaway view of the TEG module arrangement, and (b) geometric structure of a TE element with variable cross-section shapes

4.2.2 Material properties of the TEG module

As for a TEG module with a specific structure, its performance is mainly decided by the TE semiconductor materials' properties, involving the Seebeck coefficient (S), electrical conductivity (σ), and thermal conductivity (k). It is acknowledged that there are relationships between these material's properties and the working temperature, to the point that the TEG's performances can be considered as functions of the Seebeck coefficient, electrical conductivity, thermal conductivity, and temperature. In this way, a non-dimensional parameter, figure of merit (ZT), was first derived by Ioffe [32] to evaluate the quality of a TE material comprehensively. The figure of merit can be expressed as in Eq. (10) [32-34]

$$ZT = \frac{S^2 \sigma}{k} T \quad (10)$$

The figure of merit describes the relative magnitude of a TE material's capacity in the power generation and thermal conduction at a specific temperature [35]. An effective TE material should satisfy, commonly, three characteristics [33, 36]. First, a TE material should be equipped with an excellent Seebeck coefficient, maximizing the conversion of electrical power from heat. In order to decrease energy dissipation in the form of internal Joule heat, it is necessary to improve the TE

material's electrical conductivity as far as possible. Conversely, a low thermal conductivity can alleviate thermal conduction for a material, making it possible to enlarge the temperature difference across the TE element. Therefore, based on Eq. (10), an excellent TE material is always characterized by a high value of the figure of merit.

In this paper, modified bismuth telluride was introduced into the thermodynamic model as the TE semiconductor material, of which the properties can be found in Table 4.1.

Table 4.1. Material properties of modified bismuth telluride [16, 37]

| Material properties | P-type modified bismuth telluride | N-type modified bismuth telluride |
|---|--|--|
| Seebeck coefficient ($\mu\text{V/K}$) | $-188.2 + 2.2411T$ $- 3.0075 \times 10^{-3}T^2$ $+ 2.4914 \times 10^{-7}T^3$ | $443.49 - 4.5121T$ $+ 9.4424 \times 10^{-3}T^2$ $- 5.8362 \times 10^{-6}T^3$ |
| Thermal conductivity ($\text{W/m}\cdot\text{K}$) | $-1.8067 + 5.7529 \times 10^{-3}T$ $- \frac{64.639}{T}$ $+ \frac{1.3395 \times 10^5}{T^2}$ | $-4.6205 + 9.9277 \times 10^{-3}T$ $+ \frac{833.7}{T} + \frac{235636}{T^2}$ |
| Electrical conductivity (S/cm) | $-473.1 + 0.86507 \times T$ $+ e^{(16.637-1.6942\ln(T))}$ | $-2139.4 + 2.5778 \times T$ $+ e^{(12.795-0.89092\ln(T))}$ |

According to Eq. (10), the figure of merit of the TE materials can be calculated at various temperature, as shown in Figure 4.2. The results indicate that the ZT of P-type material is much higher than that of N-type under a temperature range between 300 K and 600 K. In this way, the performance of P-type material is better than that of N-type material in this temperature range.

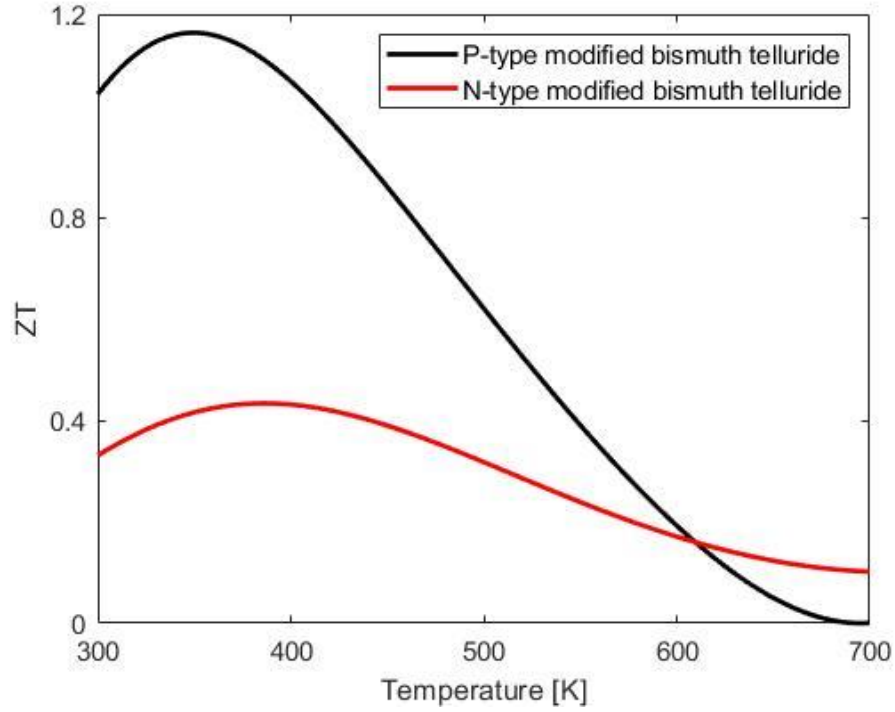


Figure 4.2. Figure of merit of the P&N-type materials

Additionally, in order to reflect the influence of temperature on the TEG performances, the average values of the TE material properties were taken into the model. Mathematically, the average value of the material's properties can be calculated by the mean value theorem of integrals along with the temperature. In this way, the general formula of the average values of the TE material properties can be shown in Eq. (11).

$$\bar{\Delta} = \frac{\int_{T_c}^{T_h} \delta(T) \cdot dT}{(T_h - T_c)} \quad (11)$$

where, $\bar{\Delta}$ represents the average values of the Seebeck coefficient, thermal conductivity, and electrical conductivity. The temperature related value of each of these properties is marked as $\delta(T)$.

4.2.3 Control equations of the TEG module

Normally, the thermal source is attached to the hot side of a TEG via a contact pad, and the thermal energy dissipates through a heat sink located on the other side of the TEG (as shown in Figure 4.3) [28]. From the figure, it can be found that there are three kinds of thermal energy

passing through the interior of TE couples, which are Fourier heat (\dot{Q}_F), Peltier heat (\dot{Q}_P), and Joule heat (\dot{Q}_J).

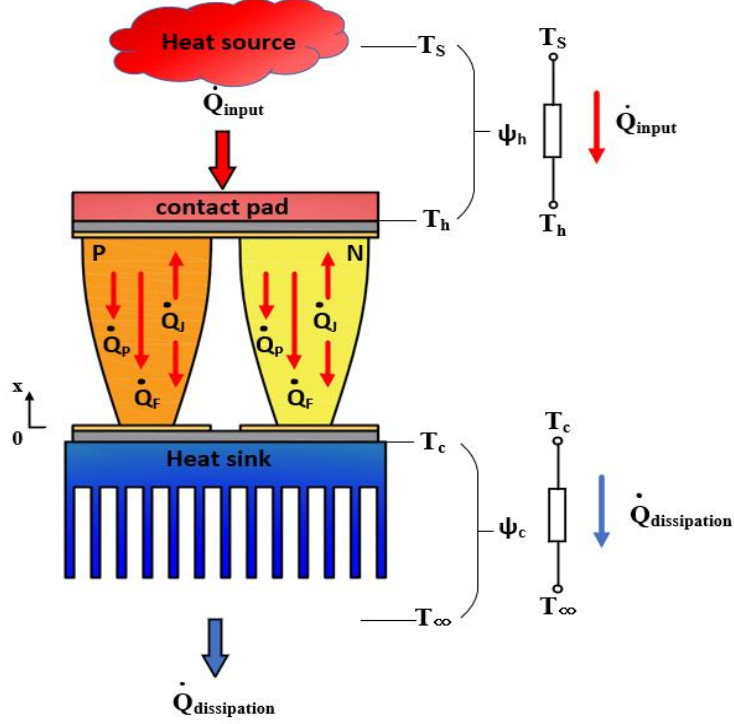


Figure 4.3. Thermal transfer processes of a variable cross-section TEG module

As for a TE couple, the Fourier heat is proportional with the temperature difference at its ends and net thermal conductance. In this way, the Fourier heat of TE couples is shown in Eq. (12) [13, 16].

$$\dot{Q}_F = \bar{K}(T_h - T_c)N_{pair} \quad (12)$$

in which, \bar{K} is the average net thermal conductance of a TE couple. As for a variable cross-sectional TE couple, the value of \bar{K} can be calculated from

$$\bar{K} = \frac{\bar{k}_P}{\int_0^L \frac{1}{A_P(x)} dx} + \frac{\bar{k}_N}{\int_0^L \frac{1}{A_N(x)} dx} \quad (13)$$

where, \bar{k}_P and \bar{k}_N are the average thermal conductivity of the P&N TE materials.

The Peltier heat for a TE couple is mainly decided by the current passing through the junction and the Peltier coefficient. The Peltier coefficient can be considered as a product of the local

temperature at the junction and the Seebeck coefficient. As for a TEG module, the Peltier heat can be calculated by Eq. (14) [13, 16].

$$\dot{Q}_P = \bar{S}T \left[\frac{\bar{S}(T_h - T_c)N_{pair}}{R_i + R_L} \right] N_{pair} = \bar{S}^2 T \frac{(T_h - T_c)N_{pair}^2}{R_i \times (1 + r_x)} \quad (14)$$

in which, \bar{S} is the average net Seebeck coefficient. T is the temperature of the hot side or cold side of the TEG module.

Moreover, it is acknowledged that the Joule heat is proportional to the square of the current and the internal resistance. As for a TEG module, the expression of the Joule heat is displayed in Eq. (15) [13, 16].

$$\dot{Q}_J = \frac{\bar{S}^2 (T_h - T_c)^2 N_{pair}^2}{(R_i + R_L)^2} R_i = \frac{\bar{S}^2 (T_h - T_c)^2 N_{pair}^2}{R_i (1 + r_x)^2} \quad (15)$$

It is noticeable that as for a kind of internal thermal source, it can be assumed that only half of Joule heat is absorbed by the hot temperature side of a TEG, and another half is dissipated into the cold temperature side [38-39].

Based on Figure 4.3, it is also found that there are two kinds of external thermal energy. The one is absorbed by the hot side of a TEG, named as energy input (\dot{Q}_{input}). Another is energy dissipation ($\dot{Q}_{dissipation}$), transferred to the surroundings through its cold side. In this way, based on the 1st law, the energy balance can be established for both the ends of a TEG, respectively (shown as the following two equations) [28, 31].

$$\dot{Q}_{input} = \dot{Q}_F + \dot{Q}_{P,h} - \frac{1}{2} \dot{Q}_J \quad (16)$$

$$\dot{Q}_{dissipation} = \dot{Q}_F + \dot{Q}_{P,c} + \frac{1}{2} \dot{Q}_J \quad (17)$$

Additionally, the energy input and dissipation can be calculated through the temperature and thermal resistance in both the ends of the TEG module. Therefore, Equations (16)-(17) can be rewritten by Eqs. (18) and (19) [28, 31].

$$\frac{T_s - T_h}{\psi_h} = \dot{Q}_F + \dot{Q}_{P,h} - \frac{1}{2} \dot{Q}_J \quad (18)$$

$$\frac{T_c - T_\infty}{\psi_c} = \dot{Q}_F + \dot{Q}_{P,c} + \frac{1}{2} \dot{Q}_J \quad (19)$$

where, T and ψ are the temperature and thermal resistance. The subscripts (c, h, S, and ∞) represent the cold side, hot side, thermal source, and ambient. According to the research from Gomez *et al.* [28], the thermal resistance of the hot side can be assumed as 1 K/W. Meanwhile, considering the cost-effectiveness and reliability of the TEG system, a passive cooling device was used as the heat sink for the cold side. According to the radiator's configuration from the manufactory, the thermal resistance of the cold side is 5.5 K/W [40].

Substituting Eqs. (12, 14-15) into the two control equations, the formulas (18) and (19) can be rearranged to the following two non-linear equations.

$$A_1 T_h^2 + A_2 T_c^2 + A_3 T_h T_c + A_4 T_h + A_5 T_c = A_6 \quad (20)$$

$$B_1 T_h^2 + B_2 T_c^2 + B_3 T_h T_c + B_4 T_h + B_5 T_c = B_6 \quad (21)$$

in which, A_i and B_i are mainly decided by TE material properties and geometric structure, as shown in Table 4.2. As for a specific TEG module, they are constant.

Table 4.2. Expressions of the constant A_i and B_i in the two control equations

| Subscript | A | B |
|--|---|--|
| 1 | $\frac{N_{pair}^2 S^2 \psi_h (1 + 2r_x)}{2R_i (1 + r_x)^2}$ | $\frac{N_{pair}^2 S^2 \psi_c}{2R_i (1 + r_x)^2}$ |
| 2 | $-\frac{N_{pair}^2 S^2 \psi_h}{2R_i (1 + r_x)^2}$ | $-\frac{N_{pair}^2 S^2 \psi_c (1 + 2r_x)}{2R_i (1 + r_x)^2}$ |
| 3 | $-\frac{N_{pair}^2 S^2 \psi_h r_x}{R_i (1 + r_x)^2}$ | $\frac{N_{pair}^2 S^2 \psi_c r_x}{R_i (1 + r_x)^2}$ |
| 4 | $N_{pair} K \psi_h + 1$ | $N_{pair} K \psi_c$ |
| 5 | $-N_{pair} K \psi_h$ | $-(N_{pair} K \psi_c + 1)$ |
| 6 | T_S | $-T_\infty$ |
| (Remained constant with 300 K in this paper) | | |

4.2.4 Methodology for the solution of the control equations based on MPSO algorithm

In this study, the specified temperature boundary conditions were taken into the TEG model. Namely, the temperature of the thermal source and ambient are specified values. Under these conditions, the parameters in the control equations (A_i and B_i) are constant for a specific TEG module. At this moment, the control equations can be considered as a binary quadratic system. Thereinto, the unknown parameters are the real temperature of both the ends of the TEG module (T_h and T_c). Therefore, the T_h and T_c can be acquired through solving the system using the MPSO algorithm, making it possible to evaluate the TEG performances.

MPSO method evolved by adding a subprogram ‘mutation’ for the PSO algorithm. As for a kind of bionic algorithm, the PSO algorithm imitates how a bird flock searches for food. During the process of the foraging, every individual in the bird flock should change their velocity continuously. Normally, the variation of the velocity is affected by the inertia, each individual’s cognitive, and social information sharing. In this way, the expression of the velocity (V_i) updating equation is displayed in Eq. (22) [41-42].

$$V_{i+1} = wV_i + C_1R_1(P_{best} - X_i) + C_2R_2(G_{best} - X_i) \quad (22)$$

where, w is the inertia weight, utilized to adjust the influence of the velocity of the previous generation particle. C_1 and C_2 are the cognitive and social parameters which are positive acceleration constants. R_1 and R_2 are random numbers ranging from 0 to 1. The local and global best positions are marked with the P_{best} and G_{best} , respectively.

Considered the unit time, the individual’s position varies with its velocity. It means that the new position is vector sum of the updated velocity and previous position as shown in Eq. (23) [41-42].

$$X_{i+1} = X_i + V_{i+1} \quad (23)$$

The calculating process of the MPSO method is displayed in Figure 4.4. According to the main sequence shown in the diagram, the objective function should be created to make sure of the optimal direction (searching the maximum or minimum value?) before applying the algorithm. Firstly, equation (20) can be rewritten into a function format through moving the right item to the left (shown as Eq. (24)).

$$f_h(T_h, T_c) = A_1 T_h^2 + A_2 T_c^2 + A_3 T_h T_c + A_4 T_h + A_5 T_c - A_6 \quad (24)$$

Similarly, equation (21) can be rearranged to Eq. (25).

$$f_c(T_h, T_c) = B_1 T_h^2 + B_2 T_c^2 + B_3 T_h T_c + B_4 T_h + B_5 T_c - B_6 \quad (25)$$

In order to make sure that the values of the two functions are zero simultaneously, an objective function (fun_1) was built through connecting the two functions using the absolute value operation (as shown in Eq. (26)). Then, utilizing the MPSO algorithm to search the minimum value for the objective function. Meanwhile, the real temperature on both the ends of the TEG module can be solved from the control equations.

$$fun_1 = \min (|f_h(T_h, T_c)| + |f_c(T_h, T_c)|) \quad (26)$$

in which, the variable searching spaces for the temperature of the thermal source and ambient are shown in Eqs. (27) and (28), respectively.

$$T_\infty \leq T_h \leq T_S \quad (27)$$

$$T_\infty \leq T_c \leq T_S \quad (28)$$

Based on the basic idea of the algorithm, the particles should adjust their velocity and location during the searching process. Therefore, it is necessary to define the relevant parameters in the updating equations (Eqs. (20) and (21)), involving C_1 and C_2 , etc. As for the cognitive and social parameters (C_1 and C_2), the values can be set arbitrarily sometimes; however, the two values always sum up to 4 [23]. Moreover, some research from algorithm engineers indicated that the recommendation for the inertia weight (w) ranges from 0.4 to 0.9, which can allow the particle to move freely enough [23]. Differing from the traditional PSO method, it is also needed to set a mutation factor (mu) for the MPSO algorithm to control the probability of the mutation being triggered. Our previous study has proven that the premature convergence in the MPSO method can be avoided effectively when the mutation factor is 0.05 [43]. Hence, the $mu=0.05$ is recommended in this paper. Overall, the parameter selection for the MPSO algorithm in this paper can be found in Table 4.3. The calculated result indicates that the accuracy can reach 0.000001 under the parameter selection for the MPSO method.

Table 4.3. Parameter selections for the MPSO algorithm

| Parameter | Value |
|----------------------------------|----------------------------------|
| cognitive parameter (C_1) | 2.0 |
| social parameter (C_2) | 2.0 |
| Particle population($Popsiz$ e) | 100 |
| Mutation factor (mu) | 0.05 |
| Inertia weight (w) | Random number in [0.4 to 0.9] |

For the next step, after generating the initial particle swarms' velocity and position vectors, the fitness for each particle can be evaluated by the objective function, which can acquire the local best and global best position for later generations. Meanwhile, if the iteration step is lower than the maximum step, each new generation particles' position and velocity will be created by the updating equations.

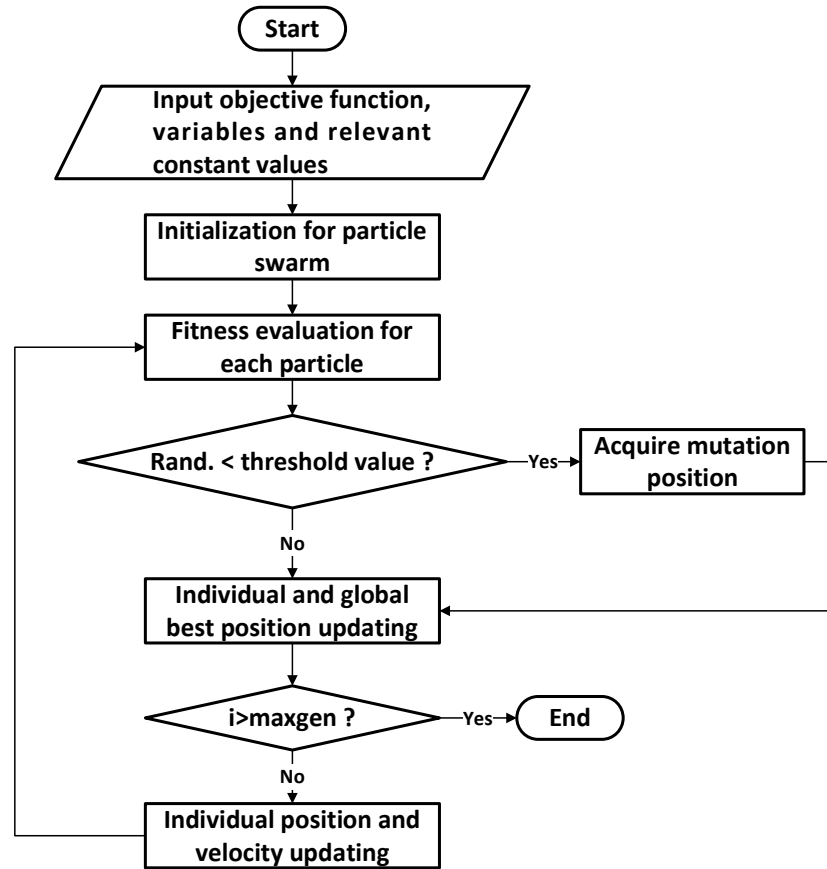


Figure 4.4. Flow chart of the M-PSO method

Additionally, the effect of the subprogram ‘mutation’ is to improve the randomization of the algorithm, making it possible to avoid the premature convergence [43-44]. According to the flow chart, the subprogram will work once the mutation condition ($Rand. < threshold\ value$) is triggered. The threshold condition can be expressed as in Eq. (29)

$$threshold\ value = (1 - (i - 1)/(maxgen - 1))^{\frac{1}{mu}} \quad (29)$$

in which, the maximum generations of particles and the mutation factor are marked as the $maxgen$ and mu .

When the subprogram ‘mutation’ is triggered, a set of position coordinates ranging from ‘ ub ’ and ‘ lb ’ can be generated by Eqs. (30) and (31).

$$lb = X_i - \delta x \quad (30)$$

$$ub = X_i + \delta x \quad (31)$$

in which, δx is a floating value which can be calculated through Eq. (32).

$$\delta x = threshold\ value \times (X_{max} - X_{min}) \quad (32)$$

However, the collection [$lb\ ub$] should not exceed the limitation of the position as shown in Eq. (33).

$$[lb\ ub] \in [X_{min}\ X_{max}] \quad (33)$$

Then, a mutation position will be generated in this collection randomly. Meanwhile, the new position will remain if its fitness is better than that of the old position.

4.3 Performance evaluation for the variable cross-sectional TEG module

In this paper, a comprehensive thermodynamic model was used to analyze the performances for a TEG with 199 cascade couples. The basic dimension for each TEG couple is 8 mm² by 6.4 mm. Keeping the volume of a TE couple unchanged, the TE element was redesigned to be in the shape of a variable cross-section using a hyperbolic function. Meanwhile, the control equations for the thermodynamic model were solved by the MPSO algorithm, making it possible to evaluate the performances of the TEG. The differences in the performance of the redesigned TEG and traditional one can also be contrasted through the comprehensive thermodynamic model. Besides, some non-dimensional parameters, such as temperature ratio, resistance ratio, and shape

parameter, *etc.*, were introduced to analyze their influences on the variable cross-sectional TEG module's performances.

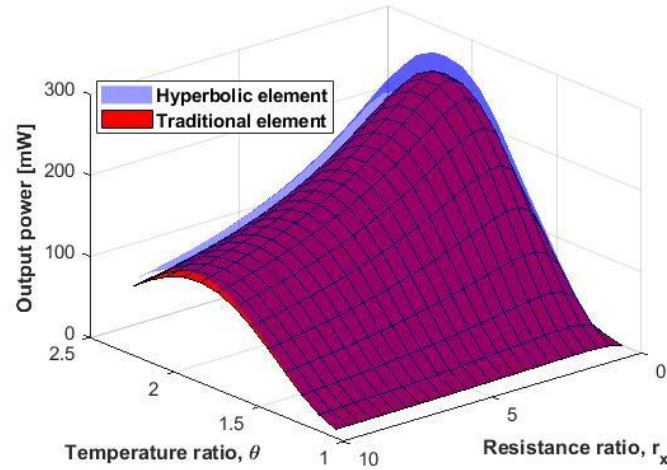
4.3.1 Thermoelectric theory for a variable cross-sectional TEG module

The output power and efficiency were used to evaluate the performances of the TEG module. The output power can be calculated by Eq. (3), and the efficiency is a ratio of the output power and energy input, that is,

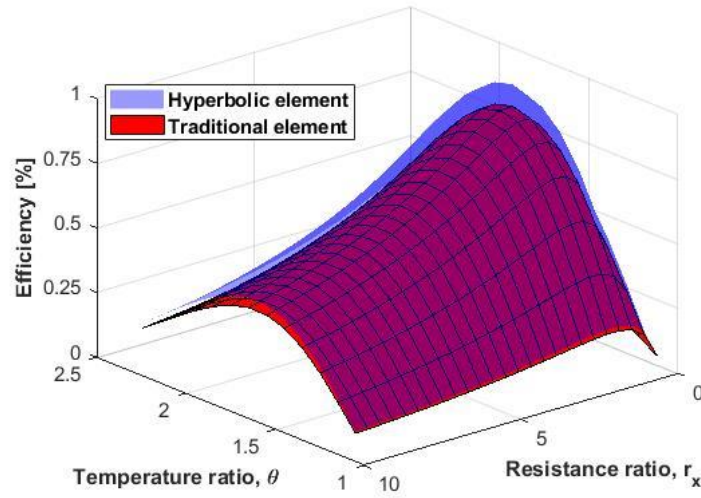
$$\eta = \frac{P}{\dot{Q}_{input}} = \frac{P}{\frac{T_s - T_h}{\psi_h}} = \frac{P}{\frac{\theta \times T_\infty - T_h}{\psi_h}} \quad (34)$$

where, θ is the temperature ratio which is a ratio between the temperature of the thermal source and ambient ($\theta = \frac{T_s}{T_\infty}$).

Based on the thermodynamic model, the output power and efficiency of the TEG modules can be acquired under different working conditions (the temperature ratio ' θ ', and resistance ratio ' r_x '). Figure 4.5 (a)-(b) displays the output power and efficiency of the variable cross-sectional TEG (its shape parameter (β) and area ratio (μ) are 1) and traditional one (which is a TEG with constant cross-sectional area).



(a)



(b)

Figure 4.5. Performances of the TEG with hyperbolic and traditional element shapes under different working conditions, (a) output power of the TEG modules and (b) efficiency of the TEG modules

The results indicate that the performance of the variable cross-sectional TEG is higher than that of the traditional one. The power and efficiency can be increased by up to 10.59% and 12.95%, respectively. In this way, through redesigning the TEG module using the hyperbolic function, its performance can be improved effectively. The calculated results show that under the same working conditions, the redesigned TEG is equipped with a higher temperature difference across the semiconductor element compared to the traditional one (displayed in Figure 4.6). The increased temperature difference is one of the reasons why the TEG performance can be improved by variable cross-sectional design.

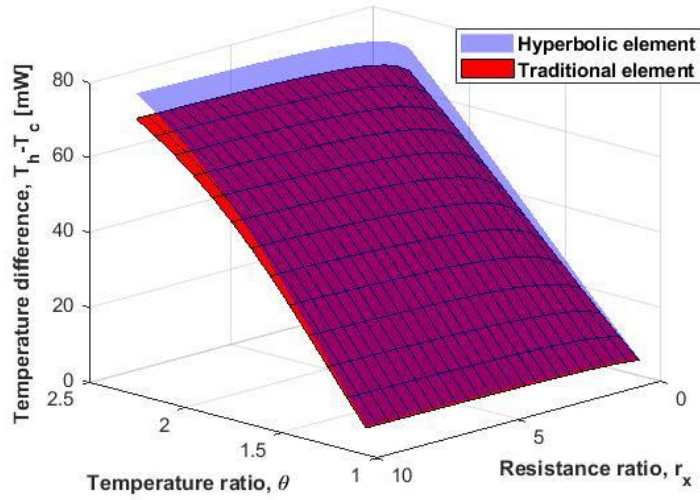


Figure 4.6. Real temperature difference at the both ends of the TEG with hyperbolic and traditional element shapes under different working conditions

In order to explore the reasons for the performance improvement further, it is necessary to calculate the internal thermal resistance and temperature distribution for the TE couple. The thermal resistance of the couple can be considered as two resistances in parallel. In this way, the total thermal resistance of a TE couple is actually a reciprocal of the sum of thermal conductance of the P and N-type elements (shown in Eq. (35)) [45].

$$\psi_{TE}(x) = \frac{1}{\frac{1}{\psi_P(x)} + \frac{1}{\psi_N(x)}} = \frac{1}{\frac{k_P(T, x) \times A_P(x)}{\Delta x} + \frac{k_N(T, x) \times A_N(x)}{\Delta x}} \quad (35)$$

where, ψ means the thermal resistance. The subscripts (TE , P , and N) represent the TE couple, P and N-type elements, respectively.

Moreover, the Peltier heat just acts on the P and N junctions located at the two ends of a TE couple. Thus, the temperature distribution inside of a TE element can be modeled by the general differential equation of a one-dimensional steady-state thermal conductivity, shown as Eq. (36) [46].

$$\frac{1}{A(x)} \frac{d}{dx} \left[kA(x) \frac{dT}{dx} \right] + \dot{G} = 0 \quad (36)$$

in which, \dot{G} represents the source item. As for a TE element, the source item is produced from the Joule heat rate.

Through the finite difference method, the above differential equation can be discretized, making it possible to acquire the internal temperature distribution of a TE element. The discretized equation is expressed as Eqs. (37)-(39) [46].

As for $i=1$

$$f_1 = T_1 \left[\frac{A(x_2)k(T_2)}{\Delta x} + \frac{A(0)k(T_c)}{\Delta x} \right] - \left[T_2 \left[\frac{A(x_2)k(T_2)}{\Delta x} \right] + T_c \left[\frac{A(0)k(T_c)}{\Delta x} \right] + \dot{g}A(x_1)\Delta x \right] \quad (37)$$

$$= 0$$

As for $i=2$ to $n-1$

$$f_i = T_i \left[\frac{A(x_{i+1})k(T_{i+1})}{\Delta x} + \frac{A(x_{i-1})k(T_{i-1})}{\Delta x} \right] \quad (38)$$

$$- \left[T_{i+1} \left[\frac{A(x_{i+1})k(T_{i+1})}{\Delta x} \right] + T_{i-1} \left[\frac{A(x_{i-1})k(T_{i-1})}{\Delta x} \right] + \dot{g}A(x_i)\Delta x \right] = 0$$

As for $i=n$

$$f_n = T_n \left[\frac{A(L)k(T_h)}{\Delta x} + \frac{A(x_{n-1})k(T_{n-1})}{\Delta x} \right] \quad (39)$$

$$- \left[T_h \left[\frac{A(L)k(T_h)}{\Delta x} \right] + T_{n-1} \left[\frac{A(x_{n-1})k(T_{n-1})}{\Delta x} \right] + \dot{g}A(x_n)\Delta x \right] = 0$$

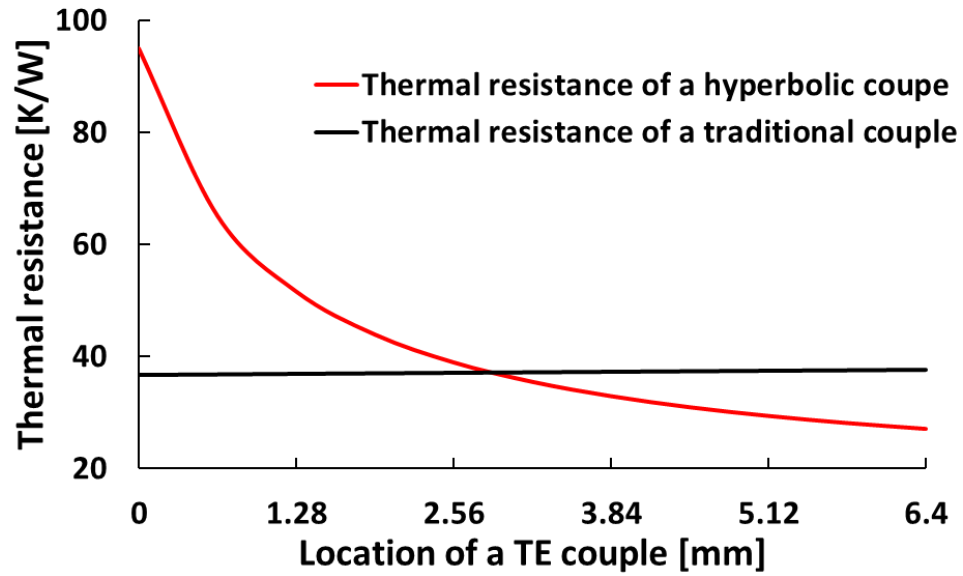
where, n is the number of nodes. \dot{g} is the Joule heat rate per unit volume, $[\text{W}/\text{m}^3]$. Δx is the unit length of a TE element.

Based on Eqs. (37)-(39), a sum formula can be established (as in Eq. (40)), which can be considered as an objective function (fun_2) for the MPSO algorithm. In this way, the unknown parameter, T_i , can be calculated by searching the minimal value of the objective function using the MPSO algorithm.

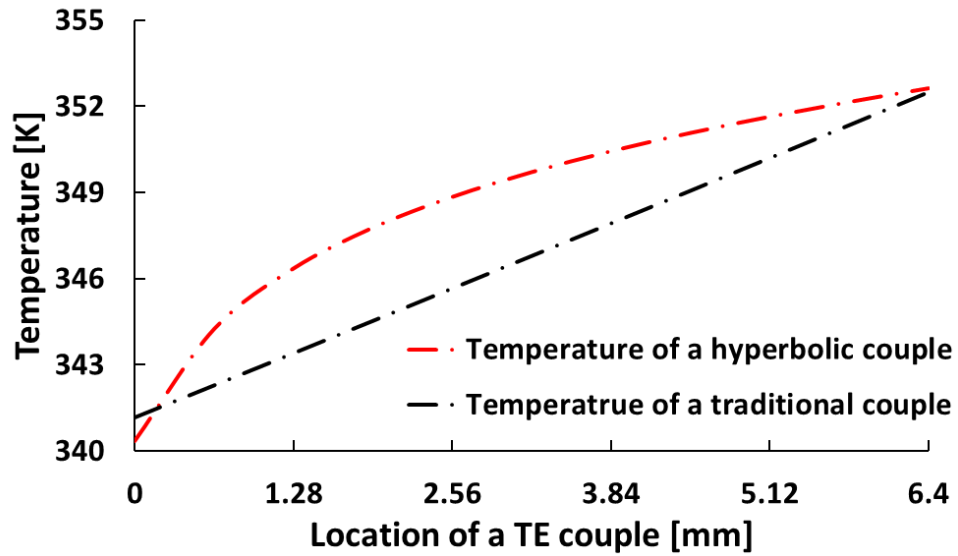
$$fun_2 = \min \left(\sum_{i=1}^n |f_i| \right) \quad (40)$$

In order to calculate thermal resistance conveniently, the TE couple was divided into 10 portions, namely $n=9$. In this way, the unit length of the TE element (Δx) was 0.64 mm. Figure 4.7 shows the thermal resistance and temperature distribution into the variable cross-sectional TE

elements (its shape parameter (β) and area ratio (μ) are 1) and traditional ones. In the figures, the origin corresponds to the cold end of the TE couple.



(a)



(b)

Figure 4.7. Internal thermal resistance and temperature distribution in the two different shapes of the TE couple

The results indicate (shown in Figure 4.7-(a)) that the thermal resistance of the hyperbolic couple is bigger than that of the traditional couple nearby the cold side, due to contraction of the area. Therefore, in the hyperbolic couple, the thermal energy is more difficult to transfer to the cold side compared to the traditional couple, making the cold temperature closer to the ambient as shown in Figure 4.7-(b). Meanwhile, it can be found from Figure 4.7-(b) that the hot temperature in the two TE shape designs is almost the same. In this way, the hyperbolic TE couple has a higher temperature difference and power output compared with the traditional couple, which is the basic reason why the TEG with non-constant area can have a higher performance.

4.3.2 Effects of working conditions on the performance of the variable cross-sectional TEG module

TEG performance is very sensitive to the variations of the working conditions, such as temperature and load resistance. Using the comprehensive thermodynamic model, both the thermal and electrical processes of a TEG module vary according to the working conditions. Hence, it is necessary to analyze the effects of the working conditions on the TEG performance. There are two non-dimensional parameters related to the working conditions concerned in this study, the resistance ratio (r_x) and temperature ratio (θ). First, the variation of the power and efficiency with the resistance ratio can be acquired through a slice of Figure 4.5 at a specific temperature ratio (Figure 4.8). The results indicate that the influences of the resistance ratio on the output power and efficiency of the TEG are non-monotonic. In a simplified TEG model (the hot and cold temperature are fixed), the TEG can be considered as a battery system, in which the relationship of the output power and resistance ratio is parabolic. Mathematically, when the resistance ratio is 1, the outpower will reach the maximum value. However, in the comprehensive TEG model, the output power of a TEG is normally decided by the electrical and thermal transfer processes because the real hot and cold temperature may vary across to the resistance ratio. When increasing the resistance ratio appropriately, the temperature difference at the two ends of a TEG can be enlarged, which has a positive effect on the output power. In this way, in the comprehensive TEG model, the optimal resistance ratio is ways greater than 1.

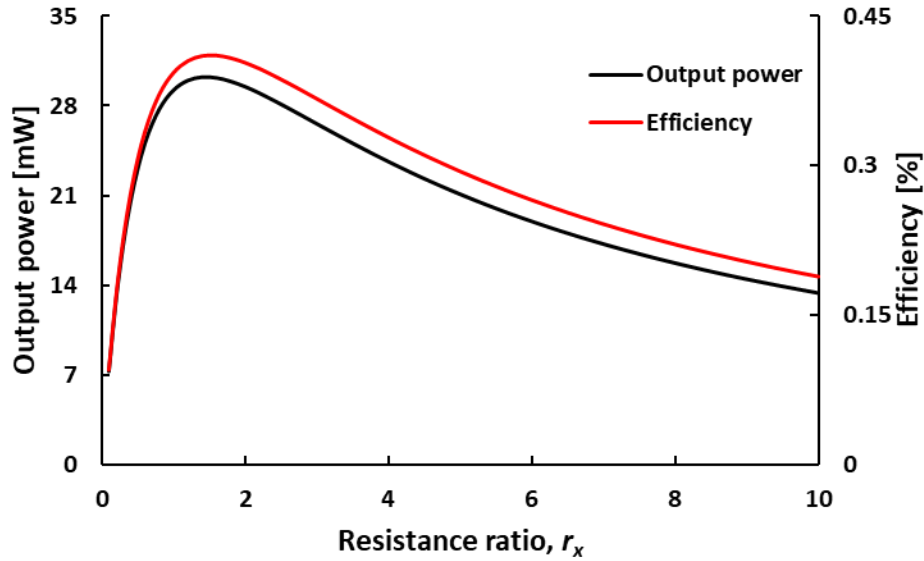


Figure 4.8. Variation of the output power and efficiency of the TEG with the load resistance ratio at a temperature ratio of 1.2

Likewise, the variation of the TEG's performances with the temperature ratio can be obtained through a slice of Figure 4.5 at a specific resistance ratio (Figure 4.9). The results show the performances of the TEG module can not be always improved through increasing temperature ratio only. There is a temperature ratio for maximum the power and efficiency of the TEG module.

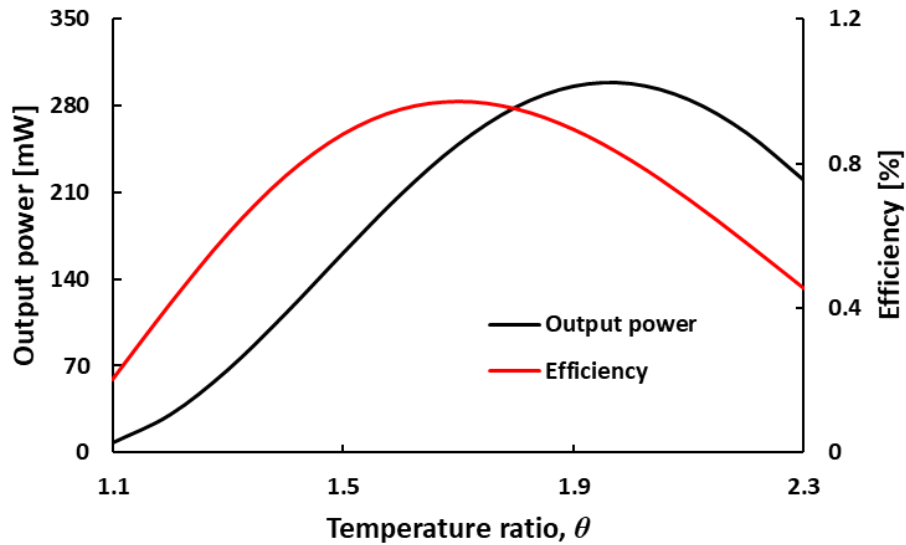


Figure 4.9. Variation of the output power and efficiency of the TEG with the temperature ratio at a resistance ratio of 1.5

The main reasons can be explained by Figure 4.10 which describes the variation of the real temperature at the ends of the TE couples with different temperature ratios. The real temperature difference at both the ends of the TEG experiences an obvious increase with the temperature ratio growth, which is the main reason for the TEG performance improvement at the early stage of Figure 4.9. Additionally, the temperature should match with the TE materials' properties in order to fully develop their thermoelectric performance. According to Figure 4.2, the recommended temperature should be in the range of 300 K and 500 K due to the TE materials equipped with an excellent ZT value under the conditions. However, with the temperature ratio increasing further, the real temperature at both the ends of the TE couples gradually deviates from the recommended range, and ZT decreases (Figure 4.2). When the enlarged temperature difference fails to compensate for the decreasing ZT , the TEG's performance will degrade.

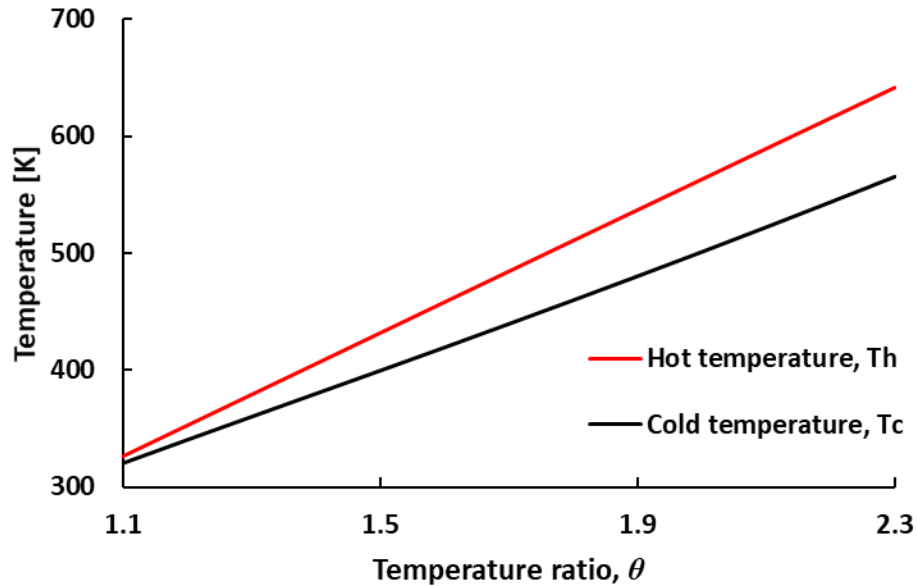


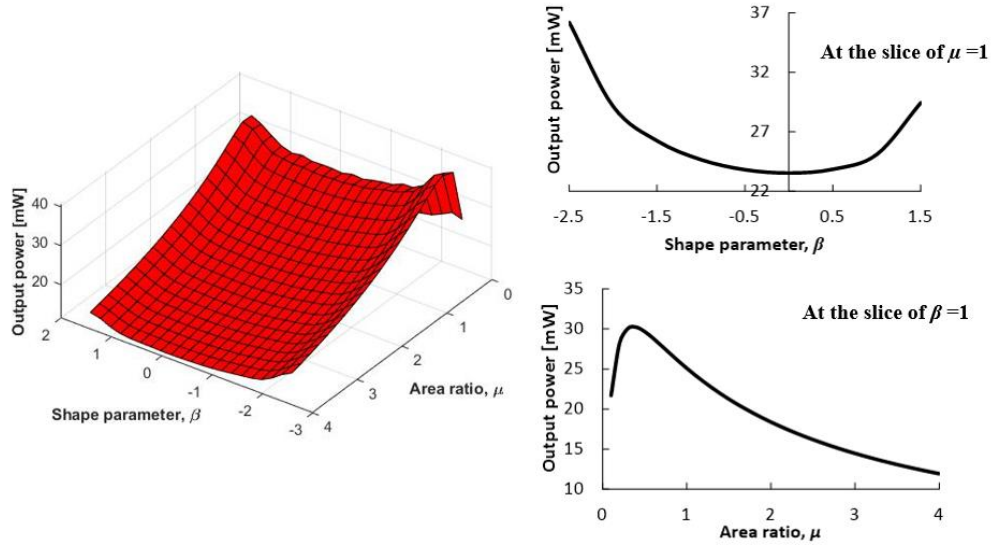
Figure 4.10. Variation of the real temperature at the ends of the TE element with different temperature ratios at a resistance ratio of 1.5

4.3.3 Effects of geometric structure on the performance of the variable cross-sectional TEG module

Based on the study mentioned in section 3.1, the variation of the cross-sectional area can lead to a difference in thermal resistance at the ends of the TE couples, enlarging the temperature difference. This is the main reason why the TEG performances can be improved by the variable cross-sectional element design. According to Eqs. (8)-(9), the cross-sectional functions can be described by the two non-dimensional parameters: shape parameter (β) and area ratio (μ).

Therefore, the studies focus on the influences of the shape parameter and area ratio on the TEG performances in the following part.

Figure 11 displays the variation of the output power (Figure 4.11-(a)) and efficiency (Figure 4.11-(b)) of the TEG with different shape parameters and area ratios (here, the temperature ratio and resistance ratio are 1.2 and 1.5). When the design for a cross-sectional TEG module, the minimum area should be greater than zero. Thereinto, considered the feasibility of the manufacture, the shape parameter (β) should be in the range of -2.5 and 1.5. As can be seen, the variation of the cross-sectional area for a high absolute value of the shape parameter ($|\beta|$) is more dramatic than in that of a low $|\beta|$, thereby making the temperature difference enlargement more obvious. Therefore, as indicated in the results, when the absolute value of the shape parameter ($|\beta|$) increases, both the power and efficiency of the TEG can be improved simultaneously. Meanwhile, it is noticeable that when the value of $|\beta|$ stays the same, the power generation and efficiency of the TE element for a positive β are a little bit higher than that for a negative β . The main reason is that compared to a negative β , a positive β can make a TE element have a smaller minimum cross-sectional area (it can be proven through Eqs. (8) or (9)), which can enlarge the temperature difference further even under a same value of $|\beta|$.



(a)

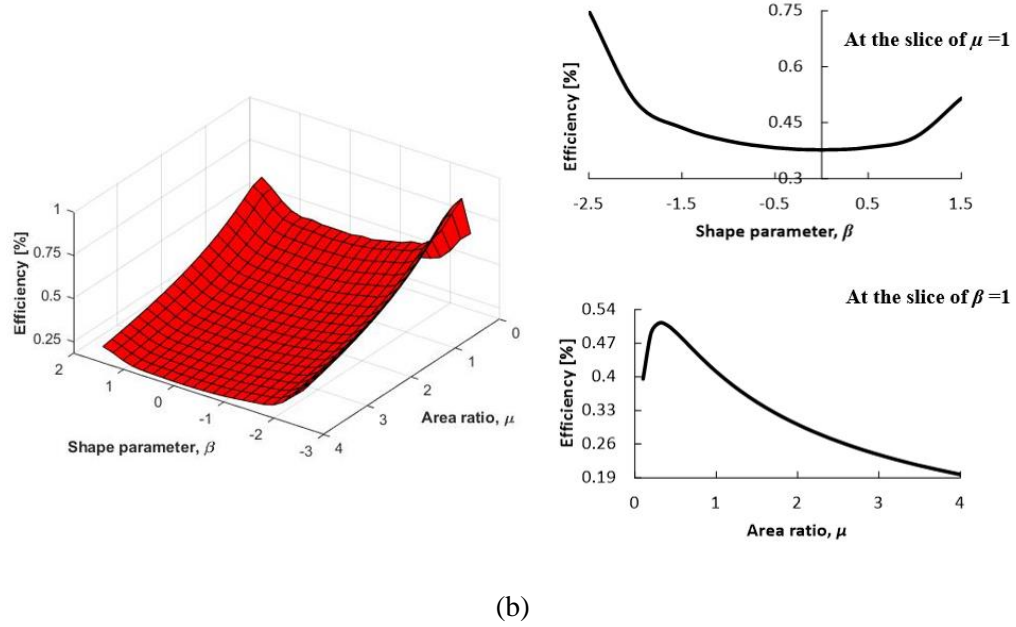


Figure 4.11. Variation of the performance of the TEG with different shape parameters and area ratios at $\theta=1.2$ and $r_x=1.5$, (a) variation of the output power, and (b) variation of the efficiency

Moreover, it can be seen from Figure 4.11 that the effects of the area ratio on the TEG's performance are non-monotonic. Meanwhile, the optimal area ratio for both the power and efficiency of the TEG is below 1 which means that compared with N-type material, the P-type should have a larger proportion in a TE couple to make the power and efficiency reach the optimum. The ZT value of the P-type material is, in general, higher than that of the N-type as shown in Figure 4.2. Therefore, in order to fully develop the thermoelectric performances of this TE material combination, the proportion of P-type material should be more than that of N-type.

4.4 Optimization the variable cross-sectional TEG module's performances based on the Dual-MPSO algorithm

The studies from the previous sections have indicated that the four non-dimensional parameters (temperature ratio (θ), resistance ratio (r_x), shape parameter (β), and area ratio (μ)) have considerable, but non-monotonic influences on the variable cross-sectional TEG module's output power and efficiency. Therefore, it is worthwhile to apply an algorithm to acquire the parameter combinations which can make the TEG module's output power and efficiency reach optima, respectively. Since a comprehensive thermodynamic model was considered in this study, it is necessary to solve the control equations before evaluating the fitness by the objective function in every iteration during the optimizing process. In this way, a dual-MPSO algorithm (its

flow chart can be displayed in Figure 4.12) was used in this paper to optimize the TEG's performance.

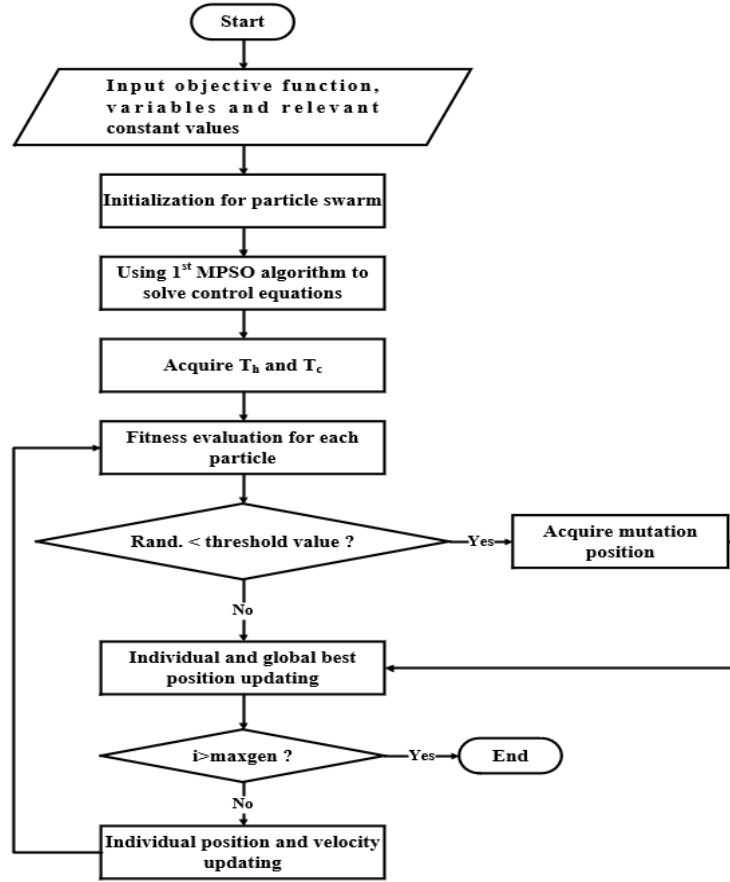


Figure 4.12. Flow chart of the M-PSO method

Based on the flow chart, in order to ensure correct optimizing direction and searching space, the objective functions, and the relevant variable ranges should be established before doing the research. The aims are to maximize the output power and efficiency for the variable cross-sectional TEG module. In this way, according to the power calculating equation (Eq. (3)), the objective function for the power generation (fun_{power}) for the TEG module can be build as shown in Eq. (37).

$$fun_{power}(\beta, \mu, \theta, r_x) = \max \left(\frac{S^2(T_h - T_c)^2 N_{pair}^2}{R_i(1 + r_x)^2} r_x \right) \quad (37)$$

Likewise, based on the efficiency calculating equation (Eq. (34)), the expression of the objective function for the efficiency ($fun_{efficiency}$) for the TEG module is displayed in Eq. (38).

$$fun_{efficiency}(\beta, \mu, \theta, r_x) = \max \left(\frac{\psi_h S^2 (T_h - T_c)^2 N_{pair}^2}{R_i (1 + r_x)^2 (\theta \times T_\infty - T_h)} r_x \right) \quad (38)$$

Meanwhile, the scopes of the variables in the two control equations can be found in Table 4.4.

Table 4.4. Relevant variables and their value ranges

| Variable | Value range |
|------------------------------------|----------------------------|
| Shape parameter (β): | $-2.5 \leq \beta \leq 1.5$ |
| Area ratio (μ): | $0.1 \leq \mu \leq 4$ |
| Temperature ratio (θ): | $1 \leq \theta \leq 2.3$ |
| Resistance ratio (r_x): | $0.1 \leq r_x \leq 10$ |

After the initialization of the particle swarm, the 1st MPSO algorithm was applied to solve the control equations, which solved for the temperature (T_h and T_c) at both the ends of the TE couple. Then, following the step of the 2nd MPSO method, the fitness was evaluated by the objective functions, making it possible to obtain the individual and global best position for later generations. Additionally, if the mutation condition (Rand. < threshold value) was triggered, a mutation was generated to improve the randomization for the algorithm. Finally, if the iteration step was lower than the maximum step, each new generation particles' position and velocity was created by the updating equations. Meanwhile, the 1st MPSO was applied to calculate the T_h and T_c in every iteration.

The optimizing processes of the output power and efficiency of the TEG module are displayed in Figure 4.13. The results indicate that after 22 and 10 steps, the output power and efficiency converge at about 554 mW and 2.17%, respectively. The relevant configurations for the optimal power and efficiency can be found in Table 4.5.

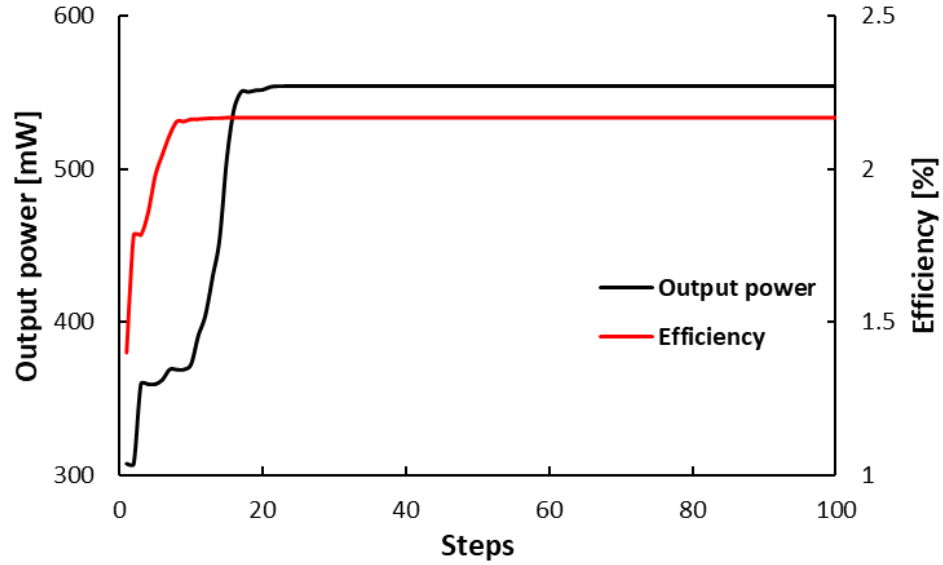


Figure 4.13. Convergence of the output power and efficiency optimizations

Table 4.5. Optimized working conditions and geometric structure configurations of the TEG

| Objective fun. | Optimal value | Shape parameter (β) | Area ratio (μ) | Temperature ratio (θ) | Resistance ratio (r_x) |
|----------------|---------------|-----------------------------|----------------------|--------------------------------|----------------------------|
| Output power | 554.18 mW | -2.5 | 0.51 | 2.07 | 1.24 |
| Efficiency | 2.17% | -2.5 | 0.42 | 1.75 | 1.43 |

Finally, it is noticeable that the single-objective optimizing results are anchor points of the Pareto frontier in the multi-objective problem. Therefore, the optimizing results in this paper will provide an important reference for the future research about the multi-objective optimization and technique for order preference by similarity to an ideal solution (TOPSIS) analysis for the hyperbolic TEG based on the comprehensive thermodynamic model.

4.5 Conclusions

In this paper, a hyperbolic function was introduced to design a variable cross-section TEG module. Based on a comprehensive thermodynamic model, the two control equations were established for the ends of the TE couples. Through solving the control equations by the MPSO

algorithm, the real temperature at both ends of the TE couples were calculated, making it possible to evaluate the TEG performance. Then, the differences in the power generation and efficiency of the newly designed TEG and a traditional one were compared. The essences of the differences can be analyzed in depth through the aspect of the internal thermal resistance. Additionally, the research indicates that the four non-dimensional parameters, shape parameter (β), area ratio (μ), temperature ratio (θ), and resistance ratio (r_x) have noticeable influences on the power generation and efficiency of the variable cross-section TEG module. In this way, the Dual- MPSO algorithm was applied to optimize the performances for the TEG module in the searching space consisting of the four parameters. The main conclusions of this work are as follows:

- 1) Compared to the traditional shape, the hyperbolic TE element is an effective design to improve the power generation and efficiency of a TEG module. The thermal resistance analysis indicates that the changing cross-sectional area can lead to the variation of the thermal resistance, making it possible to enlarge the temperature difference across the TE couple. This is the main reason that the performance of the TEG module can be improved by the hyperbolic shape design.
- 2) In the comprehensive thermodynamic model, the performance of the TEG failed to be improved through increasing the temperature ratio blindly. Initially, the real temperature difference between the two ends of the TE element can be enlarged with the temperature ratio growth, making it possible to improve the TEG performance. However, with the temperature ratio increasing further, the working temperature mismatch with the TE properties gradually to reduce the figure of merit (ZT). When the enlarging temperature difference fails to compensate for the performance loss due to the mismatch, the high-temperature ratio will have negative influences on the TEG's power generation and efficiency.
- 3) The research also verifies that there is an optimal resistance ratio for the power generation and efficiency of the TEG. The optimal value of the resistance ratio for both the power generation and efficiency is more than 1. In the comprehensive thermodynamic model, the TEG performance can be determined by the electrical and thermal processes simultaneously. In this way, the TEG can not be considered as a pure battery only, which is the main reason for the optimal resistance ratio of more than 1.
- 4) The effects of the shape parameter on the TEG's performance cannot be ignored. Normally, the variation of the cross-sectional area will increase with the absolute value of the shape parameter growth, which can intensify the difference in the thermal resistance in

a TE element. In this way, based on the findings mentioned in the first point, the performance of the TEG can be improved by increasing the absolute value of the shape parameter. In addition, it is noticeable that when the $|\beta|$ has a same value, the positive β is more preferable, compared to the negative one.

- 5) There is an optimal area ratio for the power generation and efficiency of the TEG, the value of which is below 1. When the length of a TE element remains unchanged, the area ratio actually represents the proportion of the P and N materials in the TEG system. The thermoelectric properties of the P-type material in this TEG module are superior to that of the N-type. It means that the TEG's performances can also be improved by increasing the proportion of the P-type material appropriately. Therefore, the optimal area ratios for both the power generation and efficiency of the TEG are below 1.
- 6) Finally, in order to conduct the optimization for the TEG based on the comprehensive model, it is necessary to solve the control equations in every optimizing iteration. In this way, the Dual-MPSO method was applied to this study. After the optimization, the optimal power and efficiency are about 554 mW and 2.17%, respectively.

Acknowledgments

This work was made possible by funding from the Natural Sciences and Engineering Research Council of Canada.

References

- [1] International Energy Agency (IEA, 2020), [Online], World Energy Outlook 2020, <https://www.iea.org/reports/world-energy-outlook-2020>. Accessed 10, May 2021.
- [2] S. A. Kalogirou, Solar energy engineering: processes and systems, 2nd Ed. Elsevier, UK: Oxford, 2014.
- [3] Y. V. Fan, H. H. Chin, J. J. Klemeš, P. S. Varbanov and X. Liu, "Optimisation and process design tools for cleaner production," Journal of Cleaner Production, vol. 247, p. 119181, February 2020.
- [4] International Energy Agency (IEA, 2019), [Online], Energy Efficiency 2019, <https://www.iea.org/reports/energy-efficiency-2019>. Accessed 10, May 2021.
- [5] G. Li, S. Shittu, T. M. O. Diallo, M. Yu, X. Zhao, and J. Ji, 'A review of solar photovoltaic-thermoelectric hybrid system for electricity generation', Energy, vol. 158, pp. 41–58, September 2018.

- [6] Y. Du, J. Chen, Q. Meng, Y. Dou, J. Xu and S. Z. Shen, "Thermoelectric materials and devices fabricated by additive manufacturing," *Vacuum*, vol. 178, p. 109384, August 2020.
- [7] Q. Du, X. Jiang, X. Zhang and J. Gao, "Influence of structure parameters on performance of the thermoelectric module," *Journal of Wuhan University of Technology-Mater. Sci. Ed.*, vol. 26 (3), pp. 464–468, June 2011.
- [8] B. Jang, S. Han and J. Y. Kim, "Optimal design for micro-thermoelectric generators using finite element analysis," *Microelectronic Engineering*, vol. 88 (5), pp. 775–778, May 2011.
- [9] J. Wang, Y. Li, C. Zhao, Y. Chai, L. Zhu, C. Zhang, J. Wang, W. Zhao and P. Cao, "An optimization study of structural size of parameterized thermoelectric generator module on performance," *Energy Conversion and Management*, vol. 160, pp. 176–181, March 2018.
- [10] G. E. Hoyos, K. R. Rao and D. Jerger, "Fast transient response of novel Peltier junctions," *Energy Conversion*, vol. 17 (1), pp. 45–54, February 1977.
- [11] M. Guo, D. Gu, L. Xi, H. Zhang, J. Zhang, J. Yang and R. Wang, "Selective laser melting additive manufacturing of pure tungsten: Role of volumetric energy density on densification, microstructure and mechanical properties," *International Journal of Refractory Metals and Hard Materials*, vol. 84, p. 105025, November 2019.
- [12] A. Z. Sahin and B. S. Yilbas, "The thermoelement as thermoelectric power generator: Effect of leg geometry on the efficiency and power generation," *Energy Conversion and Management*, vol. 65, pp. 26–32, January 2013.
- [13] Y. Shi, D. Mei, Z. Yao, Y. Wang, H. Liu and Z. Chen, "Nominal power density analysis of thermoelectric pins with non-constant cross sections," *Energy Conversion and Management*, vol. 97, pp. 1–6, June 2015.
- [14] Y. Wu, J. Yang, S. Chen and L. Zuo, "Thermo-element geometry optimization for high thermoelectric efficiency," *Energy*, vol. 147 (15), pp. 672–680, March 2018.
- [15] H. B. Liu, J. H. Meng, X. D. Wang and W. H. Chen, "A new design of solar thermoelectric generator with combination of segmented materials and asymmetrical legs," *Energy Conversion and Management*, vol. 175 (1), pp. 11–20, November 2018.
- [16] D. R. Karana and R. R. Sahoo, "Influence of geometric parameter on the performance of a new asymmetrical and segmented thermoelectric generator," *Energy*, vol. 179 (15), pp. 90–99, July 2019.
- [17] H. Ali, B. S. Yilbas and A. A. Sharafi, "Segmented thermoelectric generator: exponential area variation in leg," *International Journal of Energy Research*, vol. 42 (2), pp. 477–489, February 2018.
- [18] J. H. Meng, X. X. Zhang and X. D. Wang, "Multi-objective and multi-parameter optimization of a thermoelectric generator module," *Energy*, vol. 71 (15), pp. 367–376, July 2014.

- [19] Z. Liu, S. Zhu, Y. Ge, F. Shan, L. Zeng and W. Liu, "Geometry optimization of two-stage thermoelectric generators using simplified conjugate-gradient method," *Applied Energy*, vol. 190 (15), pp. 540–552, March 2017.
- [20] M. Ranjan and T. Maiti, "Device modeling and performance optimization of thermoelectric generators under isothermal and isoflux heat source condition," *Journal of Power Sources*, vol. 480 (31), p. 228867, December 2020.
- [21] L. Zhu, H. Li, S. Chen, X. Tian, X. Kang, X. Jiang and S. Qiu, "Optimization analysis of a segmented thermoelectric generator based on genetic algorithm," *Renewable Energy*, vol. 156, pp. 710-718, August 2020.
- [22] A. Yusuf, N. Bayhan, A. A. Ibrahim, H. Tiryaki and S. Ballikaya, "Geometric optimization of thermoelectric generator using genetic algorithm considering contact resistance and Thomson effect," *International Journal of Energy Research*, vol. 45 (6), pp. 9382-9395, May 2021.
- [23] Y. D. Valle, G. K. Venayagamoorthy, S. Mohagheghi, J. C. Hernandez and R. G. Harley, "Particle swarm optimization: Basic concepts, variants and applications in power systems," *IEEE Transactions on Evolutionary Computation*, vol. 12 (2), pp. 171–195, April 2008.
- [24] A. Dener, A. Denchfield and T. Munson, "Preconditioning nonlinear conjugate gradient with diagonalized quasi-newton," *PASC '19: Proceedings of the Platform for Advanced Scientific Computing Conference*, pp. 1–7, June 12–14, 2019.
- [25] Y. J. Gong, J. J. Li, Y. Zhou, Y. Li, H. S-H. Chung, Y. H. Shi and J. Zhang, "Genetic Learning Particle Swarm Optimization," *IEEE Transactions on Cybernetics*, vol. 46 (10), pp. 2277–2290, October 2016.
- [26] Q. Zhang, R. M. Ogren and S. C. Kong, "A comparative study of biodiesel engine performance optimization using enhanced hybrid PSO–GA and basic GA," *Applied Energy*, vol. 165, pp. 676–684, March 2016.
- [27] R. Yang, Y. Yuan, R. Ying, B. Shen, and T. Long, "A Novel Energy Management Strategy for a Ship's Hybrid Solar Energy Generation System Using a Particle Swarm Optimization Algorithm," *Energies*, vol. 13 (6), p. 1380, March 2020.
- [28] M. Gomez, R. Reid, B. Ohara and H. Lee, "Influence of electrical current variance and thermal resistances on optimum working conditions and geometry for thermoelectric energy harvesting," *Journal of Applied Physics*, vol. 113, p. 174908, May 2013.
- [29] F. Yang, M. Gao, J. Cong and P. Wang, "System dynamics modeling and experimental study of railway track with thermoelectric heater/generator in extreme weather conditions" *Journal of Cleaner Production*, vol. 249 (10), p. 119367, March 2020.
- [30] E. Bellos and C. Tzivanidis, "Energy and financial analysis of a solar driven thermoelectric generator" *Journal of Cleaner Production*, vol.264 (10), p. 121534, August 2020.

- [31] D. Champier, J. P. Bédécarrats, T. Kousksou, M. Rivaletto, F. Strub and P. Pignolet, "Study of a TE (thermoelectric) generator incorporated in a multifunction wood stove," *Energy*, vol. 36 (3), pp. 1518–1526, March 2011.
- [32] A. F. Ioffe, L. S. Stil'bans, E. K. Iordanishvili, T. S. Stavitskaya, and A. Gelbtuch, "Semiconductor thermoelements and thermoelectric cooling," *Physics Today*, vol. 12 (5), p. 42, May 1959.
- [33] H. Jouhara, A. Żabnieńska-Góra, N. Khordehgah, Q. Doraghi, L. Ahmad, L. Norman, B. Axcell, L. Wrobel and S. Dai, "Thermoelectric generator (TEG) technologies and applications," *International Journal of Thermofluids*, vol. 9, p. 100063, February 2021.
- [34] Y. Kishita, Y. Ohishi, M. Uwasu, M. Kuroda, H. Takeda and K. Hara, "Evaluating the life cycle CO₂ emissions and costs of thermoelectric generators for passenger automobiles: a scenario analysis," *Journal of Cleaner Production*, vol. 126 (10), pp. 607–619, July 2016.
- [35] K. Yazawa, J. H. Bahk and A. J. Ghajar, *Thermoelectric energy conversion devices and systems*, vol. 7, World Scientific, UK: London, 2021.
- [36] Z. H. Dughaish, "Lead telluride as a thermoelectric material for thermoelectric power generation," *Physica B: Condensed Matter*, vol. 322 (1-2), pp. 205–223, September 2002.
- [37] J. D'Angelo, E. D. Case, N. Matchanov, C. Wu, T. P. Hogan, J. Barnard, C. Cauchy, T. Hendrick and M. G. Kanatzidis, "Electrical, thermal, and mechanical characterization of novel segmented-leg thermoelectric modules," *Journal of Electronic Materials* volume, vol. 40, pp. 2051–2062, August 2011.
- [38] E. Kanimba, M. Pearson, J. Sharp, D. Stokes, S. Priya and Z. Tian, "A comprehensive model of a lead telluride thermoelectric generator," *Energy*, vol. 142, pp. 813–821, October 2017.
- [39] D. Patil, R. Arakerimath and P. Walke, "Thermoelectric materials and heat exchangers for power generation – A review," *Renewable and Sustainable Energy Reviews*, vol. 95, pp. 1–22, July 2018.
- [40] Coolinnovations, [Online], Sparse Configuration| Aluminum, <http://www.coolinnovations.com/datasheets/3-4141XXM.pdf>. Accessed 10, May 2021.
- [41] M. Clerc, *Particle swarm optimization*, 1st Ed. John Wiley & Sons, UK: London, 2010.
- [42] Q. Bai, "Analysis of particle swarm optimization algorithm," *Computer and information science*, vol. 3 (1), pp. 180–184, February 2010.
- [43] X. Wang, D. S. -K. Ting and P. Henshaw, "Mutation particle swarm optimization (M-PSO) of a thermoelectric generator in a multi-variable space," *Energy Conversion and Management*, vol. 224 (15), p. 113387, November 2020.

- [44] G. Xu, Q. Cui, X. Shi, H. Ge, Z. H. Zhan, H. P. Lee, Y. Liang, R. Tai and C. Wu, “Particle swarm optimization based on dimensional learning strategy,” *Swarm and Evolutionary Computation*, vol. 45, pp. 33–51, January 2019.
- [45] Y. A. Çengel and A. Shakouri, *Heat and mass transfer fundamentals and applications*, 5th Ed. McGraw Hill Education, USA: New York, 2015.
- [46] S. V. Patankar, *Numerical heat transfer and fluid flow*, 1st Ed. CRC Press., USA: New York, 1980.

CHAPTER 5

USING A HYPERBOLIC STRUCTURE TO ENHANCE THE DYNAMIC PERFORMANCE OF A THERMOELECTRIC GENERATOR

X. Wang, P. Henshaw, and D. S-K Ting, "Using a hyperbolic structure to enhance the dynamic performance of a thermoelectric generator," To be submitted

5.1 Introduction

The rapid rise of energy-intensive industries in the world has led to a long-term trend of increasing energy demand in the past decades. There was almost a threefold increase in energy consumption during the period from 1971 to 2018 [1]. Most of the energy was provided through fossil fuel combustion in this period [2, 3]. Due to the emissions of greenhouse gases during the combustion processes, a series of environmental problems, such as global warming, are threatening the existence of humans [4, 5]. In order to tackle the environmental crisis, many governments in the world have reached a consensus on carbon neutrality by 2050 [6]. However, the relevant statistics from the International Energy Agency (IEA) indicate that in the scenario of carbon neutrality, it is necessary to limit the growth of energy usage to less than 0.9% per year to 2030 [6]. In this way, except for energy mix changes, energy-saving technology, such as thermal recovery systems, also have become the focus of investment in recent years. Thermoelectrical generators (TEGs) are a kind of solid-state energy device, which can convert wasted heat to electrical power without producing any carbon emissions [7]. TEGs are considered as having a huge potential in the thermal recovery field, thereby, attracting the attention of many researchers.

It is probably worthwhile to mention that most studies on TEG are steady state whereas this is seldom the case in reality [8, 9]. In other words, the dynamic behavior is important. Chen *et al.* [10] established a transient model to investigate a TEG's performance under oscillating temperatures at the hot and cold sides. They found that the mean power output and efficiency of the TEG can be improved obviously through increasing delay between the temperature variations at the cold and hot sides [10]. Based on the transient model, Chen *et al.* [11] also verified that the amplitude of the oscillating temperature has a crucial effect on the power output [11]. According to the results, there is an 18% increase in the output power of the TEG when the temperature amplitude is raised from 0 K to 75 K [11].

Additionally, a TEG's performance under transient operation is not only affected by the variations of the source temperature, but is susceptible to its geometric structure. Jia *et al.* [12] built a transient model for a linear-shaped thermoelectrical generator (L-TEG), in which the P-type leg and N-leg are placed horizontally. A shape parameter (θ), the ratio of the length of P-type legs to the total length of TE legs, was used to describe the geometric characteristics of the L-TEG. In both the linear and exponential heating processes for the TEG, they found that a lower shape parameter can lead to a more obvious shock effect on the power output, and prolong the response time of the power to the heating process [12].

It is worth noting that semiconductor processing technology has developed at an astounding pace, making it possible to produce TEG legs with complex shapes, such as variable cross-section structures [13]. Recently, research related to the variable cross-section TEG under a steady-state condition was reported. Through modeling for a tapered TEG, Sahin, and Yilbas [14] verified that the tapered structure had advantages in improving thermoelectrical conversion efficiency. Meanwhile, Shi *et al.* [15] found that both the power output and efficiency of a tapered TEG was the highest compared to two other shape designs: quadratic and exponential. In addition, Liu *et al.* [16] derived the efficiency expression for constant and variable cross-section TEGs under eight kinds of thermal boundary conditions. Based on the analytical expression, they found that the variable cross-section structure always has a higher conversion efficiency compared to the traditional design (constant cross-section structure) [16]. A TEG consisting of X-legs (where the cross-section decreases and then increases along the length) was introduced by Ibeagwu [17]. The results indicated that the TEG with X-legs can boost the output power by 19.13% over the traditional leg shape [17]. Moreover, the research from Doraghi *et al.* [18] reported that compared to the traditional leg, a diamond-leg can increase the TEG output voltage under the same thermal boundary condition [18].

However, the research about the performance of a variable cross-section TEG under a dynamic thermal process, especially with a periodic heat source, is rarely reported. Moreover, the periodic thermal source can be found in many industrial processes, such as the Stirling engine and batch-type combustor in an incineration system [19, 20]. The temperature in these processes always oscillate periodically, which can be described by a sinusoidal function [19, 20]. In this way, there are practical significances to studying a variable cross-section TEG's performance under an oscillating thermal source temperature, which is the motivation for this research.

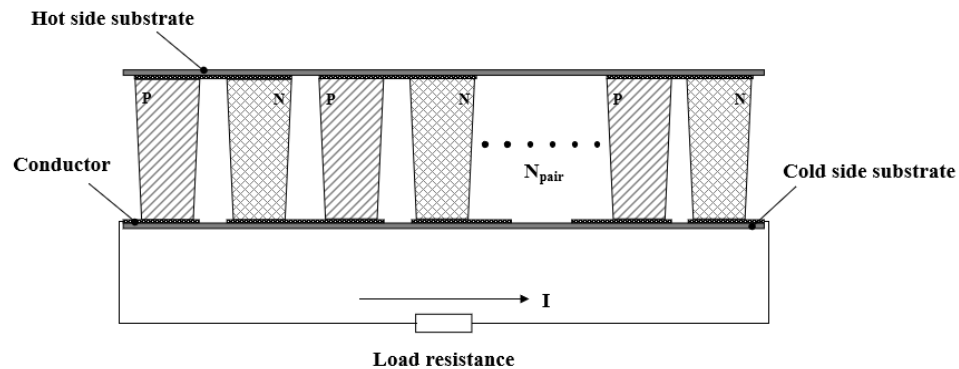
In this paper, a hyperbolic function was introduced as a variable cross-section TEG, while a sinusoidal varying thermal source was considered. Based on a transient model built in SIMULINK, differences in the transient performances between the hyperbolic and traditional TEGs under the oscillating source temperature were simulated. The mechanism causing the performance differences was explored by analyzing the hot and cold temperature variations of the two kinds of TEGs. Besides, some literature indicates that the features of the dynamic source temperature and the TEG's geometric structure have crucial influences on the TEG's performances [10-12]. In this way, this study investigated the hyperbolic TEG's performances, such as the mean power output and overall efficiency, under different periods of the oscillating temperature and TEG leg shape parameters.

5.2 TEG model established in SIMULINK

The working principle of a TEG is that the temperature difference causes the migrations of electrons and holes in the N and P semiconductors to form the current [21, 22]. In this way, a TEG model always consists of two different parts: thermal network structure and electrical network structure. A periodic thermal source, where the source temperature oscillates as a sinusoidal function, was considered as a thermal boundary condition for the TEG model.

5.2.1 Electrical network structure

Cascaded TE elements, conductors, and substrate are the basic components of a TEG module, as shown in Figure 5.1-(a). A TEG can produce a voltage under a temperature difference due to the migrations of electrons and holes in the semiconductors [21, 22]. When connecting a load, a current will be generated in the loop of the TEG system. In this way, the electrical process of a TEG can be simplified as a general DC power supply [23]. Figure 5.1-(b) is a sketch of the electrical network structure established in SIMULINK.



(a)

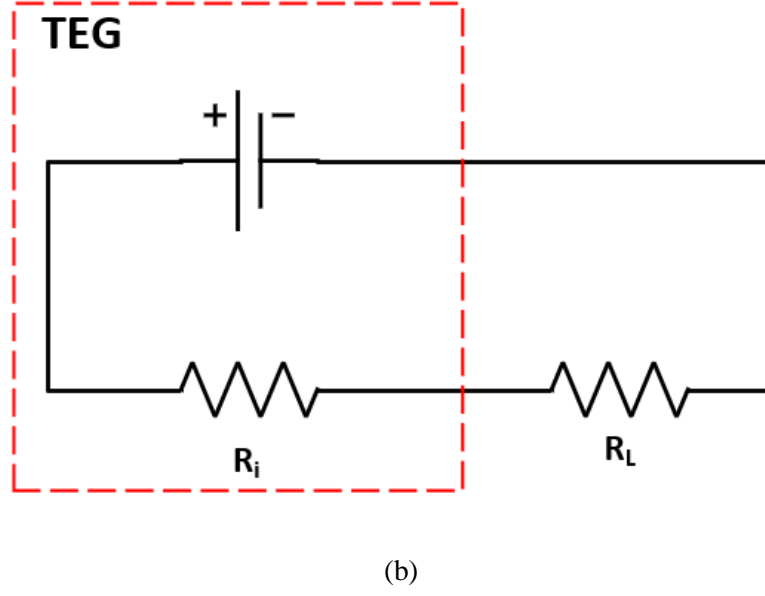


Figure 5.1. Schematic diagram of a TEG module, (a) cutaway view of a TEG module arrangement, and (b) equivalent circuit diagram of a TEG

According to the thermoelectric effect, a TEG's Seebeck voltage (V) is proportional to the temperature difference at its ends, which can be calculated from Eq. (1) [23-25].

$$V = S(T_h - T_c)N_{pair} \quad (1)$$

where N_{pair} is the number of TE couples, which is 199 pairs in this study. The hot and cold temperatures are presented as T_h and T_c . S is the overall Seebeck coefficient. Due to the empty holes and electronics equipped with positive and negative charges, the Seebeck coefficients of P-type and N-type materials have a positive and negative values, respectively. In this way, the value of S , which is used to evaluate the overall Seebeck effect, is a sum of the absolute values of the two materials' Seebeck coefficients, shown as Eq. (2).

$$S = S_p + |S_N| \quad (2)$$

where S_p and S_N are the Seebeck coefficients of P and N semiconductors, respectively.

The power supply process of a TEG is also consistent with Ohm's law. Thus, the current (I) in the loop is a ratio of the Seebeck voltage and the total resistance, that is,

$$I = \frac{V}{R_i + R_L} = \frac{SN_{pair}(T_h - T_c)}{R_i(1 + r_x)} \quad (3)$$

The output power is proportional to the square of the current and the load resistance (R_L) [23-25],

$$P = I^2(r_x R_i) = \frac{S^2 r_x (T_h - T_c)^2 N_{pair}^2}{R_i (1 + r_x)^2} \quad (4)$$

in which R_i is the internal resistance of a TEG, and r_x is the ratio of the load and internal resistance.

Normally, the internal resistance (R_i) of a TEG mainly consists of two different parts: the resistances of conductors (r_c) and TE couples (r_{teg}). For the resistance of conductors, their electrical resistance is proportional to the length and reciprocal of the cross-section area. Meanwhile, the welding resistances were considered in the TEG model. Thus, the total resistance of conductors can be calculated by Eq. (5)

$$r_c = \left(\frac{L_c}{\sigma_c A_c} \right) (2N_{pair} + 1) + r_{ct} \times 4N_{pair} \quad (5)$$

where the conductor's cross-sectional area and length are symbolized as A_c , L_c . r_{ct} and σ_c are the welding resistance and conductor's electrical conductivity.

The junction between the conductor and TE leg can be simplified in the model as an extra homogeneous layer, as shown in Figure 5.2-(a) [26]. In this way, Equation (6) can be used to evaluate the welding resistance [26].

$$r_{ct} = \frac{H_{ct}}{\sigma_{ct} A_{ct}} \quad (6)$$

in which H_{ct} and A_{ct} are the thickness and cross-section area of the extra homogeneous layer. The electrical conductivity of the extra homogeneous layer is symbolled as σ_{ct} . Based on the research of Qing *et al.* [26], value of σ_{ct} can be affected by the heat sink at the cold side of a TEG. As for a TEG system with a passive cooling format, the value is suggested to be 1.03×10^3 S/cm [26].

Similarly, the resistance of the semiconductor is proportional to the length and a reciprocal of the cross-section area. The resistance for an infinitesimal length for a TE couple is

$$dr_{TEG} = \left[\frac{1}{\sigma_P A_P(x)} + \frac{1}{\sigma_N A_N(x)} \right] dx \quad (7)$$

The total resistance can be obtained by integration along with the length of the element (L), [15, 27],

$$r_{TEG} = N_{pair} \int_0^L \left[\frac{1}{\sigma_P A_P(x)} + \frac{1}{\sigma_N A_N(x)} \right] dx \quad (8)$$

in which the cross-section area of the P-type and N-type elements are presented as $A_P(x)$ and $A_N(x)$. σ_P and σ_N are the electrical conductivities of the P-type and N-type materials.

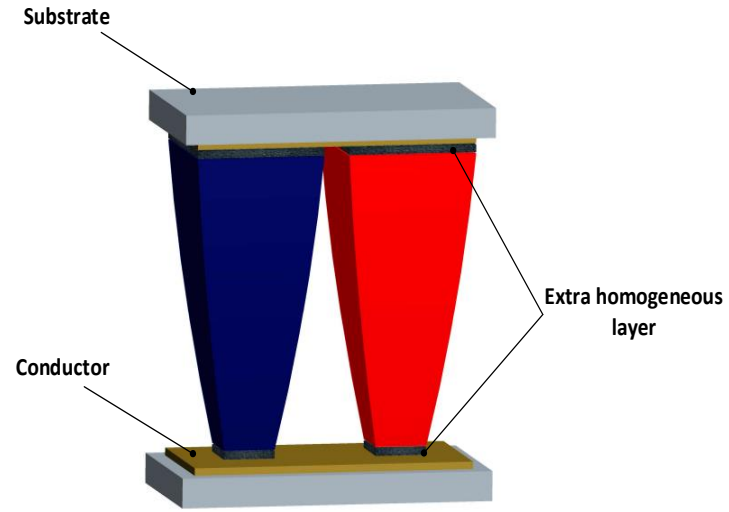
In this study, a novel variable cross-section TEG was defined by a hyperbolic function. The cross-section area of this TE element can be described as

$$A(x) = \frac{A_0}{2} + \beta A_0 \ln 2 - \frac{\beta A_0 L}{x + L} \quad (9)$$

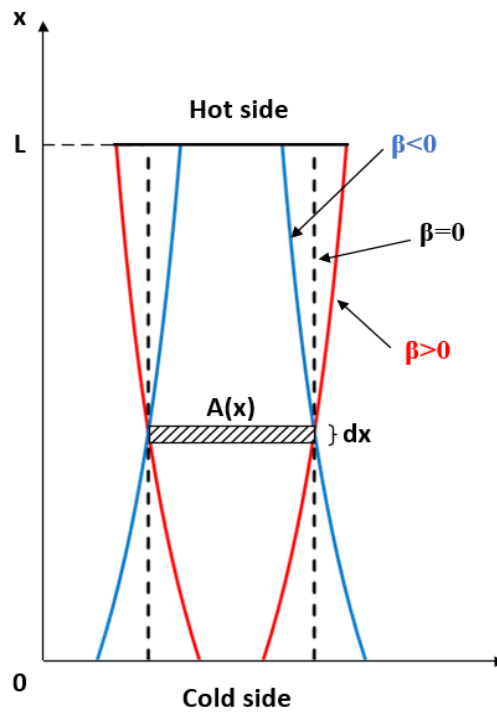
The volume of a pair of the hyperbolic elements can be held constant at $A_0 L$, while studying the effect of the shape (β).

where A_0 is the total average cross-sectional area of the P and N-type semiconductors, kept constant at 8 mm^2 in this study. In the hyperbolic TEG leg model, the minimum area should be greater than zero. Meanwhile, considering the feasibility of the manufacture, the shape parameter (β) was limited to the range of -2.5 and 1.5 in this study.

It is worth noting that the shape parameter, β , is used to describe the geometry of the TEG. According to Figure 5.2-(b), when the cross-sectional area decreases from the hot to the cold side, the value of β is bigger than zero. $\beta = 0$ means the cross-sectional area is constant. When the cross-sectional area increases from the hot to the cold side, the value of β is lower than zero.



(a)



(b)

Figure 5.2. Schematic diagram of the variable cross-section TE legs, (a) isometric view, and (b) longitudinal section

5.2.2 Thermal network structure

A transient heat transfer process in the TEG model was also simulated in SIMULINK by using an electrothermal analogy. Namely, a thermal transfer problem can be solved as an electrical circuit through this method. The electrothermal analogy can assist to understand many thermal processes visually through presenting them in circuit terms [23]. Meanwhile, due to the mathematical equivalence, a transient behavior in a thermal process can be solved and recognized by a circuit simulator [23]. Recently, some studies have been reported applying the electrothermal analogy to evaluate performance for a TEG [28-30].

The transient thermal transfer process of a TEG can be described by the general formula (as shown Eq. (10)) [31]

$$\dot{Q}_x - \dot{Q}_{x+\Delta x} + \dot{G}_{element} = \frac{\Delta E_{element}}{\Delta t} \quad (10)$$

in which ΔE , \dot{G} , and \dot{Q} represent the energy content variation rate, heat conduction rate, and heat generation rate.

There are three items in the general formula, which are heat flux item, heat generation item, and heat capacity item. In the electrothermal analogy, these three items are equivalent to current, DC current supply, and capacitor. Besides, the other two important elements in a thermal process, temperature and thermal resistance correspond to potential and resistance in the circuit.

The transient thermal model for the TE elements is displayed in Figure 5.3. In the model, the TEG is divided into n parts along the leg length direction. The local thermal resistance of each part is symbolled as $\psi_{TE}(x_i)$, which can be evaluated by Eq. (11) [15, 27]

$$\psi_{TE}(x) = \frac{1}{N_{pair} \left(\frac{\overline{k_P}}{\int_x^{x+\Delta x} \frac{1}{A_P(x)} dx} + \frac{\overline{k_N}}{\int_x^{x+\Delta x} \frac{1}{A_N(x)} dx} \right)} \quad (11)$$

where $\overline{k_P}$ and $\overline{k_N}$ are the average thermal conductivity of the P & N materials, respectively.

A TE element mainly consists of junction and inside parts shown as in Figure 5.3. For the junction parts, there are three kinds of thermal energy, which are the Fourier heat, Peltier heat, and Joule heat. The Fourier heat (\dot{Q}_F) can be considered as a ratio of the temperature difference and thermal resistance, shown as Eq. (12) [31]

$$\dot{Q}_F(x) = \frac{T(x + \Delta x) - T(x)}{\psi_{TE}(x)} \quad (12)$$

The current may cause a heat absorption or dissipation at a TE junction, which is named as Peltier heat (\dot{Q}_P). The Peltier heat is normally absorbed at the hot side, but released at the cold side of a TE element [23]. Equation (13) is the general expression of the Peltier heat [23]

$$\dot{Q}_P = SIT(x)N_{pair} \quad (13)$$

Meanwhile, when a current passes through a conductor or semiconductor, thermal energy will be produced due to its resistance, which is the Joule heat (\dot{Q}_J). The Joule heat can be calculated by Eq. (14)

$$\dot{Q}_J(x) = I^2 R_i(x) \quad (14)$$

In this way, based on Eq. (10), the transient thermal process at the junctions of a TE element can be described by the following equation (Eq. (15))

$$d\dot{Q} = \dot{Q}_F(x) - \dot{Q}_F(x + dx) = C_{TE}(x) \frac{dT(x)}{dt} - I^2 R_i(x) \pm SIT(x)N_{pair} \quad (15)$$

in which, $C_{TE}(x)$ is the local heat capacity, which can be calculated by Eq. (16)

$$C_{TE}(x) = \rho_{TE} V_{TE}(x) c_{th} \quad (16)$$

where c_{th} and ρ_{TE} are the specific heat and density of the TE elements, which are 155 J/kg·K and 8160 kg/m³, respectively [32]. $V_{TE}(x)$ represents the local of the TE elements' volume.

The Peltier effect just acts on the TE junctions. Therefore, the thermal energy movement inside of a TE element mainly consists of the Fourier heat and Joule heat. Equation (17) is used to control the transient heat process of internal TE elements [33]

$$d\dot{Q} = \dot{Q}_F(x) - \dot{Q}_F(x + dx) = C_{TE}(x) \frac{dT(x)}{dt} - I^2 R_i(x) \quad (17)$$

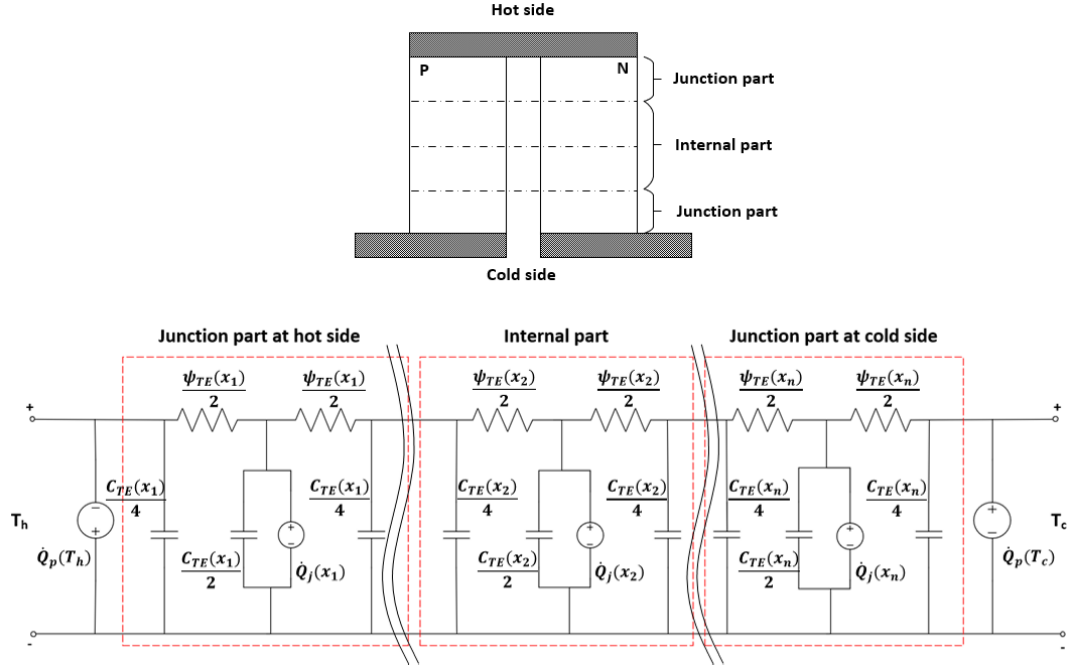


Figure 5.3. Schematic diagram of the thermal model for the TEG in the SIMULINK

Additionally, during the processes of absorbing energy from a thermal source and dissipating energy to the surroundings for a TEG, the heat energy may pass through several non-thermoelectric parts, such as the substrate and radiator. In order to improve the quality of the transient TEG model, some thermal resistances were considered in this paper. The thermal network of the non-thermoelectric parts in the SIMULINK is displayed in Figure 5.4.

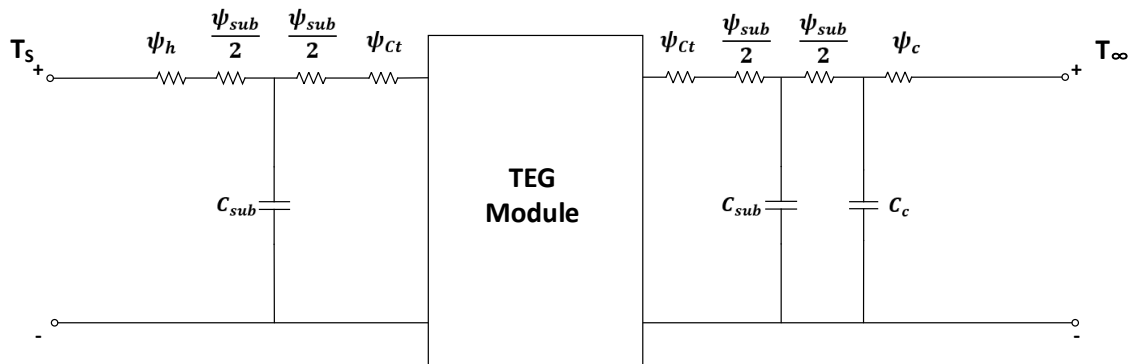


Figure 5.4. Schematic diagram of the thermal model for the non-thermoelectric parts in the SIMULINK

In the transient model, the thermal resistance of the substrates, heat reservoirs, and interfaces are presented as ψ_{sub} , $\psi_{h/c}$, and ψ_{ct} , respectively. Based on the theory of thermal conductivity, the thermal resistance of the substrate layer can be evaluated by Eq. (18)

$$\psi_{sub} = \frac{H_{sub}}{k_{sub}A_{sub}} \quad (18)$$

where H_{sub} and A_{sub} are the thickness and cross-section area of the substrate layer. The thermal conductivity of the substrate layer is marked as k_{sub} .

For a TEG, the hot side is attached to a thermal source [34]. Based on the research from Gomez *et al.* [34], the thermal resistance of the hot side (ψ_h) can be assumed as 1 K/W. Meanwhile, the heat sink on the cold side is a passive cooling format due to its cost-effectiveness and reliability. The radiator's configuration from the manufacturer indicates that the thermal resistance of the cold side is 5.5 K/W [35].

As it's known, there is a contact thermal resistance at every interface between adjacent materials. In a TE leg, these contact thermal resistances are connected in a series along with the heat transfer direction. In this way, these interfaces can be equivalent to an extra homogeneous layer at the hot and cold sides, respectively [26]. The contact thermal resistance (ψ_{ct}) on the layer can be calculated by Eq. (19)

$$\psi_{ct} = \frac{H_{ct}}{k_{ct}A_{ct}} \quad (19)$$

where the equivalent thermal conductivity of the extra homogeneous layer is denoted as k_{ct} . Referring the research of Qing *et al.* [26], the value of k_{ct} is 2.18 W/m·K.

5.2.3 Boundary conditions and physical qualities

This study mainly focuses on the transient behaviors of the hyperbolic TEG under a periodic temperature fluctuation. The source temperature (T_S) is varied by a sinusoidal function as shown Eq. (20)

$$T_S(t) = T_{S,0} + A_S \sin\left(\frac{2\pi t}{\lambda_S}\right) \quad (20)$$

in which A_S , $T_{S,0}$, t , and λ_S are the temperature of the amplitude, offset distance, time, and period. Thereinto, the values of A_S , $T_{S,0}$, and λ_S were 50 K, 423 K, and 60 mins, respectively.

Meanwhile, a constant temperature was used as the boundary condition at the cold reservoir, shown as Eq. (21)

$$T_{\infty}(t) = 300 \text{ K} \quad (21)$$

where T_{∞} is the ambient temperature.

Additionally, in the transient heat transfer problem, its initial temperature of the TEG is the same as the ambient temperature.

In addition, the two indices, the mean output power, and overall efficiency were introduced to evaluate the transient performance of the hyperbolic TEG under the oscillating source temperature. The mean power (\bar{P}) can be calculated by the total work and time (a total time of 18000 s was considered in the study) as shown in Eq. (22) [10, 11]. The overall efficiency (η) is defined by the ratio of the mean power output and mean input heat rate ($\overline{\dot{Q}_{input}}$), which is displayed by Eqs. (23) and (24) [10, 11]

$$\bar{P} = \frac{\int_{0s}^{3600s} P(t) dt}{\int_{0s}^{3600s} dt} \quad (22)$$

$$\overline{\dot{Q}_{input}} = \frac{\int_{0s}^{3600s} \frac{T_s(t) - T_h(t)}{\psi_h + \psi_{sub} + \psi_{ct}} dt}{\int_{0s}^{3600s} dt} \quad (23)$$

$$\eta = \frac{\bar{P}}{\overline{\dot{Q}_{input}}} = \frac{\int_{0s}^{3600s} P(t) dt}{\int_{0s}^{3600s} \frac{T_s(t) - T_h(t)}{\psi_h + \psi_{sub} + \psi_{ct}} dt} \quad (24)$$

in which $T_h(t)$ represents the temperature at the TEG's hot side.

5.2.4 Material properties

There are three important material properties related to the thermoelectric conversion performance, which are the Seebeck coefficient (S), electrical conductivity (σ), and thermal conductivity (k).

In this paper, the thermoelectric material for the TEG was modified bismuth telluride, for which the properties can be found in Table 5.1.

Table 5.1. Material properties of modified bismuth telluride [27, 36]

| Material properties | P-type modified bismuth telluride | N-type modified bismuth telluride |
|---|---|--|
| Seebeck coefficient ($\mu\text{V/K}$) | $-188.2 + 2.2411T$ $- 3.0075 \times 10^{-3}T^2$ $+ 2.4914 \times 10^{-7}T^3$ | $443.49 - 4.5121T$ $+ 9.4424 \times 10^{-3}T^2$ $- 5.8362 \times 10^{-6}T^3$ |
| Thermal conductivity ($\text{W/m}\cdot\text{K}$) | $-1.8067 + 5.7529 \times 10^{-3}T - \frac{64.639}{T}$ $+ \frac{1.3395 \times 10^5}{T^2}$ | $-4.6205 + 9.9277 \times 10^{-3}T$ $+ \frac{833.7}{T} + \frac{235636}{T^2}$ |
| Electrical conductivity (S/cm) | $-473.1 + 0.86507 \times T$ $+ e^{(16.637-1.6942\ln(T))}$ | $-2139.4 + 2.5778 \times T$ $+ e^{(12.795-0.89092\ln(T))}$ |

In order to reflect the influence of temperature on the TEG performances, the average values of the TE material properties were taken into the model. Mathematically, the average value of the material's properties can be calculated by the mean value theorem of integrals along with the temperature. In this way, the general formula of the average values of the TE material properties can be shown in Eq. (25)

$$\bar{\Delta} = \frac{\int_{T_c}^{T_h} \delta(T) \cdot dT}{(T_h - T_c)} \quad (25)$$

where $\bar{\Delta}$ represents the average values of the Seebeck coefficient, thermal conductivity, and electrical conductivity. The temperature-related value of each of these properties is marked as $\delta(T)$.

5.3 Modelling validation

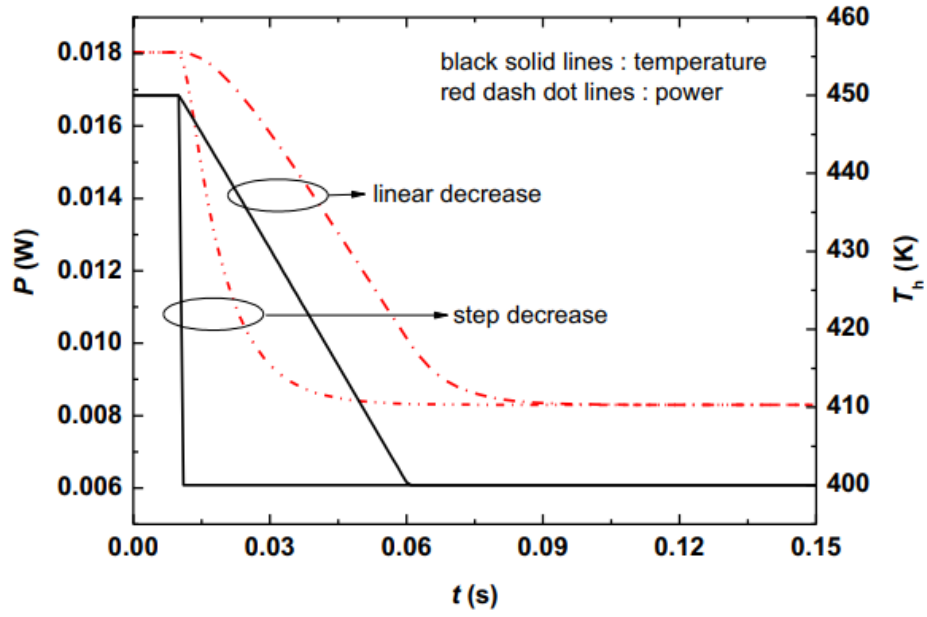
Before conducting the research, it is necessary to validate the transient TEG model. In this way, work in the modeling validation is divided into two different parts. In the first part, under a steady-state, the TEG model was validated by the experimental data from the study of Chen *et al.* [37]. In their experiment, a TEG with 127 pairs of elements were tested under a constant temperature boundary condition [37]. Therefore, the same case was simulated by our model in

SIMULINK. Besides, In the SIMULINK model, the TEG was divided into n parts, and the branch thermal resistances of the n parts are in series. Three kinds of values of n were tested in the modelling validation. Table 5.2 displays the simulation results and the experimental data from Chen *et al.* [37]. From the table, it can be found that the simulation results are close to the experimental data. Meanwhile, under the steady-state operation, the effects of the value of n on the TEG's output results can be ignored because the total thermal resistance of the TEG keeps the same in the different values of n .

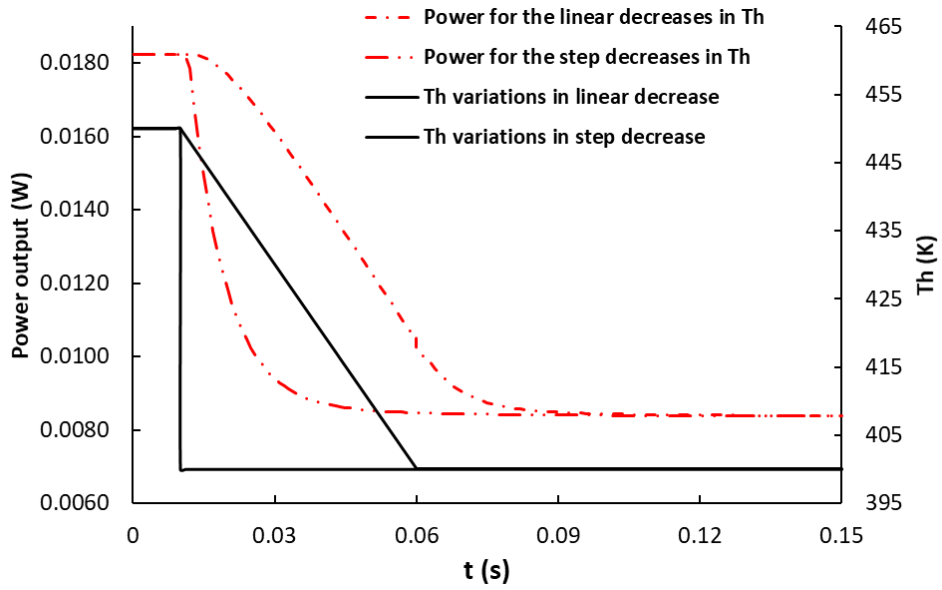
Table 5.2. Comparison between experiment and steady-state model for the TEG ($T_h=423$ K and $T_c= 303$ K)

| Quantity | Experimental data [38] | Results of the model ($n=2$) | Results of the model ($n=4$) | Results of the model ($n=8$) |
|---------------------|------------------------|--------------------------------|--------------------------------|--------------------------------|
| Input heat rate (W) | 70 | 71 | 71 | 71 |
| Output power (W) | 2.51 | 2.78 | 2.78 | 2.78 |
| Current (A) | 0.86 | 0.91 | 0.91 | 0.91 |
| Efficiency (%) | 3.6 | 3.9 | 3.9 | 3.9 |

In order to validate our TEG model under a dynamic operation, the simulation results from Meng *et al.* [38] were referred in another part. In the study of Meng *et al.* [38], they mainly focus on a pair of TE elements' transient behaviors under stepped and linear changes in temperature, respectively. The same cases were simulated by our model in SIMULINK. The results are displayed in Figure 5.5. In the transient problem, the response time is defined as the time required to reach a new steady-state (99% of the final value) after the input ends changing [38]. Table 5.3 indicates the response times of Meng *et al.* [38] and the TEG model in this study.



(a)



(b)

Figure 5.5. Comparison between previous and present transient TEG models, (a) results from Meng *et al.* [38], and (b) results from the present TEG model with $n=4$

Table 5.3. Comparison between experiment and steady-state model for the pair of TE elements

| Quantity | | Meng <i>et al.</i> [39] data | Results of this model ($n=2$) | Results of this model ($n=4$) | Results of this model ($n=8$) |
|----------------------|---------------|---------------------------------|------------------------------------|------------------------------------|------------------------------------|
| Response time (s) | Step change | 0.042 | 0.037 | 0.039 | 0.040 |
| | Linear change | 0.026 | 0.023 | 0.024 | 0.025 |

Under the hot temperature varied with the step decrease, the power converges to 0.0083 W, and the response time is 0.042 s in the research of Meng *et al.* [38]. For our result with $n=4$, the converged power and response time are 0.0085 W and 0.039s, respectively, which are within 10% of the literature values.

With the hot temperature decreasing linearly, the converged power is the same as that of the step-change in the research of Meng *et al.* [38] and in this simulation. The response time of the linear change is 0.0026 s for Meng *et al.* [38] and 0.0024 s in this study with $n=4$. In this way, when n is 4, the transient result of the model in this study is very close to that of Meng *et al.* [38] under both the hot temperature step change and linear change.

5.4 Transient performances of the hyperbolic TEG under the periodic source temperature

In the study, the shape designs with $\beta=0$ and 1.5 were taken as examples to compare the differences in the hyperbolic and traditional TEG transient behaviors under the oscillating source temperature. Meanwhile, the resistance ratio (r_x) was kept constant at 1.5 in the two cases. Before conducting the study, it was also necessary to select a time step (Δt) for the transient problem. Six levels of time step were tested for the TEG with $\beta=0$. The results are displayed in Table 5.4.

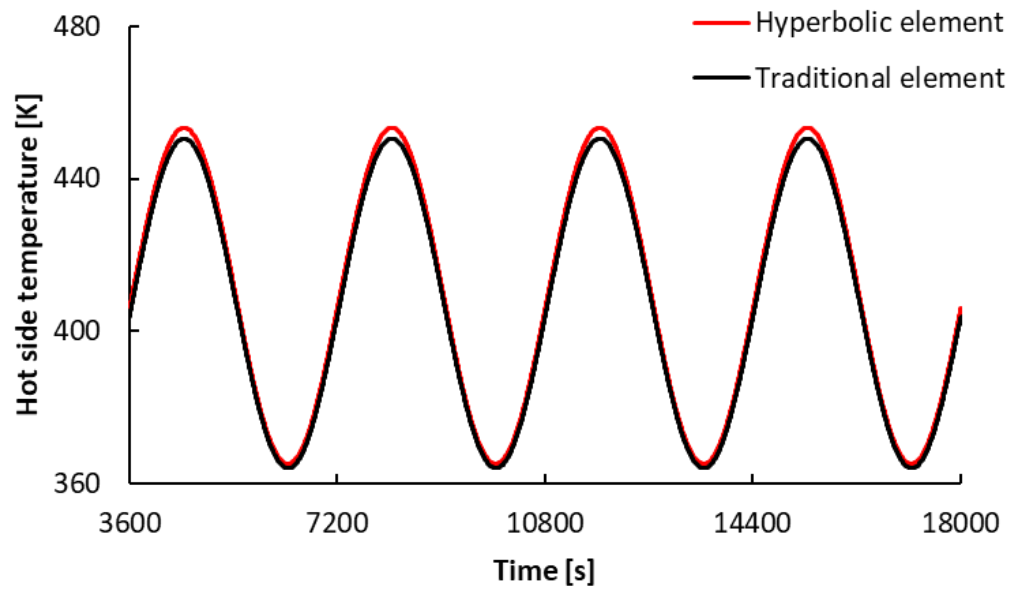
Table 5.4. Comparison in different time steps for a TEG ($\beta=0$)

| Quantity | $\Delta t=2$ s | $\Delta t=1$ s | $\Delta t=0.1$ s | $\Delta t=0.01$ s | $\Delta t=0.001$ s | $\Delta t=0.0001$ s |
|---------------------------------|----------------|----------------|------------------|-------------------|--------------------|---------------------|
| Mean power [W] | 0.1216 | 0.1217 | 0.1220 | 0.1220 | 0.1220 | 0.1220 |
| Mean input heat rate [W] | 16.49 | 16.50 | 16.51 | 16.51 | 16.51 | 16.51 |
| Overall efficiency [%] | 0.7374 | 0.7376 | 0.7389 | 0.7389 | 0.7389 | 0.7389 |

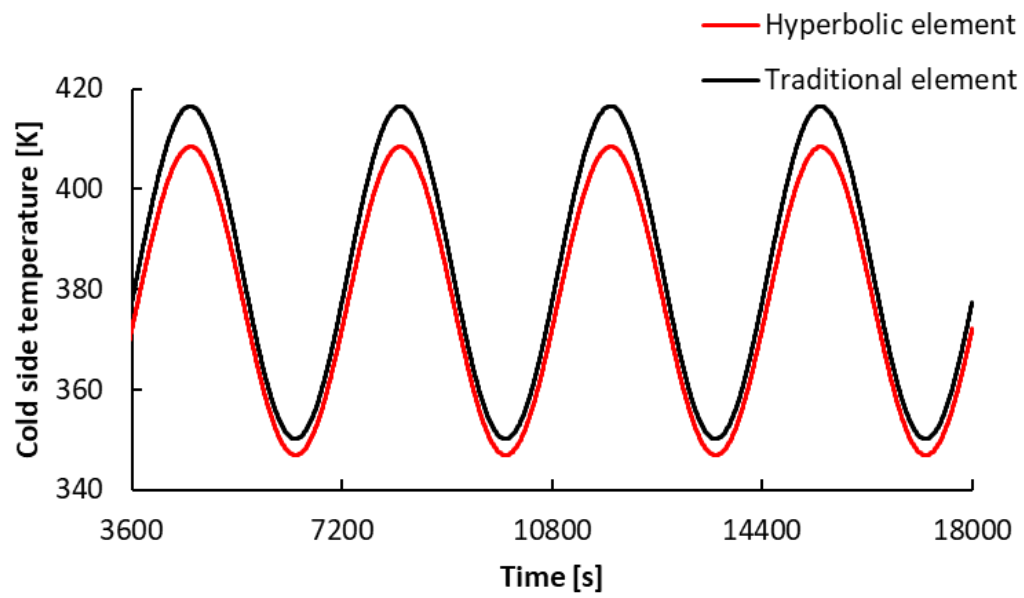
From Table 5.4, when the time step reached 0.1 s, the results, involving the mean power output, mean input heat rate, and overall efficiency, remained stable. Therefore, 0.1 s were used to be the time step for the following study.

The temperature variations at the hot side and cold side of the two leg geometries are displayed in Figures 5.6-(a) and (b). It took a couple of cycles for the simulation to reach steady state, producing repeatable sinusoidal signals that represent the real cycles. As such, the first 60 minutes of the simulated results were discarded.

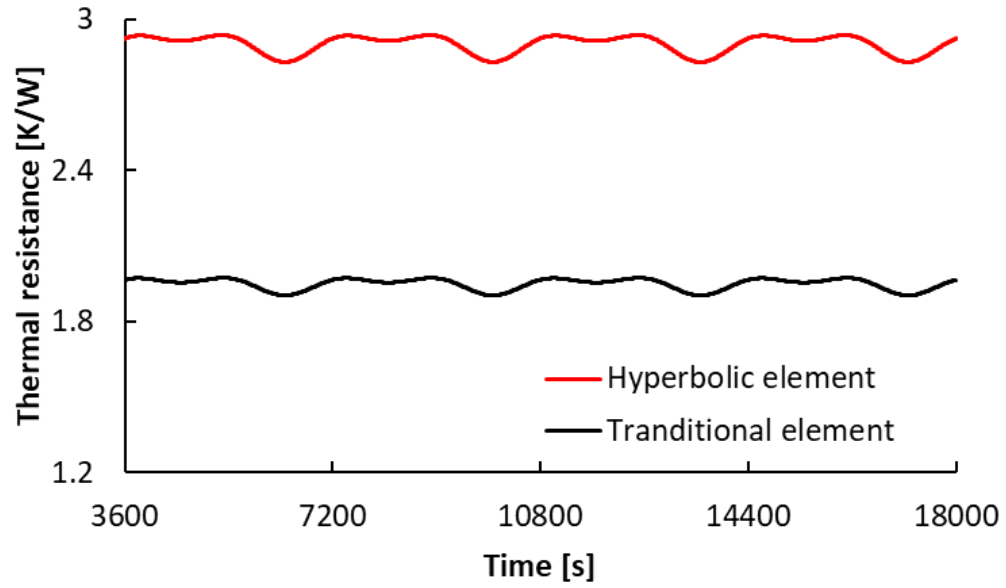
The results indicate that there are similar temperature profiles on the hot side for the two geometries. As for the cold side, the hyperbolic TEG have a lower cold side temperature, compared to the TEG consisting of traditional elements (shown as Figure 5.6-(b)). The main reason is the hyperbolic design can amplify the thermal resistance under the same volume shown as Figure 5.6-(c).



(a)



(b)



(c)

Figure 5.6. Comparison in the temperature and thermal resistance variations of the hyperbolic and traditional TEG, (a) hot temperature, (b) cold temperature, and (c) thermal resistance

The temperature difference of the TEG is calculated by a subtracting the hot temperature from the cold temperature. In this way, except for the initial stage, the hyperbolic shape design can also increase the temperature difference over most of the TEG in a cycle as shown in Figure 5.7.

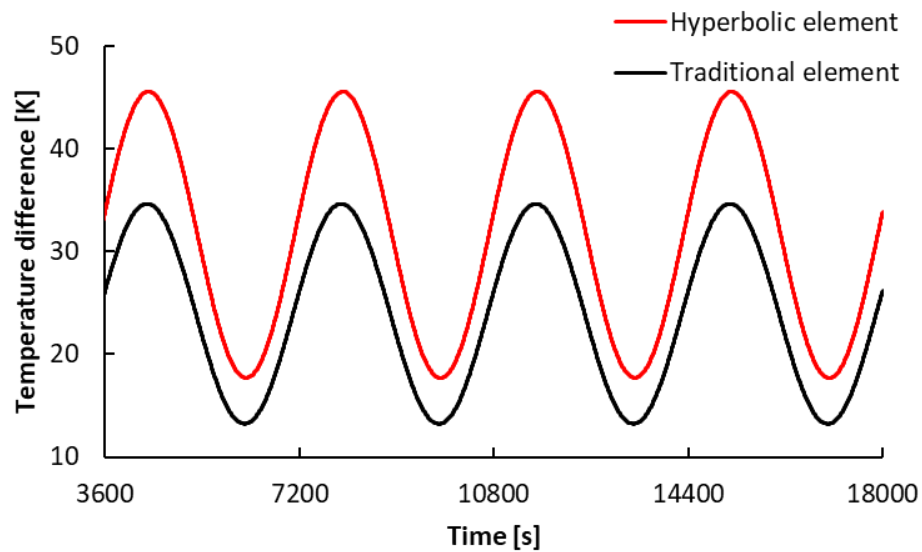


Figure 5.7. Comparison in the temperature difference variations of the hyperbolic and traditional TEGs

Figure 5.8 displays the power variations of the two kinds of TEGs under the sinusoidal thermal source. Similar to the tendency in the temperature difference, the hyperbolic TEG can output more electric work during the total time. In this way, the mean output power of the hyperbolic TEG in a cycle is higher than that of the traditional one.

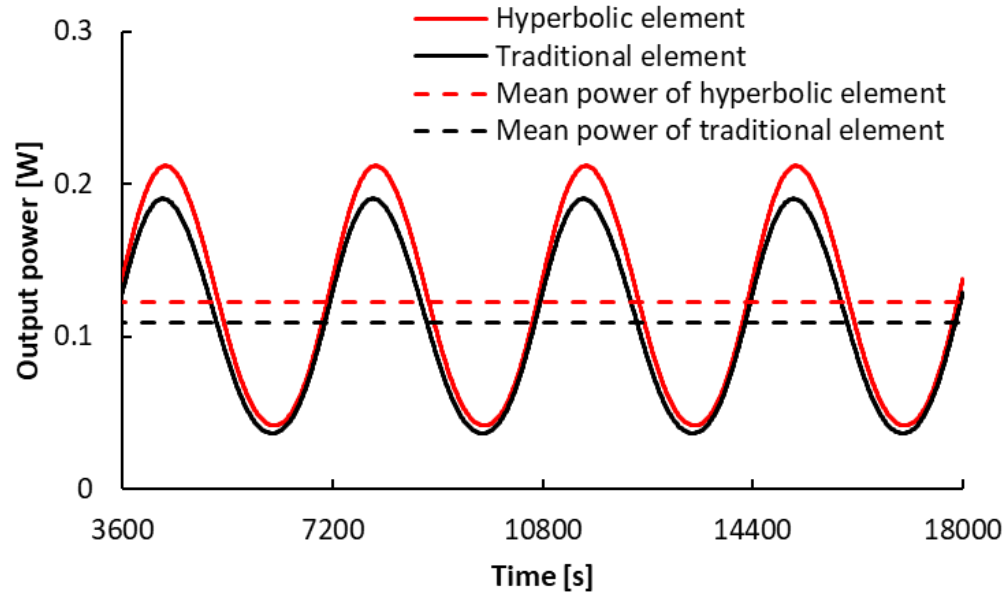
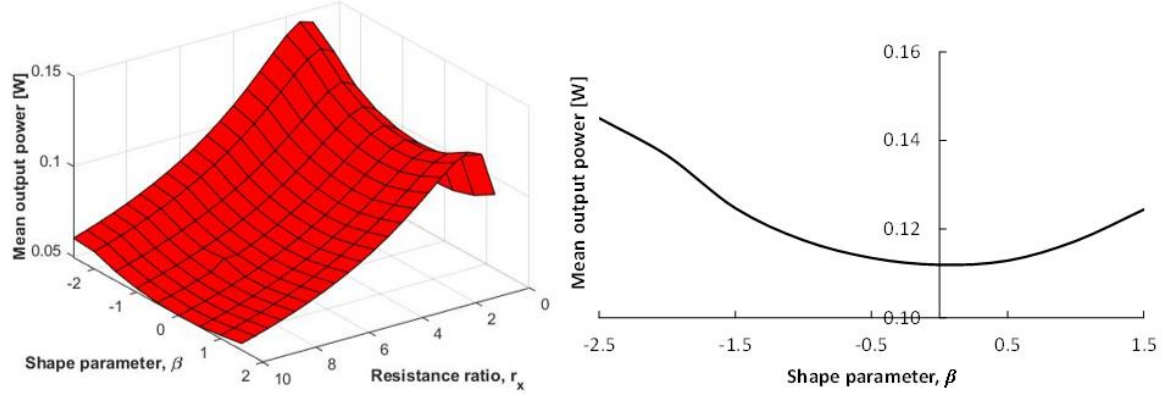


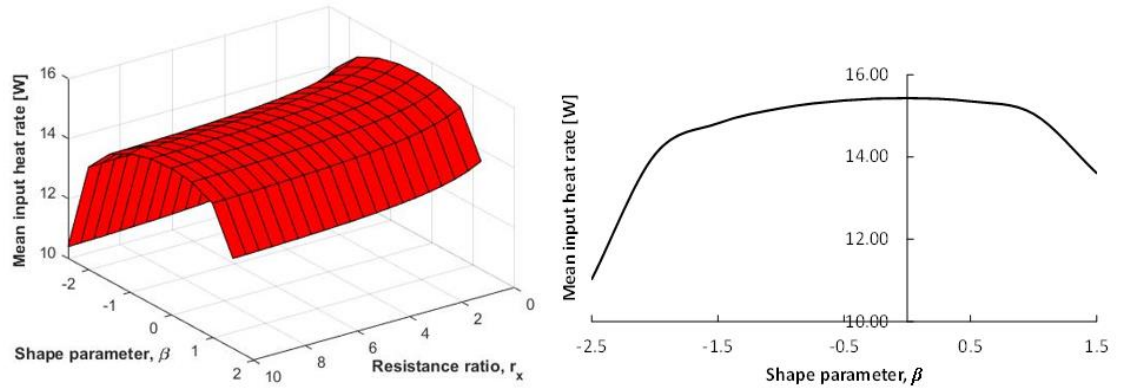
Figure 5.8. Comparison in the output power of the hyperbolic and traditional TEGs, (a) output power variations, and (b) mean output power

Additionally, in order to further verify the effects of variable cross-section design on the TEG's performance under a periodic thermal source, the hyperbolic TEG was modeled with different shape parameters and resistance ratios. It is noted that a shape parameter (β) of zero means the TE element is untapered; namely, it is a traditional TEG. The results shown in Figure 5.9-(a) indicate that the hyperbolic shape design can be used to improve the mean output power of the TEG under different resistance ratios. Meanwhile, since the hyperbolic shape design can enlarge the thermal resistance compared to the traditional TEG, there is a lower mean input heat rate for the hyperbolic TEG compared to the traditional one as shown in Figure 5.9-(b). The overall efficiency is a ratio between the mean output power and mean input heat rate. In this way, the overall efficiency of the hyperbolic TEG is higher than that of the traditional one as shown in Figure 5.9-(c). The results also disclose that there are obvious increases in both mean output power and overall efficiency with the absolute value of the shape parameter growth. Compared to the traditional TEG, the hyperbolic one designated by $\beta=-2.5$ can increase the mean power output and overall efficiency by 35.5% and 86.6%, respectively. Besides, there is almost the same power

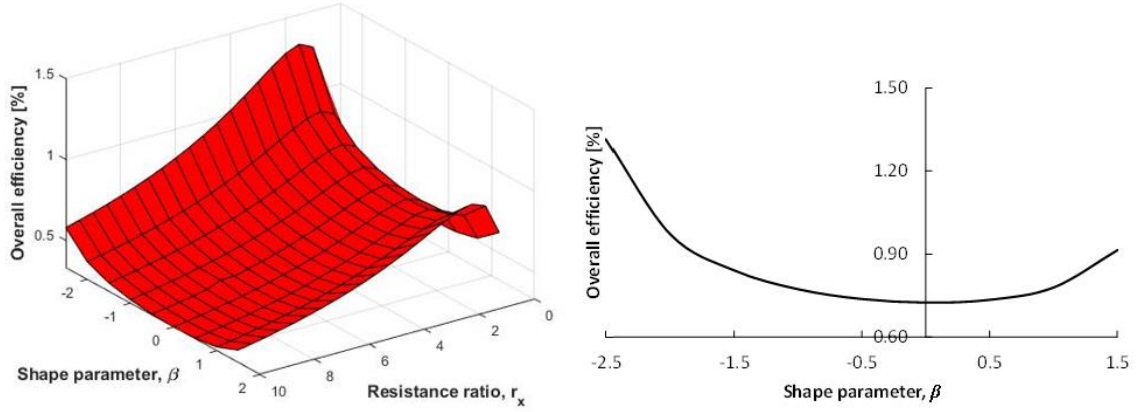
output by the hyperbolic TEG designed by a positive and negative value of β . However, compared to a negative value of β , the shape parameter with a positive value may enlarge the thermal resistance further, making a lower mean input heat rate in the TEG with a positive value of β . Therefore, when the value of $|\beta|$ stays the same, the overall efficiency of the TEG with $\beta > 0$ is a little bit better than that with $\beta < 0$ under the dynamic condition.



(a)



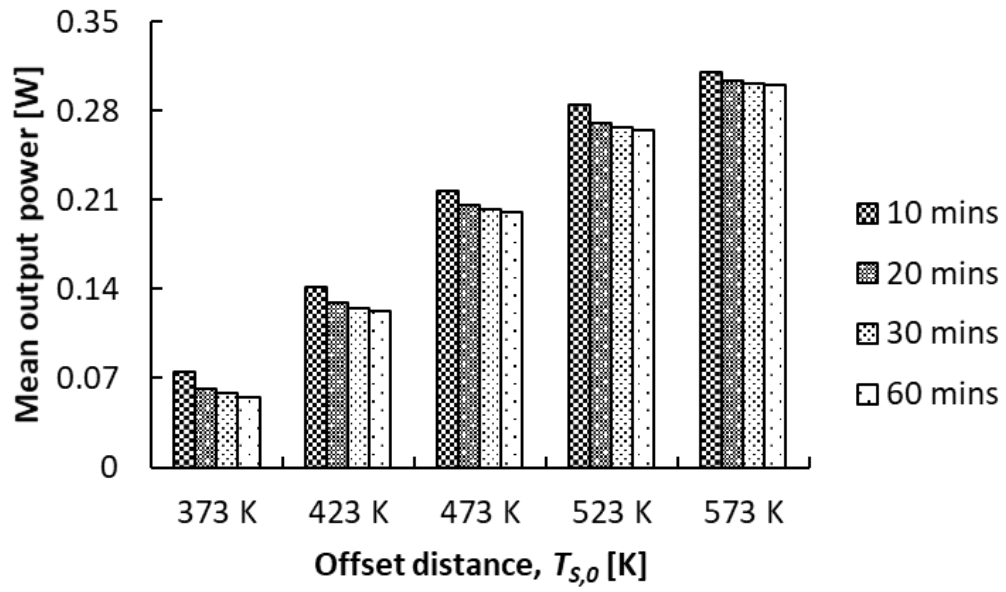
(b)



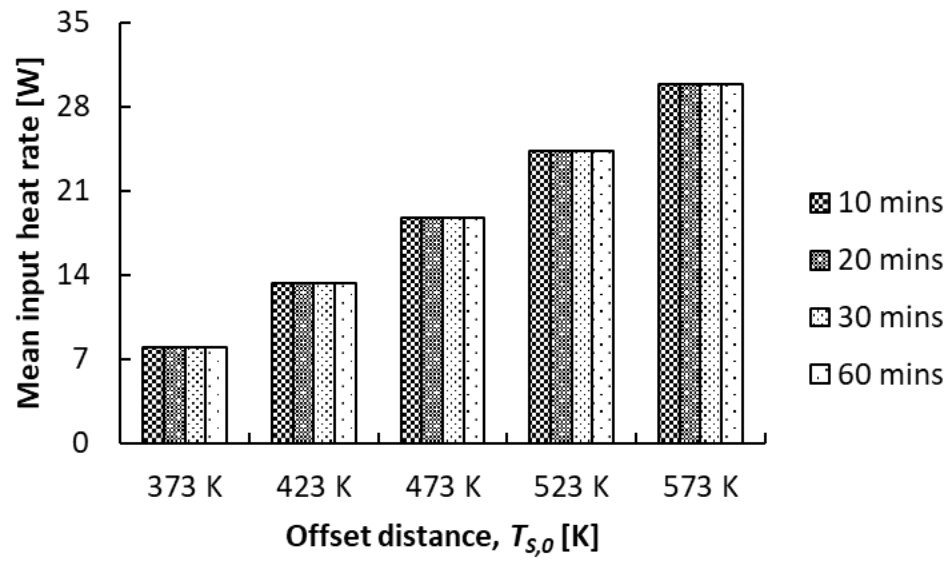
(c)

Figure 5.9. Transient performances of the hyperbolic TEG with different shape parameters and resistance ratios, (a) variation of the mean output power, (b) variation of the mean input heat rate, and (c) variation of the overall efficiency

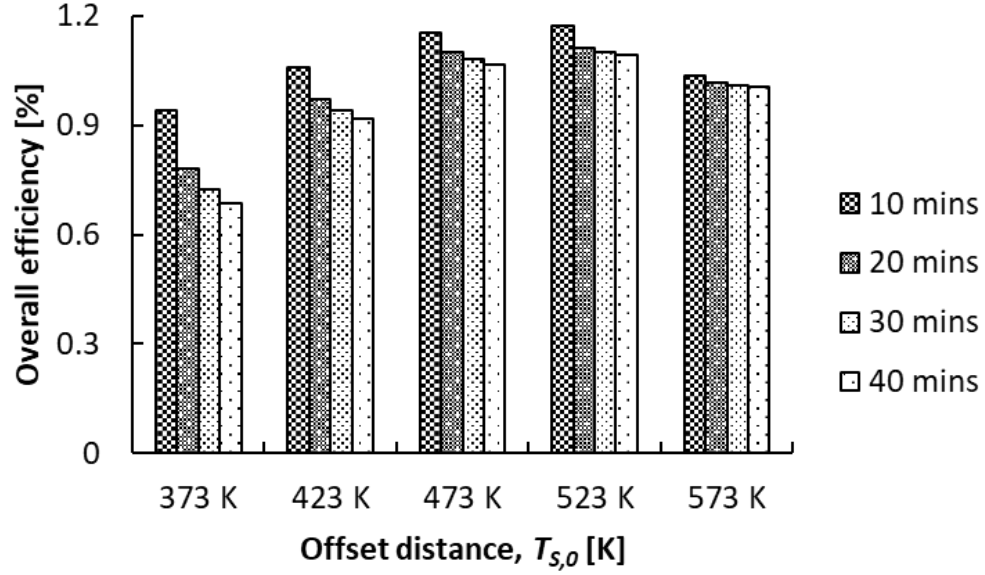
Due to the thermal inertia, the temperature variations at the hot and cold sides of the TEG are not synchronous. In this way, it is possible for the oscillating period of the heat source temperature to have an important influence on the temperature difference between the two ends of the TEG. It also means that the oscillating period may play an important role in the TEG's performance. In order to illustrate the effect of the oscillating period on the TEG's performance, a hyperbolic TEG with $\beta=1.5$ was modeled under different oscillating periods (λ_s) and offset distances ($T_{s,0}$). The thermoelectrical conversion performances of the hyperbolic TEG are displayed in Figure 5.10, involving the mean input heat rate, mean power output, and the overall efficiency. The results indicate that the mean input heat rate mainly depends on the offset distance of the source temperature rather than the oscillating period (shown as Figure 5.10-(a)). However, it can be seen in Figure 5.10-(b) that a shortened oscillating period can always increase the mean output power of the hyperbolic TEG no matter what is the offset distance of the source temperature. Combining the variations of the mean input heat rate and output power, decreasing the oscillating period can also improve the overall efficiency of the hyperbolic as shown in Figure 5.10-(c).



(a)



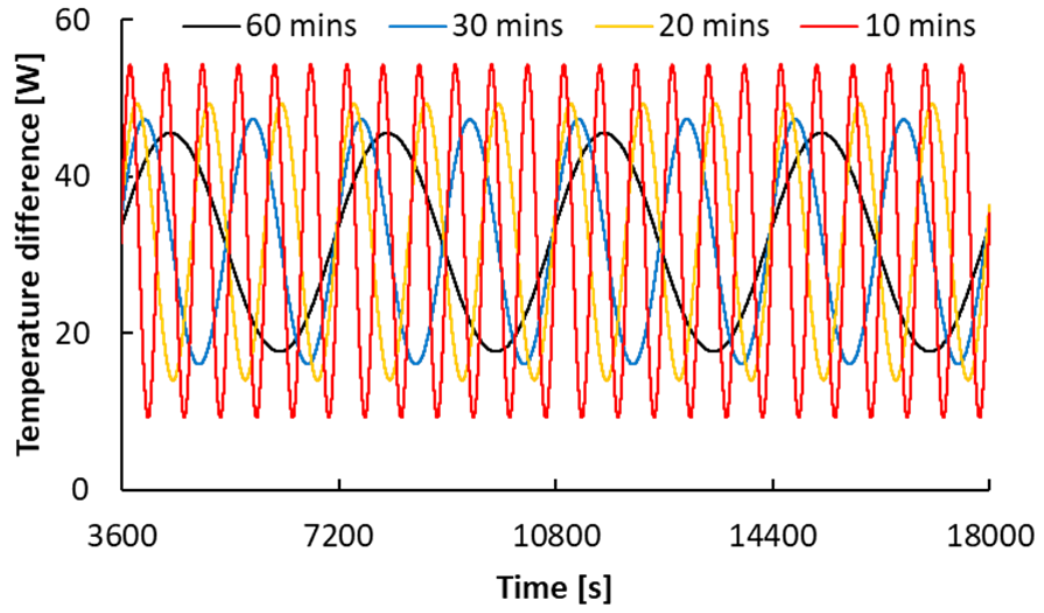
(b)



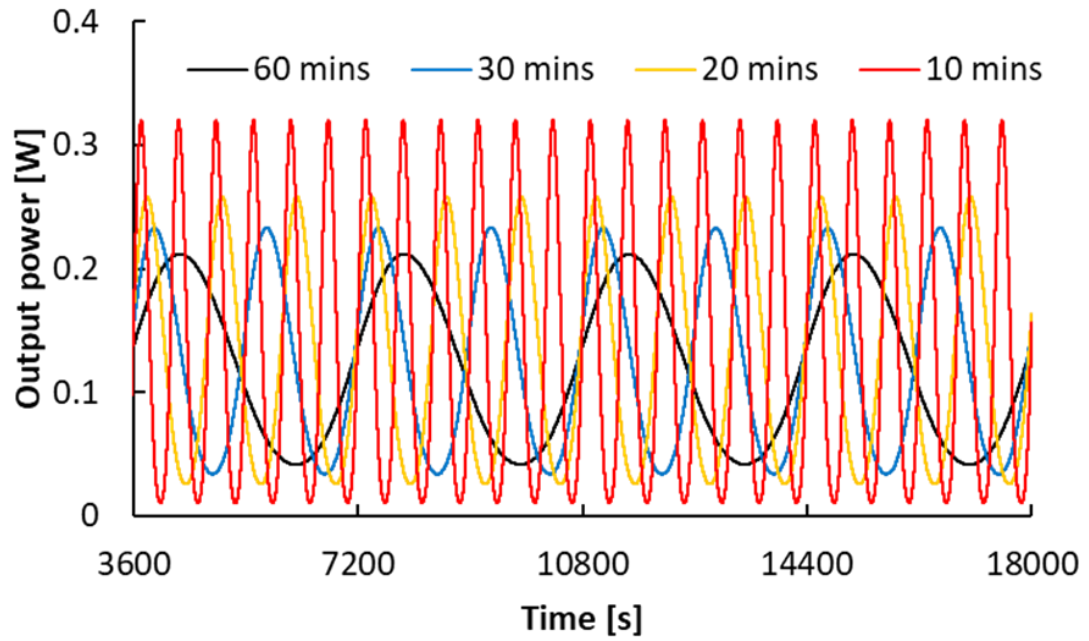
(c)

Figure 5.10. Transient performances of the hyperbolic TEG with different source periods and offset distances, (a) variation of the mean output power, (b) variation of the mean input heat rate, and (c) variation of the overall efficiency

Additionally, in order to investigate the mechanism of the mean power improvement in a short oscillating period, the transient data for the temperature difference and power output at $T_{s,0}=423$ K were extracted, shown as Figure 5.11. For a TEG, the response to the variation of the source temperature at the hot side is faster than that at the cold side due to the thermal inertia. With a shortened period of the oscillating source temperature, the lag effect becomes more obvious, making it possible to enlarge the oscillating amplitude of the temperature difference between the hot and cold side of the TEG (as shown in Figure 5.11-(a)). The output power of a TEG is a function of the temperature difference squared. Increasing temperature difference amplitude can lead to the larger the power at the crest compared to the valley (as shown in Figure 5.11-(b)), making it possible to increase the total electrical work. In this way, decreasing the period may have a positive effect on the mean power output of the TEG.



(a)



(b)

Figure 5.11. Comparison in the temperature difference and output power variations of the hyperbolic TEG under different source periods, (a) temperature difference variations, and (b) output power variations

5.5 Conclusions

In this paper, a hyperbolic shape design was introduced to improve a TEG's performance under a periodic thermal source. Based on the electrothermal analogy, a transient TEG model was established in SIMULINK. In this model, the source temperature oscillates with a sinusoidal function, and the ambient temperature is kept constant at 300 K. The TEG model was validated under steady-state and dynamic operation. Then, it was used to show differences in the transient behaviors of hyperbolic and traditional shaped TEGs under the periodic thermal source. Meanwhile, based on the TEG model, the two important parameters, the shape parameter, and source temperature period, were verified to have considerable effects on the transient performances of the hyperbolic TEG. The main conclusions of this work are as follows:

- 1) Due to the thermal inertia, there is a higher power output of the traditional TEG compared to that of the hyperbolic one at the initial stage. However, the hyperbolic design can enlarge the thermal resistance under the same volume of a TE element. With lower heat transfer, the hyperbolic TEG ends up with a higher temperature difference than that of the traditional one, making it possible to produce more power for most of the cycle. In this way, under a continuously oscillating source temperature, the hyperbolic shape design can be used to improve the mean output power and overall efficiency of a TEG.
- 2) Additionally, the shape parameter, β , is used to describe the geometry of the hyperbolic TEG. Increasing the absolute value of the shape parameter ($|\beta|$) makes the TE element's shape more tapered, which can enlarge the thermal resistance further. Therefore, a high value of $|\beta|$ has positive effects on the transient performances of the hyperbolic TEG.
- 3) Finally, there is a delay in the temperature variations from the hot to the cold side of the TEG. A shortened period of the source temperature oscillation can increase the amplitude in the oscillating temperature difference at two ends of the TEG, thereby, having a positive effect on the mean power output. The result indicates that the effect of the period on the input heat can be ignored. In this way, decreasing the period can also improve the overall efficiency of the TEG.

Acknowledgments

This work was made possible by funding from the Natural Sciences and Engineering Research Council of Canada.

References

- [1] International Energy Agency (IEA, 2020), [Online], World Energy Outlook 2020, <https://www.iea.org/reports/world-energy-outlook-2020>. Accessed 5, May 2022.
- [2] International Energy Agency (IEA, 2022), [Online], Data and statistics, <https://www.iea.org/data-and-statistics/data-browser/?country=WORLD&fuel=Energy%20supply&indicator=TESbySource>. Accessed 5, January 2022.
- [3] S. A. Kalogirou, Solar energy engineering: processes and systems, 2nd Ed. Elsevier, UK: Oxford, 2014.
- [4] M. E. Fernandez, J. O. Gentili, and A. M. Campo, “Solar access: Review of the effective legal framework for an average argentine city,” Renewable and Sustainable Energy Reviews, vol. 156, p. 112008, December 2021.
- [5] S. R. Paramati, U. Shahzad, and B. Dogan, ‘The role of environmental technology for energy demand and energy efficiency: Evidence from OECD countries’, Renewable and Sustainable Energy Reviews, vol. 153, p. 111735, October 2021.
- [6] International Energy Agency (IEA, 2022), [Online], Tracking Industry 2021, <https://www.iea.org/reports/tracking-industry-2021>. Accessed 5, January 2022.
- [7] G. Li, S. Shittu, T. M. O. Diallo, M. Yu, X. Zhao, and J. Ji, ‘A review of solar photovoltaic-thermoelectric hybrid system for electricity generation’, Energy, vol. 158, pp. 41–58, September 2018.
- [8] C. C. Bomberger, P. M. Attia, A. K. Prasad, and J. M. O. Zide, “Modeling passive power generation in a temporally-varying temperature environment via thermoelectrics,” Applied Thermal Engineering, vol. 56, pp. 152–158, March 2013.
- [9] D. Luo, Yuying Yan, R. Wang, and W. Zhou, “Numerical investigation on the dynamic response characteristics of a thermoelectric generator module under transient temperature excitations,” Renewable Energy, vol. 170, pp. 811–823, February 2021.
- [10] W. H. Chen, P. H. Wu, X. D. Wang, and Y. L. Lin, “Power output and efficiency of a thermoelectric generator under temperature control,” Energy Conversion and Management, vol. 127, pp. 404–415, September 2016.
- [11] W. H. Chen, S. R. Huang, X. D. Wang, P. H. Wu, and Y. L. Lin, “Performance of a thermoelectric generator intensified by temperature oscillation,” Energy, vol. 133, pp. 257-267, May 2017.

- [12] X. D. Jia, Y. J. Wang, and Y. W. Gao, "Numerical simulation of thermoelectric performance of linear-shaped thermoelectric generators under transient heat supply," *Energy*, vol. 130, pp. 276–285, April 2017.
- [13] M. Guo, D. Gu, L. Xi, H. Zhang, J. Zhang, J. Yang and R. Wang, "Selective laser melting additive manufacturing of pure tungsten: Role of volumetric energy density on densification, microstructure and mechanical properties," *International Journal of Refractory Metals and Hard Materials*, vol. 84, p. 105025, November 2019.
- [14] A. Z. Sahin and B. S. Yilbas, "The thermoelement as thermoelectric power generator: Effect of leg geometry on the efficiency and power generation," *Energy Conversion and Management*, vol. 65, pp. 26–32, January 2013.
- [15] Y. Shi, D. Mei, Z. Yao, Y. Wang, H. Liu and Z. Chen, "Nominal power density analysis of thermoelectric pins with non-constant cross sections," *Energy Conversion and Management*, vol. 97, pp. 1–6, June 2015.
- [16] H. B. Liu, S. L. Wang, Y. R. Yang, W. H. Chen, and X. D. Wang, "Theoretical analysis of performance of variable cross-section thermoelectric generators: Effects of shape factor and thermal boundary conditions," *Energy*, vol. 201, p. 117660, April 2020.
- [17] O. I. Ibeagwu, "Modelling and comprehensive analysis of TEGs with diverse variable leg geometry," *Energy*, vol. 180, pp. 90–106, May 2019.
- [18] Q. Doraghi, N. Khordehgah, A. Zabnienska-Góra, L. Ahmad, L. Norman, D. Ahmad, and H. Jouhara, "Investigation and computational modelling of variable TEG leg geometries," *ChemEngineering*, vol. 5 (3), p. 5030045, August 2021.
- [19] S. C. Costa, M. Tutar, I. Barreno, J. A. Esnaola, H. Barrutia, D. García, M. A. Gonzalez, and J. I. Prieto, "Experimental and numerical flow investigation of Stirling engine regenerator," *Energy*, vol. 72, pp. 800–812, June 2014.
- [20] W. H. Chen and J. C. Chen, "Combustion characteristics and energy recovery of a small mass burn incinerator," *International Communications in Heat and Mass Transfer*, vol. 28 (3), pp. 299–310, April 2001.
- [21] K. Yazawa, J. H. Bahk and A. J. Ghajar, *Thermoelectric energy conversion devices and systems*, vol. 7, World Scientific, UK: London, 2021.
- [22] H. Adachi, K. Uchida, E. Saitoh¹, and S. Maekawa, "Theory of the spin Seebeck effect," *Reports on Progress in Physics*, vol. 76, p. 036501, February 2013.
- [23] M. Chen, L. A. Rosendahl, T. J. Condra, and J. K. Pedersen, "Numerical modeling of thermoelectric generators with varying material properties in a circuit simulator," *IEEE Transactions on Energy Conversion*, vol. 24 (1), pp. 112–124, March 2009.

- [24] Y. Shi, X. Lu, Q. Xiang, J. Li, X. Shao, and W. Bao, "Stretchable thermoelectric generator for wearable power source and temperature detection applications," *Energy Conversion and Management*, vol. 253, p. 115167, December 2021.
- [25] J. Chen, R. Wang, D. Luo, and W. Zhou, "Performance optimization of a segmented converging thermoelectric generator for waste heat recovery," *Applied Thermal Engineering*, vol. 202, p. 117843, November 2021.
- [26] S. Qing, H. Yuan, C. Chen, S. Tang, X. Wen, J. Zhong, and X. Gou, "Characteristics and single/multi-objective optimization of thermoelectric generator by comprehensively considering inner-connection-and-contact effects and side-surface heat loss," *Energy Conversion and Management*, vol. 251, p. 115003, November 2021.
- [27] D. R. Karana and R. R. Sahoo, "Influence of geometric parameter on the performance of a new asymmetrical and segmented thermoelectric generator," *Energy*, vol. 179 (15), pp. 90–99, July 2019.
- [28] A. Montecucco, J. R. Buckle and A. R. Knox, "Solution to the 1-D unsteady heat conduction equation with internal Joule heat generation for thermoelectric devices," *Applied Thermal Engineering*, vol. 35, pp. 177–184, October 2011.
- [29] G. Fraisse, J. Ramousse, D. Sgorlon, and C. Goupil, "Comparison of different modeling approaches for thermoelectric elements," *Energy Conversion and Management*, vol. 65, pp. 351–365, October 2012.
- [30] A. Piggott, "Detailed transient multiphysics model for fast and accurate design, simulation and optimization of a thermoelectric generator (TEG) or thermal energy harvesting device," *Journal of Electronic Materials*, vol. 48 (9), pp. 90–99, January 2019.
- [31] Y. A. Çengel and A. Shakouri, *Heat and mass transfer fundamentals and applications*, 5th Ed. McGraw Hill Education, USA: New York, 2015.
- [32] P. E. Ruiz-Ortega, M. A. Olivares-Robles, and O. Y. Enciso-Montes de Oca, "Segmented Thermoelectric Generator under Variable Pulsed Heat Input Power" *Entropy*, vol. 21, p. 1100929, September 2019.
- [33] A. Montecucco, J. R. Buckle, and A. R. Knox, "Solution to the 1-D unsteady heat conduction equation with internal Joule heat generation for thermoelectric devices" *Applied Thermal Engineering*, vol. 35, pp. 177-184, October 2011.
- [34] M. Gomez, R. Reid, B. Ohara and H. Lee, "Influence of electrical current variance and thermal resistances on optimum working conditions and geometry for thermoelectric energy harvesting," *Journal of Applied Physics*, vol. 113, p. 174908, May 2013.
- [35] Coolinnovations, [Online], Sparse Configuration| Aluminum, <http://www.coolinnovations.com/datasheets/3-4141XXM.pdf>. Accessed 10, May 2021.

- [36] J. D'Angelo, E. D. Case, N. Matchanov, C. Wu, T. P. Hogan, J. Barnard, C. Cauchy, T. Hendrick and M. G. Kanatzidis, "Electrical, thermal, and mechanical characterization of novel segmented-leg thermoelectric modules," *Journal of Electronic Materials* volume, vol. 40, pp. 2051–2062, August 2011.
- [37] M. Chen, L. A. Rosendahl, and T. Condra, "A three-dimensional numerical model of thermoelectric generators in fluidpower systems," *International Journal of Heat and Mass Transfer*, vol. 54, pp. 345-355, October 2010.
- [38] J. H. Meng, X. X. Zhang and X. D. Wang, "Dynamic response characteristics of thermoelectric generator predicted by a three-dimensional heat-electricity coupled model," *Journal of Power Sources*, vol. 245, pp. 262-269, July 2013.

CHAPTER 6

CONCLUSIONS AND RECOMMENDATIONS

6.1 Summary and Conclusions

The main objective in this study is to enhance a TEG's performance through novel geometric structures and optimized working conditions. The contributions are mainly focused on two aspects, which are the improvement of the TEG optimization algorithm, and variable cross-section shape design. The main conclusions are summarized in this chapter.

6.1.1 Improvement of TEG optimization algorithm

A mutation subprogram was used to improve the PSO method when the TEG's performance is optimized by this algorithm. The mutation is an effective method to avoid premature convergence for the PSO algorithm. Besides, the mutation can decrease the need for trial-and-error calculations or tuning parameters in the optimization.

The results also demonstrated that the optimal configurations of the geometric structure and working conditions may vary with different performance indices of a TEG. It is necessary to conduct multi-objective optimization for a TEG in order to balance the design based on different performance indicators. The weighted approach can be introduced in the M-PSO algorithm to solve the multi-objective optimization for a TEG. However, the selection of the weighting factor is arbitrary. This drawback can be avoided through introducing the epsilon-constraint method into the M-PSO algorithm. A series of solutions that satisfy the constraints can be acquired by this method. It was demonstrated that an ideal solution can be selected from the set of solutions through applying the technique for order preference by similarity ideal solution (TOPSIS) method.

Additionally, there is a limitation on the M-PSO algorithm when a TEG is optimized based on a comprehensive thermodynamic model where the temperatures at the ends of a TEG are unknown. This limitation can be overcome through loop nesting of the M-PSO algorithm (which is named as Dual-MPSO).

Overall, the M-PSO is an effective algorithm to optimize a TEG's performance. Meanwhile, through using the epsilon-constraint and TOPSIS method cooperatively, a reasonable optimal configuration for a TEG in the multi-objective optimization can be acquired by the M-PSO algorithm. Besides, the M-PSO method was utilized twice when optimizing a TEG based on a comprehensive thermodynamic model. This method is called the Dual-MPSO algorithm.

6.1.2 Hyperbolic shaped design for a TEG

A hyperbolic structure was used to optimize a TEG's performance. The results indicated that under a steady-state operation, the hyperbolic TEG has a higher output power and efficiency compared to the constant cross-section TEG (traditional TEG). According to the thermal resistance analysis, the changing cross-sectional area can lead to the variation of the thermal resistance, making it possible to enlarge the temperature difference across the TE couple. This is the main mechanism by which the performance of the TEG module is improved in the hyperbolic shape design. Besides, the shape parameter (β), used to describe the geometric feature of the hyperbolic TEG, has considerable effects on the TEG's performance. With the increasing of the $|\beta|$, the output power and efficiency of the hyperbolic TEG can be improved. It is also noticeable that when the $|\beta|$ has the same value, the positive β is more preferable, compared to the negative one (*i.e.*, narrowing the hot end of the TEG is more effective than narrowing the cold side).

The hyperbolic structure can not only be used to increase the power output and efficiency under a steady-state operation, but it has positive effects on the dynamic performance of a TEG. Under a periodically oscillating source temperature, the mean output power and overall efficiency of the hyperbolic TEG are higher than that of the traditional one. The mean power output and overall efficiency of the hyperbolic TEG can be improved further through enlarging the value of the $|\beta|$. Besides, under dynamic operation, the effects of the oscillating period of the source temperature on the hyperbolic TEG's dynamic performance should not be ignored. The results disclosed that decreasing the oscillating period results in enhancements in the mean power output and overall efficiency of the hyperbolic TEG.

6.1.3 Limitations

Although the MPSO algorithm can be used to optimize a TEG in many applications, there are some limitations to the variable range selections in these studies. Firstly, the TE materials in this thesis are bismuth telluride and modified bismuth telluride. The relevant literature indicated that these materials are suitable for waste heat recovery at a medium temperature range, meaning the source temperature is normally between 503 K and 923 K [1, 2]. In this way, the temperatures in this thesis range from 273 K to 900 K. Additionally, in the optimization, the load resistance is in a range between 0.01 Ω to 10 Ω , and the internal resistance of the TEG depends on the materials' properties, temperature and structure. The optimization algorithm is independent of the load resistance, and the power and efficiency depend on the load resistance. However, based on Ohm's law, when the load resistance is roughly equal to the internal resistance, the TEG will reach its optimal performance (in the thesis, the variation of the internal resistance of the TEG is between

0.09 Ω to 8.81 Ω under different temperatures and geometric structures). In this way, the range of the load resistance should cover the internal resistance variations, which is the main reason why the load resistance ranges from 0.01 Ω to 10 Ω .

6.2 Recommendations

For the research about the TEG's performance optimization, there are two aspects which should be improved further: the TEG model and algorithm. Firstly, based on the practical application, it is necessary to establish a detailed model for a TEG system, involving the TEG module and cooling devices, making it possible to conduct a comprehensive optimization for a TEG system. Moreover, a segmented TEG model, consisted of two or three different TE materials, should be focused in future studies, which is a useful way to improve the TEG's performance under a high temperature environment. Specially, some complicated geometric structures, such as diamond structure or X-shaped structure, can be used to design and optimize the segmented TEG's performance.

Additionally, an increasing number of novel bionic algorithms, such as the Student Psychology-Based Optimization (SPBO) and Poor and Rich Optimization (PRO), *etc.*, have been proposed in recent years. These algorithms improve the convergence. In this way, it is worthwhile to apply novel algorithms in the TEG optimization research, to further avoid premature convergence, and decrease the processes of trial-and-error calculations or tuning parameters.


Finally, from the dynamic research, it is difficult for a TEG to output power at its optimal state continuously since the surroundings are always changing. Thus, similar to other renewable energy systems, like solar power systems, it is required for a TEG to develop a Maximum Power Point Tracking (MPPT) system, making it possible to output the maximum power continuously. However, the algorithm failure caused by premature convergence is still one of the main challenges for the MPPT system. In this way, improving the algorithm for the MPPT system is also a popular topic in future studies.

References

- [1] R. Ovik, B. D. Long, M. C. Barma, M. Riaz, M. F. M. Sabri, S. M. Said, and R. Saidur, 'A review on nanostructures of high-temperature thermoelectric materials for waste heat recovery', *Renewable and Sustainable Energy Reviews*, vol. 64, pp. 635–659, July 2016.
- [2] A. J. Minnich, M. S. Dresselhaus, Z. F. Ren, and G. Chen, 'Bulk nanostructured thermoelectric materials: current research and future prospects', *Energy & Environmental Science*, vol. 2 (5), pp. 466–479, February 2009.

APPENDICE

Appendix A Permissions of the chapters 2 and 3 from the publishers



Mutation particle swarm optimization (M-PSO) of a thermoelectric generator in a multi-variable space

Author: Xi Wang, David S-K Ting, Paul Henshaw
Publication: Energy Conversion and Management
Publisher: Elsevier
Date: 15 November 2020
© 2020 Elsevier Ltd. All rights reserved.


Journal Author Rights

Please note that, as the author of this Elsevier article, you retain the right to include it in a thesis or dissertation, provided it is not published commercially. Permission is not required, but please ensure that you reference the journal as the original source. For more information on this and on your other retained rights, please visit: <https://www.elsevier.com/about/our-business/policies/copyright#Author-rights>

BACK

CLOSE WINDOW

© 2022 Copyright - All Rights Reserved | Copyright Clearance Center, Inc. | Privacy statement | Terms and Conditions
Comments? We would like to hear from you. E-mail us at customer-care@copyright.com



Exergoeconomic analysis for a thermoelectric generator using mutation particle swarm optimization (M-PSO)

Author: Xi Wang, Paul Henshaw, David S-K Ting
Publication: Applied Energy
Publisher: Elsevier
Date: 15 July 2021
© 2021 Elsevier Ltd. All rights reserved.

Journal Author Rights

Please note that, as the author of this Elsevier article, you retain the right to include it in a thesis or dissertation, provided it is not published commercially. Permission is not required, but please ensure that you reference the journal as the original source. For more information on this and on your other retained rights, please visit: <https://www.elsevier.com/about/our-business/policies/copyright#Author-rights>

BACK

CLOSE WINDOW

© 2022 Copyright - All Rights Reserved | Copyright Clearance Center, Inc. | Privacy statement | Terms and Conditions
Comments? We would like to hear from you. E-mail us at customer-care@copyright.com

VITA AUCTORIS

NAME: Xi (William) Wang

PLACE OF BIRTH: Beijing, China

YEAR OF BIRTH: 1990

EDUCATION: Beijing the 31st Middle School, Beijing, China, 2008
Chang'an University, B.Sc., Xi'an, China, 2013
Chang'an University, M.Sc., Xi'an, China, 2016
University of Windsor, Windsor, ON, 2022